2013-01-01

Integrated Geological and Geophysical Studies of the Indio Mountains and Hueco Bolson, West Texas

Pawan Budhathoki
University of Texas at El Paso, pawanbt@hotmail.com

INTEGRATED GEOLOGICAL AND GEOPHYSICAL STUDIES OF THE INDIO MOUNTAINS AND HUECO BOLSON, WEST TEXAS

PAWAN BUDHATHOKI

Department of Geological Sciences

APPROVED:

Richard P. Langford , Ph.D., Chair

Diane I. Doser, Ph.D., Co-Chair

Terry L. Pavlis, Ph.D.

Philip C. Goodell, Ph.D.

Jose M. Hurtado, Jr., Ph.D.

Jerry D. Johnson, Ph.D.

Benjamin C. Flores, Ph.D.
Dean of the Graduate School

Dedication

To my lovely family…

INTEGRATED GEOLOGICAL AND GEOPHYSICAL STUDIES OF THE INDIO MOUNTAINS AND HUECO BOLSON, WEST TEXAS

by

PAWAN BUDHATHOKI, M.S., B.S.

DISSERTATION

Presented to the Faculty of the Graduate School of

The University of Texas at El Paso

in Partial Fulfillment

of the Requirements

for the Degree of

DOCTOR OF PHILOSOPHY

Department of Geological Sciences

THE UNIVERSITY OF TEXAS AT EL PASO

December 2013

Acknowledgements

I wish to express my heartfelt gratitude to my advisors and dissertation committee chair and co-chair Dr. Richard Langford and Dr. Diane Doser who made it possible to complete this dissertation, and provided continuous guidance, suggestions and tremendous supports. Dr. Langford introduced me the research project of the sequence stratigraphic framework of the Cox Sandstone of the Indio Mountains, and Dr. Doser offered me an opportunity to work with her on the Hueco bolson project. Dr. Langford deserves extra thanks for his tremendous help in fieldwork, untiring guidance and encouragement throughout my study at the University of Texas at El Paso. I will be forever grateful with Dr. Doser for her undying patience and endless support during the course of the project and my academic term. My gratitude and sincere appreciations also go to Dr. Terry Pavlis, Dr. Jose Hurtado, Dr. Philip Goodell, and Dr. Jerry Johnson for serving this dissertation committee, and for their helpful guidance.

I am grateful to Dr. Mark Baker for discussion related to log analysis, and Alfredo Ruiz of El Paso Water Utilities for providing the well logs. I would like to thank Galen Kaip for teaching me to use geophysical equipment, and Carlos Montana for his assistance in the computer work. I thank Dr. Niti Mankhemthong, Seth Page, Felix Ziwu, Martin Sandoval, Victor Avilla (Yogi), Alay Gebregiorgis, Raju Sitaula, and Mark Lucero for their assistance during the fieldwork. I also like to thank Sandy Marrufo for providing the gravity data used in this study.

I would like to thank the Department of Geological Sciences, University of Texas at El Paso for providing me teaching assistantship during my study. I, also, would like to thank the staff of the Department of Geological Sciences, the Graduate School, and the Office of International Programs for support and help. My special thanks go to Pam Hart, Head Administrative Assistant and Tina Carrick, former Graduate Coordinator of the Department of Geological Sciences for their tireless supports.

I thank the American Association of Petroleum Geologist's Foundation Grant, the Southwest section of American Association of Petroleum Geologist, the West Texas Geological

Foundation, the Geological Society of America and the Society of Exploration Geophysicist for providing scholarships and travel grants.

I could not go this far without support, patience, understanding, love and care from my dear wife and friend Anita Thapalia. My son, Keidas, has always been blessings and inspiration to my studies. I am deeply indebted to my mother and brother, Tara Budhathoki and Suman Budhathoki, for their love, encouragement and never-ending supports.

Pawan Budhathoki

December, 2013

Abstract

This dissertation consists of two different projects. The first project describes the results of an outcrop based sequence stratigraphic study of the Albian Cox Sandstone in the Indio Mountains of west Texas. The depositional environment of the Cox Sandstone ranges from shallow marine to the coastal plain deposited in four sequences where sequence 1 and sequence 2 consists of transgressive system tracts (TST) followed by highstand system tracts (HST). The highstand system tract (HST) is missing in sequence 3 and the transgressive systems tract is missing in sequence 4. The Cox changes in thickness from 320 m in the northern end of the outcrop belt to 365 m in the southern end. This thickness change is accommodated during transgression where shales drape topography that is actively being shaped by faults and block rotation recorded in exposed growth strata. During Highstand, coarse fluvial-deltaic systems truncate shales on topographic high levelling the topography. Systems tracts and sequences change thickness due to block rotation and erosion as well as deposition from a point source near the center of the outcrop belt. The second project involves the integrated study of gravity and well log data in the northern Hueco bolson. The objective of this study is to demarcate subsurface faults that appear to control the locations of fresh and brackish water. In this study 28 gravity anomalies were identified that correlate with previously mapped (Collins and Raney, 2000) and new faults, and some of them can be extended further south to south east to join with previously mapped faults by Collins and Raney (2000) and Marrufo (2011). Structural cross sections of well logs also suggest that at least some faults are present between them. The four depositional environments inferred from the gamma log responses and their stacking patterns are consistent with the previous interpretation of Doser and Langford (2006) and Marrufo (2011).

Table of Contents

List of Tables

List of Figures

SECTION 1

Outcrop Study of Sequence Stratigraphic Framework and Depositional Environment: the Cox Sandstone of the Chihuahua Trough, the Indio Mountains, Texas, USA

1.1 Abstract

Excellent exposure of the Albian Cox sandstone in the Indio Mountains of west Texas provides outcrop opportunities to study sequence stratigraphic framework of a rift basin margin. The depositional environment of the Cox ranges from shallow marine to the coastal plain deposited in four sequences where sequence 1 and sequence 2 consists of transgressive system tracts (TST) followed by highstand system tracts (HST). The highstand system tract (HST) is missing in sequence 3 and the transgressive systems tract is missing in sequence 4. The Cox changes in thickness from 320 m in the northern end of the outcrop belt to 365 m in the southern end. This thickness change is accommodated during transgression where shales drape topography that is actively being shaped by faults and block rotation recorded in exposed growth strata. During Highstand, coarse fluvial-deltaic systems truncate shales on topographic high levelling the topography. Systems tracts and sequences change thickness due to block rotation and erosion as well as deposition from a point source near the center of the outcrop belt.

1.2 Introduction

This study describes the sedimentary response to complex intrabasinal deformation in exposed Cretaceous rift sediments. We use a sequence stratigraphic approach to document facies distributions and patterns of sedimentation that accommodate faulting and expansion of the section. Many studies of rift deposition describe the alluvial fan and lacustrine fill deposited during the early filling of rift basins. This paper describes a later-stage of rifting, during which transgression has created a narrow sea, which is effected by eustatic as well as tectonic events.

The Cretaceous Border Rift System has been used to describe a Mesozoic extensional terrane with basins that formed along the US-Mexico border between Texas and eastern California (Dickinson & Lawton, 2001). At least the western part of this system records a two-phase deformation history with an unconformity separating Jurassic from Early Cretaceous. These basins are typically deep and narrow. The Chihuahua Trough, the rift basin that forms the focus of this study, contains 5 km of Cretaceous strata (Haenggi, 2001). The Chihuahua trough portion of the rift is bounded by Diablo and Aladama Platforms in the North and South respectively (Haenggi, 2001) (Fig. 1.1). The Indio Mountains, which are located approximately 120 miles southeast of El Paso, expose the northern flank of this extensional basin (Fig. 1.1), and offer exposures that link sedimentation and tectonism.

1.3 Regional Geology

The Chihuahua trough is a NW-SE elongated mid-Mesozoic extensional basin. Though many authors used "Chihuahua trough" for the first time in 1964 (Bridges, 1964; Deford, 1964; Pearson, 1964), their extent of trough was uncertain. Later, Gries and Haenggi (1970) defined the Chihuahua trough as "a relatively narrow, northwest-southeast trending negative feature flanked by the Aldama and Diablo Platforms". More precisely, (Haenggi, 2001, 2002) defined Chihuahua trough as the area of north-eastern Chihuahua and adjacent parts of Texas, New Mexico and Sonora placing north-western limit along the 109th Meridian, and arbitrary southern boundary at the edge of North American craton. Lawton and Mcmillan (1999) and Dickinson and Lawton (2001) introduced the concept of the Border rift system, and included the Sabinas basin, Chihuahua trough, Bisbee basin, and McCoy basin in their Border rift system (Fig. 1.1). However, the absence of Jurassic igneous activity in the Chihuahua trough led Haenggi (2002) and Haenggi and Muehlberger (2005 to treat the Chihuahua trough as a different basin than the coeval Sabinas and Bisbee basins. A recent study from Peryam et al. (2012) also described the Chihuahua trough as a part of the Border rift system.

The Chihuahua trough initiated as a rift basin during the Jurassic (Oxfordian) and extended from the Gulf of Mexico to Southern Arizona along the international border between the United States and Mexico (Haenggi, 2002). The interpretation of tectonic setting of the basin varies widely (Lawton & Mcmillan, 1999) and Dickinson & Lawton, (2001) advocated a back-arc basin setting with Cordilleran slab rollback as a mechanism for basin development. Lawton & McMillan (1999) proposed a three phase tectonic model to explain the borderland rift system: 1) normal subduction; 2) early slab retreat, lithospheric magmatism, and basin formation; and 3) rapid basin subsidence and asthenospheric magmatism. Stern and Dickinson (2010) have described the Gulf of Mexico as a Jurassic back-arc basin, and the Border rift system as intra-arc basin, and related their association with Nazas magmatic arc. Anderson and Nourse (2005) disagreed with the backarc model for the Border rift system, and inferred a sinistral transtensional basin system along the Mojave-Sonora megashear (Anderson & Silver, 1979). They infer that initial sedimentation within the trough was controlled by northwest and east-striking faults, and formed en route to pull-apart basin development at releasing steps along left-lateral faults (Anderson & Nourse, 2005). In contrast, Haenggi and others (Haenggi, 2001, 2002; Haenggi & Muehlberger, 2005) have proposeda dextral transtensional model to explain the evolution of the Chihuahua troughwith the Chihuahua trough forming as a right-lateral pull apart basin during the Oxfordian (159-156 Ma). They related dextral motion to counter clockwise rotation of the North American plate in response to opening of the Atlantic Ocean (Haenggi, 2002; Haenggi & Muehlberger, 2005). Most recently, in describing the Bisbee Basin, Peryam et al. (2012) noted that it, like the Chihuahua trough, exhibits a two-phase deformation and ascribed rifting to the Jurassic phase and a back arc setting to the Middle Cretaceous phase, and noted a prominent lower Cretaceous unconformity. In the Chihuahua Trough portion of the system, Jurassic sediments are largely buried and Neocomian (Early Cretaceous) sediments are not exposed.

The strata exposed in the study area are from the later phase of extension, which began in the Aptian. During the Aptian through the Cenomanian, over 5 km of sediments were deposited

immediately south of the study area. This pattern of deposition came to an end during the Turonian, when increased clastic deposition and the formation of a clastic-dominated basin overlapped the edge of the trough. Mack (1987) described a similar change in deposition that occurred in the Cenomanian in Southern New Mexico to the west of the study area.

During the Laramide orogeny (84 to ~45Ma in this region), the Chihuahua trough was inverted, leading to compression and shortening in the region (Deford, 1958; Henning, 1994; Haenggi, 2002). The Laramide fold belt in Texas and Chihuahua is commonly called the Chihuahua tectonic belt (Deford, 1958; Gries, 1980). Jurassic evaporites of La Casita Formation are thought to form the principal decollement of the Chihuahua tectonic belt above which, the Cretaceous rocks were transported to the Northeast (Haenggi, 2002). Based on the presence of Jurassic salts, several authors advocated evaporite tectonics as the primary control for later Laramide structures. (Haenggi & Gries, 1970; Gries & Haenggi, 1970; Drewes, 1978; Gries, 1980; Dickerson, 1985; Haenggi, 2002).

In the study area several thrust faults exhumed the Aptian through Cenomanian rift fill (Reaser and Underwood, 1980; Underwood, 1980; Carciumaru and Ortega 2008; Page, 2011). Recent restoration of the thrust system indicates that two thrust sheets expose different part of the rift basin (Page, 2011). The lower, thrust sheet was displaced 7 km from the Southwest, and contains a thinner, more basin margin stratigraphy, whereas the upper thrust plate exposes thicker and more distal strata from 18 km to the Southwest (Page, 2011). The area was exhumed during the Paleogene and overlain by Paleogene volcanic rocks but during the Neogene, the Mesozoic strata were re-exhumed along north-northwest trending extensional faults that formed the present-day Indio Mountains. These faults cut across the thrusts and the depositional trends of the Chihuahua trough sediment, exposing both thrust plates. The result of this complex depositional and tectonic history is an outcrop belt that exposes two slices of the Cretaceous Rift fill in panels oblique to the Border Rift margin. This study is a detailed examination of one formation, the Cox Sandstone along one of these panels, showing detailed changes related sedimentation during the Cretaceous rifting.

1.4 General Stratigraphy

The stratigraphy of the Chihuahua trough differs from basin margin to basin center (Cordoba *et al.*, 1970; DeFord & Haenggi, 1971; Haenggi & Gries, 1970). The Mesozoic succession varies in thickness from 200 m in the basin margin (King, 1965; Albritton & Smith, 1965) to 4,700 m in the basin (Haenggi, 2002). Significant facies variations and accompanying lithostratigraphic nomencclature variations occur in association with these thickness variations (Fig. 1.2). The oldest rocks exposed in the Chihuahua trough are the Jurassic La Casita formation. Evaporites deposits (Tithonian-Necomian) in the Chihuahua trough are assigned as "unnamed gypsum" (Spiegelberg, 1961) or "unnamed evaporites sequences" (DeFord and Haenggi, 1970) or "Loma Blanca Formation" (Cordoba *et al.*, 1970). The rocks of the Indio Mountains were deposited toward the basin margin, where (Underwood, 1975) described the Yucca Formation, Bluff Mesa Formation, Cox Sandstone, Finlay Limestone, Benevides Formation, Espy Limestone and Buda Limestone of the Cretaceous (Fig. 1.2).

Interestingly, Kimmeridgian to upper Aptian rocks are absent in the Chihuahua trough margin. The origin of this unconformity has been uncertain by but Peryam *et al.*, (2012) showed that in the Bisbee Basin this interval was an angular unconformity separates the Lower Cretaceous strata from Upper Jurassic rocks (Peryam *et al.*, 2012). If the Bisbee basin and Chihuahua trough are the parts of same Border rift system, these data suggest an unconformity separates Upper Jurassic rock from Lower Cretaceous strata in Chihuahua trough and the Lower Cretaceous assemblage records tectonic events distinct from the Jurassic assemblage of the basin.

1.4.1 COX SANDSTONE

The Cox Sandstone (Campbell, 1959) outcrops in many localities in Trans-Pecos Texas and Mexican region. Richardson (1904) used the term "Cox" for first time in his Finlay Mountains section. Though this unit is easily traced throughout the Chihuahua trough, the lateral variation in lithology and thickness is conspicuous. DeFord and Haenggi (1971) correlated the

lower part of the Cox sandstone with the Glen Rose formation in the upper part of the Trinity Group of Central Texas, and the upper part with the lower part of the Fredericksburg Group.

Deford and Haenggi (1970) also proposed the name Lagrima Formation for the lateral equivalent of the Cox sandstone in Sierra Lagrima or Sierra del Hueso area. The overall thickness of the Lagrima formation in Sierra Lagrima is estimated to be 1,000 to 1,100 m (DeFord and Haenggi, 1970). Haenggi (1966) studied the relationship between Cox sandstone and the Lagrima Formation in El Cuervo area, northeastern Chihuahua, Mexico; and found an abrupt change in lithofacies from predominant sandstone to predominant limestone from the Cox Sandstone to the Lagrima Formation.

The minimum measured thickness of the Cox Sandstone is 51 m (135 ft) in the Kent area (Brand & Deford, 1958), and the maximum is 785 m in El Cuervo area (Haenggi, 1966). Hicks (1997) studied the depositional environments and diagenesis of the Cox Sandstone in the Finlay Mountains area, where he measure 185 m maximum thickness and divided the sandstone into four lithofacies. Several authors, studying ranges south and west of the study area, divided the Cox into upper and lower sandstones, separated by a limestone member (Haenggi, 1966; Deford and Haenggi, 1970; Jones and Reaser, 1970). The upper contact of the Cox with the overlying Finlay Limestone has been described as both gradational and unconformable (Brunson, 1954; Wade, 1954; Albritton and Smith, 1965; Haenggi, 1966; Underwood, 1975). However, as will be described below, the lithologic contact between the formations is an intertonguing contact within a sequence.

Regionally, the Cox Sandstone overlies lithologically varied strata that are known as the Bluff Mesa Formation, Quitman Formation and Campogrande Formation in Trans Pecos Texas, the Beningo Formation in Northern Mexico (Underwood, 1962; Haenggi, 1966; Hicks, 1997). Outside the Border Rift, the Cox unconformably overlies Permian limestone (Mount, 1960; Albritton and Smith 1965). Within the study area, the Cox rests on a well-exposed sequence boundary that separates it from the underlying limestones of the Bluff Mesa Formation.

The Cox and its correlative formations have been ascribed to the middle Albian in age (Underwood, 1962; Albriton and Smith 1965). The initial marine transgression into the Indio Mountains area occurs just below the Bluff Mesa Formation, in the underlying upperYucca Formation. The Bluff Mesa Formation is dominantly a marine deposit, but deposition did not extend beyond the margins of the subsiding Chihuahua Trough/Border Rift (Haenggi, 1966; Cordoba, 1969). The Cox Sandstone and overlying Finlay Limestone mark the initial transgression beyond the margins of the Border Rift as part of a regional transgression (Cheatham, 1984). Although the Cox extends across the Diablo Plateau, it thins from 365 m in the study area to 60 m thick outside the Rift (Albritton and Smith, 1965). Because it thickens within the trough, it is ideal unit to study the effects of tectonism on a unit that extends beyond local fault blocks.

1.5 Methods

A detailed outcrop analysis provided the data to distinguish the facies associations. Facies were interpreted based on lithology, sedimentary structures, texture, bedding, fossils, and trace fossils (Walker, 1984; Bhattacharya & Walker, 1992; Walker & Plint, 1992; Allen & Posamentier, 1994; Kamola & Van Wagoner, 1995; Yoshida, 2000; Pemberton, 1992). Sections were measured along the footwall of the Indio Normal fault that exhumes the lower thrust plate (Fig. 1.3). Environments were inferred from facies associations that together provided information about processes and fauna. The outcrops were correlated through walking of contacts as well as the use of high-resolution photographs from Google Earth and the U.S. National Map. These images also provided sections of facies geometries and how thickness changes were accommodated between sections, including recognition of growth-strata relationships.

The sequence stratigraphic model of the Cox sandstone is based on correlation of 8 closely spaced (0.5 km to 1 km) measured outcrop sections with a cumulative 1465m thickness (Fig.1.3). In this study, we basically considered stacking trends and patterns, stratal geometries,

chronostratigraphic surfaces and substrate controlled ichnofacies to delineate the sequence stratigraphic surfaces, system tracts and stratigraphic sequences (Posamentier & Vail, 1988; Van Wagoner *et al.*, 1988, 1990; Taylor & Lovell, 1995; Kamola & Van Wagoner, 1995; O'Byrne & Flint, 1996; Catuneanu, 2002; Catuneanu *et al.*, 2009).

1.6 Facies Associations and Depositional Environments

Six facies associations were inferred from the Cox Sandstone strata in the Indio Mountains (Table 1). We considered lithology, sedimentary structures, nature of bedding contacts, and distribution of bioturbation to describe the facies associations. These facies associations are used as a guide to aid in the synthesis of a sequence stratigraphic framework of the Cox Sandstone.

1.6.1 FA1: MASSIVE MUDSTONE, LIMESTONE, AND CURRENT AND WAVE RIPPLE FACIES ASSOCIATION

Description

This facies association predominantly consists of greenish gray to purple shale intercalated with subordinate amount of very thin bedded greenish gray siltstone (Fig. 1.4A). Thin beds (10-20 cm) of very fine grained rippled sandstone occur sporadically throughout this facies (Fig. 1.4B). The mud facies is soft and mostly covered. Where it is exposed, the thickness of individual units varies from few meters to ten's of meters (Fig. 1.4A). The massive mudstones lack obvious burrows and primary sedimentary structures, while very fine grained sandstones encapsulated in the mudstones show intense bioturbation, suggesting the mudstones are also bioturbated. Thin limestone beds (10 -50 cm thick) are encased in the mudstone facies, but are rarely exposed, typically being covered. A single fossiliferous limestone was found at about 14 m above the base of one interval of this facies that contains turitella and several benthic foraminifera (Fig. 1.4C). The upper two-thirds of the limestone consist of about 4m thick, bluish gray fossiliferous limestone which crops out throughout the Indio Mountains region (Figs 1.4D and 1.4E). Due to poor preservation species could not be identified. Mount (1960) reported

fragments of Exogyra sp. in similar intervals and Underwood (1975) found *Exogyra texana*, Gryphea *washitaensis*, *Toucasia* sp.

Interpretation

The thick mudstone intervals with very fine grained sandstone and siltstone, parallel lamination, and current and wave ripples, and marine fossils support an interpretation of an inner shelf environment. The presence of fossil assemblages described above indicates an open marine environment. Albritton & Smith (1965) also noted the similar marine gastropods and pelecypods fossils in all sections in the northern part of Quitman Mountains and in upper part of the southern Quitman Mountains. The deposition of mudstone indicates long period of quiescent environment (Howard & Reineck, 1981).

1.6.2 FA 2: HUMMOCKY CROSS STRATIFIED SANDSTONE AND LAMINATED SANDSTONE FACIES ASSOCIATION

This facies association mostly consists of fine grained, well sorted, white sandstone with hummocky cross stratification (HCS), parallel sub-horizontal lamination, and wave ripples (Figs 1.5A, B and C). Individual sandstone beds range from few centimetre to a meter or two with general coarsening upward trend. Sandstone beds include scattered very thin beds of greenish gray siltstone. Scattered pebbles and granules, mud chip clasts are common at the base and/or within the facies. *Planolite, Paleophycus, Arenicolite, Diplocaterion, Thalassinoides* are common trace fossils found in this association (Fig. 1.5D).

Interpretation

The existence of Hummocky Cross Stratification indicates storm-waves in an environment that is normally below fair-weather wave base (Walker, 1984). The presence of laminated sandstone signifies the influence of wave working in storm conditions (Howard and Reineck, 1981). Thin wave-rippled beds in the lower part of the facies indicate oscillatory currents (Fig. 1.5C). Scattered pebbles and granules in the fine grained sandstone are interpreted as having moved onto the lower shoreface during the storm and left behind as a post-storm lag (Clifton, 2006). The occurrence of *Cruziana* Ichnofacies (Fig. 1.5D) suggests a shallow marine

environment. This facies association is influenced by storm-wave processes generated between above wave base and below fair-weather wave base and interpreted lower shoreface (Galloway & Hobday, 1996; Hampson, 2000). In contrast to the shale facies, the abundance of sandstones indicates regular shallower water and higher energy.

1.6.3 FA 3: TROUGH CROSS BEDDED, TABULAR PLANAR, BIOTURBATED SANDSTONE AND PLANAR LAMINATED SANDSTONE FACIES ASSOCIATION

Description

This facies is composed of generally well-exposed, cliff and ledge-forming sandstones consisting of fine- to medium-grained, well-sorted, and white to gray sandstone. The top part of this succession has a spectacular black and white (salt and pepper) appearance in weathered outcrop but it is white with red patches on fresh faces. The sedimentary structures include trough cross beds, sub-horizontal lamination (Figs 1.6A and B). Low angle cross strata are also common in this association. Individual cross beds are 25 cm to 1-m-thick. Fine to medium grained, cross bedded sandstone beds consists of mud chip rip up clasts. Individual sandstone beds show coarsening up to no change in grain size. In general, troughs are present in the middle of the beds. Soft sedimentation deformation features are commonly found in all the sections (Fig. 1.6C). The sandstone beds often exhibit the internal scour with mud chips conglomerate. The top of the sandstone bed is bioturbated. Vertical (*Skolithos*) and U shaped (*Diplocraterion* and *Arenicolite*) *Skolithos* ichnofacies are common and easily identified based on their shape and orientation (Fig. 1.6D).

Interpretation

This facies association in interpreted to deposited in upper shoreface to foreshore environment. Well sorted tabular and cross bedded sandstones with coarsening up to constant grain size associated with *Skolithos, Arenicolite* and *Diplocraterion* are interpreted to be in shoreface environment. Constant grain size implies that sediments were deposited aggadationally. Very low angle cross beds, and low dipping planar beds with rare *Skolithos* trace

fossils are interpreted to be in foreshore environment. Generally, trough cross beds, and low angle cross beds and sub horizontal planar beds occur together.

1.6.4 FA 4: CONGLOMERATIC SANDSTONE, TROUGH CROSS STRATIFIED SANDSTONE, PLANAR LAMINATED SANDSTONE AND QUARTZ SANDSTONES FACIES ASSOCIATION

Description

This facies association mostly consists of medium to very coarse grained sandstones with scattered pebble and gravel at the base (Fig. 1.7A). Conglomerate consists of few mm to 15 mm, sub-angular to sub-rounded chert and limestone clasts which grade upward into medium grained sandstone. The tops of some medium grained sandstone beds are bioturbated with *Skolithos* ichnofacies. In addition to the trough cross strata, current ripple laminations are found in fine grained sandstone (Fig. 1.7B). Syndepositional deformation structures are abundant in this association. Mount (1960) and Underwood (1962) also noticed conglomerate beds in the Cox Formation; however they did not mention the bioturbation in this facies. Channel-fills units occur as isolated single-storey bodies and in some places, are stacked into amalgamated multistory bodies (Fig. 1.7C). Their thickness ranges from 1 m as an isolated body to 9-15 m as multistory amalgamated bodies. Lateral accretion bed sets are commonly observed in this facies association (Fig. 1.7D).

Interpretation

Based on lithology, channel geometry, and sedimentary structures, this facies association is interpreted as deposits of meandering and braided fluvial systems. Medium- to fine-grained, isolated channels are interpreted as a meandering river deposit (Fig. 1.5D). In contrast, pebble conglomerate bearing very-coarse-grained to coarse-grained, laterally and vertically amalgamated channels are interpreted as braided river deposits. Notably, braided channel deposits are more common in the North. In some places, meandering and braided channels are so similar in outcrop appearance that they are hard to distinguish away from the sections. Also, many outcrops are indefinite in terms of braided and meandering. Due to the limited identification, we grouped these two channel system together in our description. The presence of

ripple laminated sandstone and the *Skolithos* ichnofacies suggests that the coastal environment was prevalent. At least some, generally more southern exposures of this facies were probably deposited in channels within a tidal delta.

1.6.5 FA 5: RIPPLE LAMINATED WHITE TO LIGHT GRAY SANDSTONE, INTERBEDDED SANDSTONE AND MUDSTONE FACIES ASSOCIATION

Description

This facies association is characterized by fine- to very fine-grained sandstone. Lenticular beds (20cm to 2.5 m thick cm), of internally scoured, trough cross-stratified, sandstone are common. Within individual cross sets, strata may alternate between coarse and fine grained on a 1-20 cm scale (Fig. 1.8A). The top of this facies association is marked with the spindle shaped cracks (Fig. 1.8B). Individual cracks ranges from 5 cm to 14 cm in length and tapers at both ends. This facies association also contains beds 20 cm thick, laminated, very fine grained, light gray sandstone that contains flaser and lenticular mud drapes. Generally, this mud draped sandstone unit is 1.5 to 3-m-thick, and overlain by thin beds of 0.4 to 0.7-m-thick green siltstone containing wave-ripple cross strata highlighted by diagenetic cementation (Fig. 1.8B).

Interpretation

Overall, this facies association is interpreted to be deposited in an intertidal environment. Lenticular shape, internal scour, trough cross bed, fining up sequence are evidence of channel deposition. The lenses of fine grained sandstone and alternative fine and coarse grained sandstone suggests the rapid change in environment from high energy to low energy. The lenticular and flaser bedding likewise indicate energy alternations (Reineck &Singh, 1980; Smith, 1988; Shanley et. al., 1992). The internal scours are interpreted as reactivation surfaces. The cracks are either synaeresis cracks or distorted desiccation cracks. The irregular bedding suggests deposition in a sandy tidal environment with numerous bars. The interdistributary part of a tidal delta is the most likely setting.

1.6.6 FA 6: VARIEGATED MUD AND FINE GRAINED SANDSTONE FACIES ASSOCIATION

Description

FA 6 is composed of interbedded mudstone and thin bedded fine to very fine grained sandstone and siltstone (Fig. 1.9A). Irregular "potato shaped" carbonate nodules up to 2-cm-long are common with in many of the mudstones (Fig. 1.9B). Shale thickness varies from few cm to a meter, while siltstone is 5-15 cm thick. Due to poor exposure of the shale beds, it is hard to find any root traces or wood fragments; however, scattered petrified wood was found in the top of the section. Organic matter is rarely preserved in this facies.

The variegated purple, ochre, red and orange colours of this unit are notable. It is often difficult to identify this unit due to poor exposure and it is often difficult to separate it from the marine shales in FA1.

Interpretation

This unit is interpreted flood plain deposits associated with the fluvial/deltaic channels. The variegated colours indicate changing conditions of oxidation. The carbonate nodules are not typical soil carbonates, but probably represent near water table growth of nodules. The lack of bedding in many shales may be due to soil bioturbation. The petrified wood was probably deposited during flood events. Due to poor exposure, this facies is the most difficult to identify in the field and has the fewest definite environmental clues.

1.7 Sequence Stratigraphic Framework

Study has shown that sequence stratigraphies in rift basins (Hubbard, 1988; Howell & Flint, 1996; Catuneanu, 2010; Martins-Neto & Catuneanu, 2010) differ from the classic passive margin setting (Mitchum et al., 1977; Posamentier and Vail, 1988; Posamentier et al., 1988; Van Wagoner et al., 1988; Van Wagoner et al., 1990; Mitchum and Van Wagoner, 1991; Posamentier et al., 1992; Posamentier & Allen, 1993 and Posamentier and Allen, 1999). In this section, the high-resolution sequence stratigraphic framework of Albian Cox Sandstone is interpreted from

eight closely spaced measured outcrops (Figs 1.3 and 1.10). The most representative section is shown in detail in Fig. 1.11.

1.7.1 SEQUENCE 1

A well-defined, continuous transgressive lag of large fossil fragments separates the Cox Sandstone from underlying Bluff Mesa Formation (Fig. 1.12 A). The fossils and clast composition varies from south to north. In the southern part, transgressive lag is highly fossiliferous with white and black chert pebbles (Fig. 1.12 B), while the northern part is less fossiliferous and contains iron nodules (Fig. 1.12 C). We interpreted this as a transgressive lag overlying sequence boundary (SB1). Beneath the sequence boundary are fossiliferous wackestones of the Bluff Mesa Formation. Above the transgressive lag are marine shales and tidal flat sandstones in the lower Cox Sandstone. An upward fining, retrogradational Transgressive System Tract (TST1) overlies the SB1. TST1 consists of fossiliferous limestone encased in a shale and current and wave rippled laminated fine grained sandstone of FA1 and tidal channel sandstone of FA5. Figure 1.12D shows the small channel fill sandstone directly overlying the lag deposit. This is interpreted to represent the transgressive and lowstand fill of a valley incised into SB1. In section CS1 (Fig. 1.3), tidal channel pinch out to the North. In the northern part of the outcrop belt, between sections CS 4 and CS5, channel fill sandstone directly overlies the lag deposit (Figs 1.3 and 1.12D). The tidal flat facies grades laterally and upward into shelf and lower shoreface deposits indicating transgression during deposition. The basal interval of TST1 can be observed to thin against the sequence boundary at the base of the Cox, at its contact with the Bluff Mesa Formation (Fig. 1.13).

A poorly exposed Maximum Flooding Surface (MFS1) separates TST1 from the overlying aggradational to progradational Highstand System Tract (HST1). This maximum flooding surface is within a thick shale that separates the upward fining TST 1 interval from the upward Coarsening HST 1. The condensed section in Sequence 1 is recognized by the presence

of highly bioturbated bed with abundant Thallasinoides and Skolithos trace fossils, similar to that identified by Taylor and Gawthorpe (1993) in the Lower-Middle Jurassic Halten Terrace.

Overlying the TST is a Highstand composed of channel and coastal plain deposits of facies associations FA4 and FA 6. The HST1 is thicker in the northern part where channelized sandstone bodies are thicker and more abundant (Fig. 1.10). Just north of CS 1, stratal truncations are apparent at the top of sequence 1 and the beds are observed to pinch out against the sequence boundary (SB2) (Fig. 1.13). The cliff exposure makes it difficult to take measurements related to strata truncations; however, high resolution satellite imagery clearly depicts the relationship between sequence boundary and onlapping of strata (Fig. 1.13). Overall, this sequence thickens to the south.

1.7.2 SEQUENCE 2

A flooding surface marks the change from coastal plain and channel deposit of sequence 1to shoreface deposit of transgressive system tract (TST2) (Fig. 1.10). This surface can be recognized by the abrupt change from fluvial sandstones to marine mudstones, that forms a subtle bench along the ourcrop belt. TST2 constitutes inner shelf mudstone and lower to upper shoreface sediments of facies associations FA1, FA 2 and FA3; however, foreshore sediments were not observed in this system tract. Interestingly, shale thickness changes from 6 m in north to 46m in south across 500 m of outcrop. A glossifungites ichnofacies containing *Thalassinoides*, *Diplocratarion, Arenicolite* and *Skolithos* in fine grained sandstone bed is interpreted to mark the maximum flooding surface (Fig. 1.14) (Pemberton, 1992). The overlying progradational highstand system tract (HST2) contains upper shoreface, foreshore and channel fill sandstone that increase in percentage of fluvial strata upward (facies associations FA 3 and FA4). This sequence thickens towards the basin as in south of Fig. 1.10. Martins-Neto & Catuneanu (2010) suggested that rapid creation of accomodation leads to transgression, which is marked by flooding surface as seen in sequence 2.. In the northern part of the outcrop belt (Fig.

1.10), the base of sequence 2 (SB2) appears to mark by channelization. However, we did not observe erosional truncation associated with SB2.

1.7.3 SEQUENCE 3

A well-defined transition from foreshore and channel deposits of HST2 to lower shoreface deposits marks the base of sequence 3. Sequence boundary (SB 3) is placed in the marine flooding surface that overlies the highstand system tract of sequence 2. The transgressive system tract (TST3) passes upward from trough cross bedded upper shoreface, to hummocky cross–stratified lower shoreface and finally, to massive mudstone and fossiliferous limestone of the offshore shelf environment. There is a sharp change in environment from offshore carbonate grainstones of TST3 to the coastal plain and fluvial deposit of sequence 4. Here, the Maximum Flooding Surface (MSF3) is coincident with the sequence boundary (SB4) (Figs. 1.10 and 1.15). The shales within the sequence thicken and coalesce to the South (Fig. 1.10).

1.7.4 SEQUENCE 4

The top of sequence 3 is easily observed in all places in the Indio Mountains because of the continuous exposure of a thin cliff-forming carbonate grainstone below the less resistant fluvial and coastal plain deposit (Figs 1.10 and 1.15). This sharp basinward shift in facies was traced for several kilometers (Fig. 1.10), and interpreted as a sequence boundary (SB4). The sequence boundary overlies the carbonate grainstone at the top of Sequence 3. This sharp contact is not erosional, as the limestone is present throughout the outcrop belt, but the sudden shift from marine to the nonmarine sandstones and shales in Sequence 4 indicates a sequence boundary. The uppermost parts of the Cox Sandstone constitute Highstand System Tract (HST 4) of sequence 4, which is generally coarser than the underlying transgressive and highstand system tracts. In this sequence, the Transgressive System Tract is either very thin or missing. Facies associations FA4, FA5 and FA 6 are associated with HST 4, which is dominated by fluvial and coastal channels and associated floodplain mudstones. A small channel containing highly fossiliferous alternations sandstone and carbonate was observed to rest on tidal flat sandstone in

section CS 2 (Figs 1.16 A and B) and is believed represent a fill of an incised valley marking SB 5 at the top of the Cox (Fig. 1.16A). A transgressive limestone that marks the intertonguing transition into the overlying Finlay Limestone rests on the top of sequence 4, and overlies SB 5 at the upper boundary of the Cox interval (Fig. 1.16A).

1.8 Discussion and Interpretation

The excellent exposure of shallow marine to coastal deposits of the Cox Sandstone in the Indio Mountains provides outcrop opportunity to study sequence stratigraphic framework of a rift basin margin. The Cox provides an outcrop analogue to compare depositional environments and architecture to similar rift settings elsewhere.

In the Indio Mountains, the Cox Sandstone comprises four sequences. Three major differences distinguish the rift-basin sequences from the classic sequence stratigraphic models. 1) Sequences comprise transgressive and highstands systems tracts, lowstands are absent. 2) Syntectonic deformation is evident within the Cox, thickening is accommodated within the transgressive systems tracts. 3) Facies associations, reflecting depositional environments are confined to restricted areas and abrupt changes are common, particularly within transgressive systems tracts.

It is well established that transgressive system tracts form when accommodation space outpaces the sediment supply; and when sedimentation outpaces the accommodation space, highstand system tracts form. In rift systems, transgressive and highstand system tracts have been interpreted to represent pulses of tectonic subsidence and tectonic quiescence respectively (Martins-Neto and Catuneanu, 2010). Within the Cox Sandstone, the lowstand system tract is absent, which is a typical characteristic of rift basins (Folkestad and Satur, 2008 and Martins-Neto and Catuneanu, 2010). The absence of low stand tract suggests tectonically driven subsidence rate was rapid enough to outpace eustatic sea level falls in extensional basin. (Posamentier & Allen, 1993; Gawthorpe et al., 1994; Martins-Neto and Catuneanu, 2010). The similar stratigraphic architecture has been observed in the Nukhul Formation of Suez Rift, Egypt

(Jackson el al., 2005). An alternative explanation in the case of this study is that the Rift-flank location preserved shelf transgressions and highstands and that lowstands, if they are preserved, are found within the deeper parts of the rift that remained below sea-level when sequence boundaries were being cut in the study area. This explanation is preferred because the highstands are thick and truncate rotated blocks of the underlying TSTs, which would be not expected with high accommodation.

The second difference shaped by active rifting is the dramatic thickness changes within systems tracts along the outcrop belt, which is oriented oblique to the basin margin, with the south end farther from the edge of the rift. The most dramatic thickening is within Sequence 1, where the Highstand onlaps rotated transgressive shales of TST1. The upper beds in TST1 are rotated and truncated by erosion at the base of the HST1 (Fig. 1.13). Because, this angular unconformity is not regional and is located in the area of syndepositional normal faults, it is interpreted to be the result of block rotation during normal faulting. Between sequences 1 and 2, it is difficult to distinguish whether the pinching out of the strata against the sequence boundary (SB2) is due to rotation of sequence 1, or to filling of a paleovalley in the southern half of the outcrop.

Over most of the outcrop area, there is little gross change in thickness between the base of the Cox, on SB1 and the transgressive limestone above SB4 (Fig. 1.11). However, individual sequences thicken and thin dramatically. The lower two transgressive system tracts thicken to the south, whereas highstands thicken to the north. This could be confused with a facies change from sands to the north, to shales in the south, however, beds, particularly the burrowed MFS bed, can be correlated from section to section. This along with the angular unconformity in the southern part of the outcrop (Fig 1.13), indicates that tectonism and erosion caused the observed changes in thickness. However, there is a change from continental to coastal environments to the south within several of the highstands.

The truncation of transgressive systems tracts, erosion of paleovalleys at sequence boundaries during lowstands, and the complex fill resulting from a point source and along-axis deposition result in complex thinning and thickening of sequences.

The final difference between sequences is the abrupt lateral transitions between environments along strike. These are most evident in highstands HST 1 and HST 4. In these units, the 30 to 50 m thick intervals are fluvial in the center and tidally influenced coastal deposits 3 km away to the north and south. This argues for a point source of fluvial sediment near the center of the outcrop belt.

The interplay between accommodation space and sediment supply has been reported to be the key factor for sequence stratigraphic architecture (Coe et al., 2003). In passive margin settings, accommodation is mainly controlled by eustatic fluctuations in sea level (Posamentier & Vail, 1988; Plint, 1991; Nichol et al., 1996) and tectonism coupled with climate, source areas and base level change (Catuneanu, 2002). Previous research has shown that sequence stratigraphic architecture for extensional basins may differ from the classic sequence stratigraphic models proposed for passive margins (Hubbard, 1988; Howell & Flint, 1996; Bosence, 1998; Folkestad & Satur, 2008; Martins-Neto & Catuneanu, 2010). In rift basins, accommodation space, local changes in relative sea level, and sediment supply can affect the stratigraphic cyclicity, whereas tectonic subsidence is the dominant factor for controlling accommodation (Jackson et. al, 2005; Ranvas and Steel, 1998; Martins-Neto and Catuneanu, 2010) and variation in basin topography (Howell and Flint, 1996). Rifts are less effected by eustatic fluctuations (Martins-Neto & Catuneanu , 2010), and hence have different stratigraphic architecture, stratal geometries and facies stacking patterns (Jackson et. al, 2005; Martins-Neto & Catuneanu , 2010).

In this study, eustacy is apparent and creastes four correlable sequences. However, a point supply of sediment and tectonism result in thckening and thinning of the intervals along with internal unconformitites.

1.9 Conclusions

The Albian Cox Sandstone of the Chihuahua trough, Indio Mountains, SW Texas, consists of six facies associations. Detailed outcrop facies analysis reveals four high frequency sequences. The sequence stratigraphic architecture of the Cox Sandstone is dominated by TST and HST though HST of sequence 3 and TST of sequence 4 are missing. In most of the sequences, the Transgressive systems tracts, and particularly the shales, thicken to the south. This is due to the rotation of beds to the south and west. Rotation of beds creates accommodation space, which is later filled by shale during the subsequent rise in sea level.

1.10 Acknowledgments

The Authors would like to thank Seth Page, Niti Mankhemthong, and Raju Sitaula for their assistant during field work. This research was supported by American Association of Petroleum Geologist (AAPG) foundation Grants-in-Aid fund. Pawan Budhathoki was 2010 Grants-in-Aid Recipient. We also gratefully acknowledge the logistical support of the Indio Mountains Research Station operated by the University of Texas at El Paso and its director, Dr. Jerry Johnson.

References

Albritton, C. C. Jr. and **Smith, J.F. Jr.** (1965) Geology of the Sierra Blanca area, Hudspeth County, Texas. *US Geol. Surv. Prof. Pap.*, **479**, 131pp.

Allen, G.P. and **Posamentier, H.W.** (*1994*) Transgressive facies and sequence architecture in mixed tide- and wave-dominated incised valleys: example from the Gironde Estuary, France. In*: Incised Valley Systems: Origin and Sedimentary Sequences* (Eds R.W.Dalrymple*,* R.Boyd and B.A.Zaitlin*), SEPM Spec. Publ.,* **51***,* 225–240.

Anderson, T. H. and **Silver, L.T.** (1979) The role of the Mojave-Sonora megashear in the evolution of northern Sonora. In: *Geology of northern Sonora* (Eds T.H. Anderson, and J. Roldán-Quintana), *Geol. Soc. Am. Fieldguide* , **27**, 59–6.

Anderson, T.H. and **Nourse, J.A.** (2005) Pull-apart basins at releasing bends of the sinistral Late Jurassic Mojave-Sonora fault system. *Geol. Soc. Am. Spec. Pap.*, pp. 97–122.

Bhattacharya, J.P. and **Walker, R.G.** (1992) Deltas. In:*Facies Models: Response to Sea-Level Change* (Eds R.G. Walker and N.P. James), Geol. Assoc. Can., pp. 157–177.

Bosence, D.W.J. (1998) Stratigraphic and sedimentologicalmodels of riftbasins. In: *Sedimentological evolution of the Red Sea-Gulf of Aden Basin* (Eds B.H. Purser, D.W.J. Bosence), pp. 9–15, Chapman and Hall, London.

Brand, J. P. and **DeFord, R. K.** (1958) Comanchean stratigraphy of Kent quadrangle, Trans-Pecos Texas. *AAPG Bull*., **42**, 371-386.

Brunson, W.E. (1954) Type Sections of Cox and Finlay Formations, Hudspeth County, Trans-Pecos Texas. University of Texas, Austin, 216 pp.

Bridges, L.W. (1964) Stratigraphy of Mina Plomosas-Placer de Guadalupe area. In: *Geology of Mina Plomosas-Placer de Guadalupe area, Chihuahua, Mexico*, West Texas Geol. Soc. Field Trip Guidebook, **64-50**, 50-59.

Campbell, R. A. (1959) Stratigraphy of Borrachera anticline, municipio de Ojinaga, Chihuahua, Mexico. University of Texas, Austin, 78 pp.

Carciumaru, D. and **Roberto, O.** (2008) Geologic structure of the northern margin of the Chihuahua trough: Evidence for controlled deformation during Laramide Orogeny. *Boletín de la Sociedad Geológica Mexicana*, **60**, 43–69.

Catuneanu, O. (2002) Sequence stratigraphy of clastic systems: concepts, merits, and pitfalls. *J. Afr. Earth Sci.*, **35**, 1–43.

Catuneanu, O., Abreu, V., Bhattacharya, J.P., Blum, M.D., Dalrymple, R.W., Eriksson, P.G., Fielding, C.R., Fisher, W.L., Galloway, W.E., Gibling, M.R., Giles, K.A., Holbrook, J.M., Jordan, R., Kendall, C.G.S.C., Macurda, B., Martinsen, O.J., Miall, A.D., Neal, J.E., Nummedal, D., Pomar, L., Posamentier, H.W., Pratt, B.R., Sarg, J.F., Shanley, K.W., Steel, R.J., Strasser, A., Tucker, M.E. and **Winker, C.** (2009) Towards the standardization of sequence stratigraphy. *Earth-Sci. Rev.,* **92***,* 1–33.

Cheatham, T. L. (1984). Paleoenvironments of late Albian stage (early Cretaceous) of eastern Trans-Pecos, Texas. *AAPG Bull.*, **68**, 461 (CONF-8405216).

Clifton, H.E. (2006) A re-examination of facies models for clastic shorelines. In: *Facies Models Revisited* (Eds H.W. Posamentier and R.G. Walker)*, SEPM Spec. Publ.,* **84***,* 293–337.

Coe, A., Bosence, D., Church, K., Flint, S., Howell, J. *and* ***Wilson, C.*** *(2003) The Sedimentary Record of Sea-level Change. The Open University, Milton Keynes, 285 pp.*

Cordoba, D.A. (1969) Mesozoic Stratigraphy of Northwestern Chihuahua Mexico. In: *Guidebook of the border region* (Eds. Cordoba, D. A., Wengerd, S. A., and Shomaker, J), *New Mexico Geol. Soc.*, 20th Field Conference, 91-96.

Cordoba, D.A., Rodriguez –Torres, R. and Guerrero-Garcia, J. (1970) Mesozoic Stratigraphy of the northern portion of the Chihuahua trough. In: *The Geologic Framework of the Chihuahua Tectonic Belt* (Eds Seewald K. and Sundeen D.), *West Texas Geol. Soc. Publ.,* **71-59**, 83-98.

DeFord, R.K. (1958) Cretaceous platform and geosyncline, Culbertson and Hudspeth counties, Texas: Van Horn, Texas. In: *SEPM, Permian Section, Guidebook 1958 Field Trip*, **58-4**.

Deford, R.K. (1964) History of geological exploration in Chihuahua. In: *Geology of Mina Plomosas-Placer de Guadalupe area, Chihuahua, Mexico*. *West Texas Geol. Soc*. Field Trip

DeFord, R.K. and **Haenggi, W.T.** (1971) Stratigraphic nomenclature of Cretaceous rocks in northeastern Chihuahua. In: *The Geologic Framework of the Chihuahua Tectonic Belt* (Eds Seewald K. and Sundeen D.), *West Texas Geol. Soc. Publ.,* **71-59**, 175-196.

Dickerson, P.W. (1985) Evidence for Late Cretaceous-early Tertiary transpression in Trans Pecos Texas and adjacent Mexico. In: *Structure and Tectonics of Trans-Pecos Texas* (Eds P.W. Dickerson, and W.R. Muehlberger), *West Texas Geol. Soc. Publ.*, **85-81**, 185–194.

Dickinson, W.R. and **Lawton, T.F.** (2001) Tectonic setting and sandstone petrofacies of the Bisbee basin (USA–Mexico). *J. S. Am. Earth Sci*., **14**, 475–504.

Drewes, H. (1978) The Cordilleran orogenic belt between Nevada and Chihuahua. *Geol. Soc. Am. Bull.*, **89**, 641–657.

Folkestad, A. and Satur, N. (2008) Regressive and transgressive cycles in a rift-basin: Depositional model and sedimentary partitioning of the Middle Jurassic Hugin Formation, Southern Viking Graben, North Sea. *Sed. Geol.*, **207**, 1-21.

Galloway, W. E. and **Hobday, D.K.** (1996). *Terrigenous clastic depositional systems* (*2nd Ed.*). Heidelberg, Springer-Verlag, 489pp.

Gawthorpe, R.L., Collier, R.E.L. and **Fraser, A.J.** (1994) Sequence stratigraphy in active extensional basins: implications for the interpretation of ancient basin fills. *Marine and Petrol. Geol.,* **11**, 642–658.

Gries, J.C. and **Haenggi, W.T.** (1970) Structural evolution of the eastern Chihuahua Tectonic Belt. In: *The geologic framework of the Chihuahua Tectonic Belt* (Eds K. Seewald and D. Sundeen), *West Texas Geol. Soc. Publ.*,**70-12**, 119–137.

Gries, J.C. (1980) Laramide evaporate tectonics along the Texas-northern Chihuahua Border. In: *New Mexico Geol. Soc. Guidebook 31st Field Conference, Trans-Pecos Region*, 93-100.

Gries, J.C. and **Haenggi, W.T.** (1970) Structural evolution of the eastern Chihuahua Tectonic Belt. In: *The geologic framework of the Chihuahua Tectonic Belt* (Eds K. Seewald and D. Sundeen), *West Texas Geol. Soc. Publ.*,**70-12**, 119–137.

Haenggi, W.T. (1966) Geology of El Cuervo area, northeastern Chihuahua, Mexico. University of Texas, Austin, 403 pp.

Haenggi, W.T. and **Gries, J.C.** (1970) Structural evolution of northeastern Chihuahua Tectonic Belt. In: *The geologic framework of the Chihuahua Tectonic Belt* (Eds. K. Seewald and D. Sundeen), *West Texas Geol. Soc. Publ.*, **70-12**, 55–69.

Haenggi, W. (2001) Tectonic history of the Chihuahua trough, Mexico and adjacent USA, Part I: the pre-Mesozoic setting. *Boletínde la Sociedad Geológica Mexicana*, **Tomo LIV**, 28–66.

Haenggi, W. (2002) Tectonic history of the Chihuahua trough, Mexico and adjacent USA, Part II: Mesozoic and Cenozoic. *Boletínde la Sociedad Geológica Mexicana*, **Tomo LV**, 38–94.

Haenggi, W.T. and **Muehlberger, W.R.** (2005) Chihuahua trough - A Jurassic pull-apart basin. *Geol. Soc. Am. Spec. Pap.*, **393**, 619–630.

Hennings, P.H. (1994) Structural transect of the southern Chihuahua Fold Belt between Ojinaga and Aldama, Chihuahua, Mexico. *Tectonics*, **13**, 1445-1460.

Hampson, G.J. (2000) Discontinuity surfaces, clinoforms, and facies architecture in a wave-dominated, shoreface-shelf parasequence. *J. Sed. Res.,* **70***,* 325–340.

Howard, J.D. and **Reineck, H.E.** (1981) Depositional facies of high-energy beach-to-offshore sequence, comparison with low energy sequence. *AAPG Bull.*, **65**, 807–830.

Howell, J. A. and **Flint, S.S.** (1996) A model for high resolution sequence stratigraphy within extensional basin. In: *High Resolution Sequence Stratigraphy: Innovations and Applications* (Eds J.A. Howell and J.F. Aitken), *Geol. Soc. London Spec. Publ.,* **104***,* 129-137.

Hubbard, R. J. (1988) Age and significance of sequence boundaries on Jurassic and early Cretaceous rifted continental margins. *AAPG Bull.,* **72**, 49-72.

Jackson, C. A. L., Gawthorpe, R. L., Carr, I. D. and. **Sharp, I . R.** (2005) Normal faulting as a control on the stratigraphic development of shallow marine syn-rift sequences: the Nukhul and Lower Rudeis Formations, Hammam Faraun fault block, Suez Rift, Egypt. *Sedimentology*, **52**, 313-318.

Jones, B.R., and **Reaser, D.F.** (1970) Geology of southern Quitman Mountains, Hudspeth County, Texas. *Bur. Econ. Geol. Univ. Tex. Austin Rep*. Geologic Quadrangle Map No. 39.

Kamola, D.L. and **Van Wagoner, J.C.** (1995) Stratigraphy and facies architecture of parasequences with examples from the Spring Canyon Member, Blackhawk Formation, Utah. In: *Sequence Stratigraphy of Foreland Basin Deposits – Outcrop and Subsurface Examples from the Cretaceous of North America* (Eds. J.C. Van Wagoner and G.T. Bertram), *AAPG Mem.*, **64**, 27-54.

King, P.B. (1965) Geology of the Sierra Diablo region, Texas. *US Geol. Surv. Prof. Pap.*, **480**, 185pp.

Lawton, T.F. and **Mcmillan, N.J.** (1999) Arc abandonment as a cause for passive continental rifting : Comparison of the Jurassic Mexican Borderland rift and the Cenozoic Rio Grande rift. *Geology,* **27**, 779–782.

Mack, G.H. (1987) Mid-Cretaceous (late Albian) change from rift to retroarc foreland basin in southwestern New Mexico. *Geol. Soc. Am. Bull.*, **98**, 507–514.

Martins-Neto, M.A. and **Catuneanu, O.** (2010) Rift sequence stratigraphy. *Marine and Petroleum Geology*, **27**, 247–253.

Mitchum, R.M.Jr*,* **Vail, P.R.** and **Thompson, S.** (1977) Seismic stratigraphy and global changes of sea-level, part 2: the depositional sequence as a basic unit for stratigraphic analysis. In: *Seismic Stratigraphy - Applications to Hydrocarbon Exploration* (Ed. by C. E.Payton), *AAPG Mem.,* **26***,* 53–62.

Mitchum, R.M., Jr and **Van Wagoner, J.C.** (1991) High frequency sequences and their stacking patterns: sequence stratigraphic evidence of high-frequency eustatic cycles. *Sediment. Geol.,* **70***,* 131–160.

Mount, J.R. (1960) A petrofabric analysis of the Cox Sandstone, Hudspeth County, M.S. Thesis Texas. Texas Technological College, Lubbock Texas, 67 pp.

O'Byrne, C.J. and **Flint, S.** (1996) Interfluve sequence boundaries in the Grassy Member, Book Cliffs, Utah: criteria for recognition and implications for subsurface correlation. In: *High Resolution Sequence Stratigraphy: Innovations and Applications* (Eds. J.A. Howell and J.F. Aitken), Geol. Soc. London, Spec. Publ., **104**, 208–220.

Nichol, S.L., Boyd, R. and **Penland, S.** (1996) Sequence stratigraphy of a coastal-plain incised valley estuary: Lake Calcasieu, Louisiana. *J. Sed. Res.*, **66**, 847–857.

Page, S. J. (2011). Fold-thrust system overprinting syn-rift structures on the margin of an iverted rift basin: Indio Mountains, West Texas. The University of Texas at El Paso, El Paso, Texas, 68 pp.

Pemberton, S. (1992) Applications of Ichnology to Petroleum Exploration. *Soc. Econ. Palaeont. Mineral., Core Workshop Guide17*.

Pearson, B. (1964) Some regional relationships, Trans-Pecos Texas and Northeastern Chihuahua. In: *Geology of Mina Plomosas-Placer de Guadalupe area, Chihuahua, Mexico*. *West Texas Geol. Soc*. Field Trip Guidebook, **64-50**, 109-112.

Peryam, T.C., Lawton, T.F., Amato, J.M., González-León, C.M., and **Mauel, J. D.** (2012) Lower Cretaceous strata of the Sonora Bisbee Basin: A record of the tectonomagmatic evolution of northwestern Mexico. *Geol. Soc. Am. Bull.*, **124**, 532–548.

Plint, A.G. (1991) High frequency relative sea-level oscillations in Upper Cretaceous shelf clastics of the Alberta foreland basin: some possible evidence of a glacio-eustatic control? *In: Sedimentation, Tectonics and Eustacy – Sealevel Changes at Active Margins* (Ed. D.I.M. Macdonald), *Int. Assoc. Sedimentol. Spec. Publ.*, **12**, 409–428. Blackwell Scientific Publications, Oxford, UK.

Posamentier, H.W. and **Vail, P.R.** (1988) Eustatic controls on clastic deposition II – sequence and systems tracts models. In: *Sea-Level Changes: an Integrated Approach* (Eds C.K. Wilgus, B.S. Hastings, C.G.S.C. Kendall, H.W. Posamentier, C.A. Ross, and J.C.V. Wagoner), *SEPM Spec. Publ.*, **42**, 125–154.

Posamentier, H.W. and **Allen, G.P.** (1993) Variability of the sequence stratigraphic model: effects of local basin factors. *Sedim. Geol.*, **86**, 91–109.

Posamentier, H.W. and **Allen, G.P.** (1999) Siliciclastic sequence stratigraphy – concepts and applications. SEPM Concepts in Sedimentology and Paleontology, **7**, 210pp.

Reaser, D.F. and **Underwood, J.R.** (1980) Tectonic style and deformational environment in the Eagle-Southern Quitman Mountains, Western Trans-Pecos Texas. In: *Trans-Pecos Regio*n, (Eds P. W. Dickerson, J. M. Hoffer, J. F. Callender), *New Mexico Geol. Soc. Guidebook, 31st Field Conference, Trans-Pecos Region*, 123–130.

Richardson, G.B. (1904) Report of a reconnaissance in Trans-Pecos north of the Texas and Pacific Railway. *University of Texas, Mineral Sur. Bull.*, 9.

Spiegelberg, F. (1961) Stratigraphy of northern Sierra de Ventana, municipio de Ojinaga, Chihuahua, Mexico. University of Texas, Austin, 90 pp.

Taylor, A. M. and **Gawthorpe, R. L.** (1993) Application of sequence stratigraphy and trace fossil analysis to reservoir description: examples from the Jurassic of the North Sea. In: *Petroleum geology of Northwest Europe. Proceedings of the 4th conference* (Ed. J.R. Parker), *Geol. Soc. London, Petroleum Geology Conference series,* **4**, 317-335.

Taylor, D.R. and **Lovell, R.W.W.** (1995) High-frequency sequence stratigraphy and paleogeography of the Kenilworth Member, Blackhawk Formation, Book Cliffs, Utah, USA. In: *Sequence Stratigraphy of Foreland Basin Deposits: Outcrop and Subsurface Examples from the Cretaceous of North America* (Eds J.C. Van Wagoner and G.T. Bertram), *AAPG Mem.*, **64**, 257–275.

Underwood, J. R. (1962) Geology of the Eagle Mountains and vicinity, Trans-Pecos, Texas, University of Texas, Austin, 559 pp.

Underwood, J. R. (1963) Geologic map of Eagle Mountains and Vicinity, Hudspeth County, Texas, *Bur. Econ. Geol. Univ. Tex. Austin Rep*. Quad. Map No. 26, 32 pp.

Underwood, J.R. (1975) Geology of Eagle Mountains and Vicinity, Hudspetch County, Texas. In: *Geology of the Eagle Mountains and Vicinity Trans-Pecos Texas*, *SEPM Permian Basin Section Guidebook*, **75-15**, 1-32.

Underwood, J. R. (1980) Geology of the Eagle Mountains, Hudspeth County, Texas: In: *Trans-Pecos Regio*n, (Eds P. W. Dickerson, J. M. Hoffer, J. F. Callender), *New Mexico Geol. Soc. Guidebook, 31st Field Conference, Trans-Pecos Region*, 183-193.

Van Wagoner, J.S., Posamentier, H.W., Mitchum, R.M., Vail, P.R., Sarg, J.F., Loutit, T.S. and **Hardenbol, J.** (1988) An overview of the fundamentals of sequence stratigraphy and key definitions. In: *Sea-Level Changes: An Integrated Approach* (Eds C.K. Wilgus, B.S. Hastings, C.G. Kendall, H.W. Posamentier, C.A. Ross, and J.C. Van Wagoner), *SEPM* Spec. Publ., **42**, 39–45.

Van Wagoner, J.C., Mitchum, R.M., Campion, K.M. and **Rahmananian, V.D.** (1990) Siliciclastic sequence stratigraphy in well logs, cores, and outcrops : concepts for high-resolution correlation of time and facies. *AAPG Methods in Exploration Series*, **7**, Tulsa, Okla., 55 pp.

Van Wagoner, J.C. (1995) Sequence Stratigraphy and Marine to Nonmarine Facies Architecture of Foreland Basin Strata, Book Cliffs, Utah, USA. In: *Sequence Stratigraphy of Foreland Basin Deposits – Outcrop and Subsurface Examples from the Cretaceous of North America* (Eds. J.C. Van Wagoner and G.T. Bertram), *AAPG Mem.*, **64**, 137-223.

Walker, R.G. (1984) Shelf and shallow marine sands. In: *Facies Models* (Eds. R. Walker), *Geosci. Can. Repr. Series*, **1**, 141–170.

Walker, R.G. and **Plint, A.G.** (1992) Wave and storm-dominated shallow marine systems. *Facies Models: Response to Sea-Level Change* (Eds. R.G. Walker and N.P. James), *Geol. Assoc. Can.*, 219–238.

Wade, D.E. (1954) Is the Fredricksburg Group a Practical Unit in Trans-Pecos Texas? University of Texas, Austin, 160 pp.

Yoshida, S. (2000) Sequence and facies architecture of the upper Blackhawk Formation and the Lower Castlegate Sandstone (Upper Cretaceous), Book Cliffs, Utah, USA. *Sed. Geol.*, **136**, 239–276

Table1.1: General scheme of the facies associations and interpreted depositional environments of the Cox Sandstone in the Indio Mountains

Facies Association	Description	Depositional Environment
FA1: Massive mudstone, limestone, and current and wave ripple facies association	Greenish gray to purple shale intercalated with very thin bedded greenish gray siltstone. Very fine to fine grained highly bioturbated sandstone, current and wave ripples, fossiliferous limestone	Shelf and intertidal mudstones
FA2: Hummocky cross stratified sandstone and laminated sandstone facies association	Hummocky cross stratified sandstone, laminated sandstone, bioturbation	Lower shoreface
FA3: Trough cross bedded, tabular planar, bioturbated sandstone and planar laminated sandstone facies association	Trough cross bedded sandstone, tabular planar bed, bioturbation	Upper shoreface and foreshore
FA4: Conglomeratic sandstones, trough cross stratified sandstone, planar laminated sandstone and quartz sandstones facies association	Lenticular sandstone, conglomeratic sandstone, fining up units exhibiting lateral accretion	Fluvial channel fill sandstone
FA5: Ripple laminated white to light gray sandstone, interbedded sandstone and mudstone facies association	Ripple laminated sandstone, mud drapes, alternative bands of fine and coarse grained sandstone	Tidal flat
FA6: Variegated mud and fine grained sandstone facies association	Variegated mudstone interbedded with siltstone and fine to very fine grained sandstone, carbonaceous shale	Coastal plain

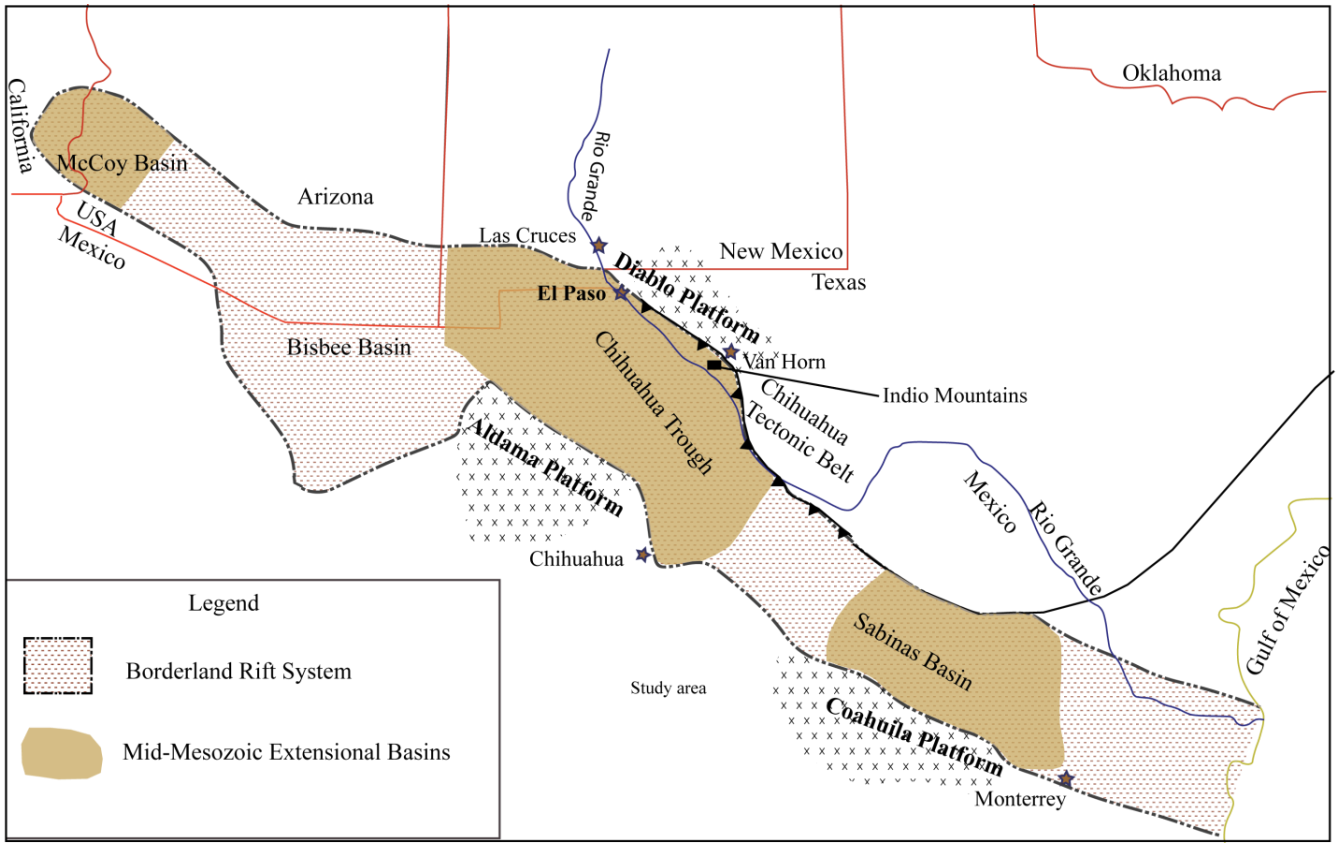

Fig. 1.1: Borderland Rift system showing Chihuahua trough (Deford, 1964) and other associated basins with the borderland rift system. Black rectangle shows the study area in the Indio Mountains (Modified from Lawton & Mcmillan, 1999; Dickinson & Lawton, 2001; Haenggi, 2001).

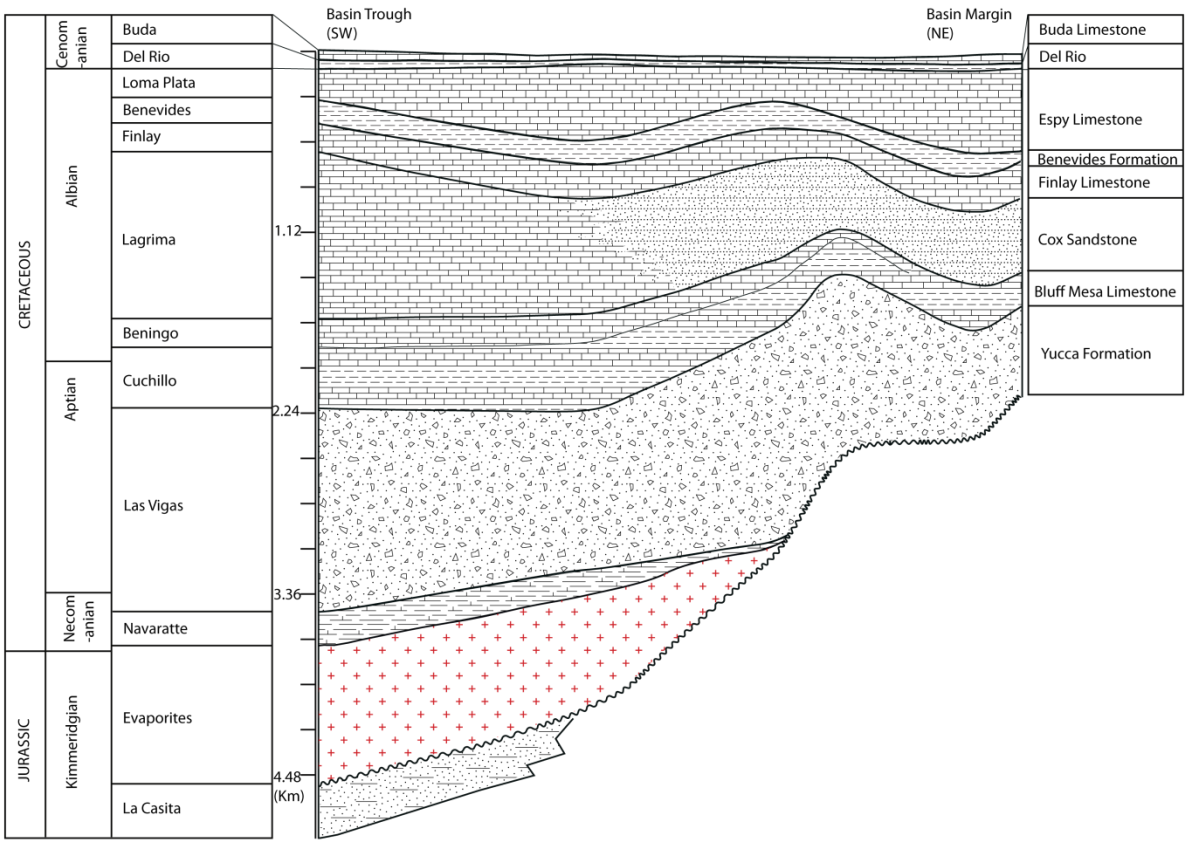

Fig. 1.2: Generalized stratigraphic column of the Chihuahua trough from basin margin to basin trough (Modified after Underwood, 1962; Haenggi, 1970). Cox Sandstone is overlain by Finlay limestone and underlain by Bluff Mesa Limestone. Recent study suggests that regional unconformity separates Upper Jurassic unit from Lower Cretaceous strata in the Chihuahua trough margin (Peryam *et al.*, 2012).

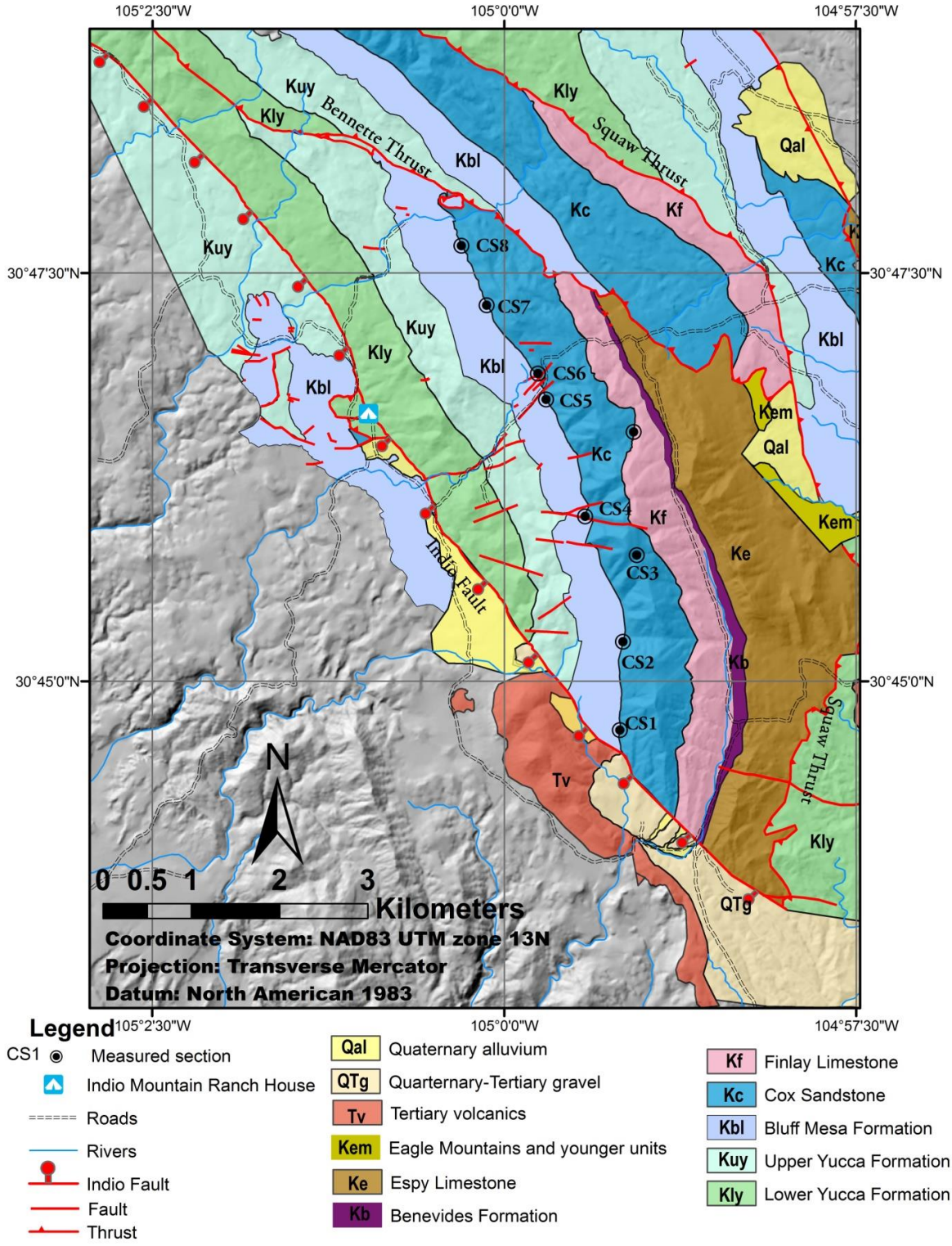

Fig. 1.3: Geological map of the study area showing measured sections. Sections were measured along the upthrown block of the thrust sheet (after Underwood, 1963; Page, 2011).

(A)

(B)

(C)

(D)

(E)

Fig. 1.4: Photographs illustrating inner shelf mudstone and sandstone facies association (FA1). (A) General view of Facies Association 1 consisting of massive mudstone intercalated with greenish

gray siltstone, looking NE; (B) Fine grained rippled laminated sandstone; (C) Fossiliferous limestone consisting of turitella (?) and forams, found at approximately 14m above the base (D) About 3.5-m-thick fossiliferous limestone at about two third of the sections from the base which can be traced the entire region and (E) Close up of the limestone showing bivalve fossils. Geologist for scale in photograph (A) is 1.8 m tall; pen (12 cm long) for scale in (B) and (E); penny (1.90 cm diameter) for scale in (C); and Jacob's staff (1.5m long) for scale in (D).

(A)

(B)

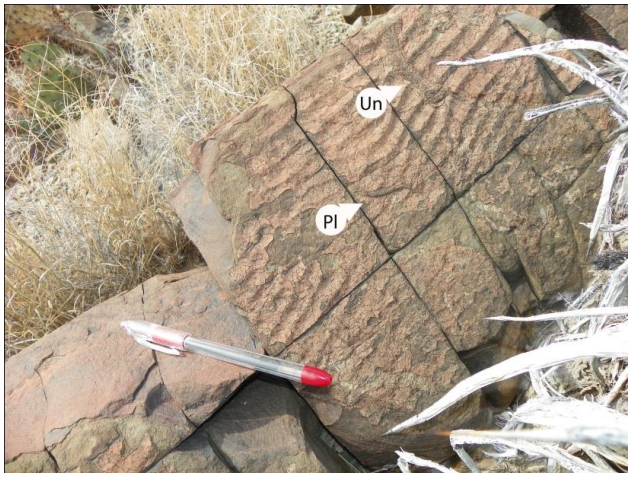

(C)

(D)

Fig. 1.5: Outcrop of photographs illustrating lower shoreface facies association (FA2). (A) Small scale Hummocky cross stratification. Lens cap is 5.2 cm in diameter; (B) Very fine grained laminated sandstone. Jacob staff for scale is 1.5 m long (C) Wave rippled sandstone with *Planolite* (Pl) and unidentified trace fossil (Un) at planar view. Pen for scale is 15 cm long; (D) Lower shoreface sandstone containing *Thalassinoides* (Th), *Paleophycus* (Pa), *Planolite* (Pl) *and Skolithos* (S). Pen cap is 4 cm long.

(A)

(B)

(C)

(D)

Fig. 1.6: Representative photographs of upper shoreface and foreshore facies association (FA3). (A) Tabular planar sandstone; Pen is 15 cm long; (B) Trough cross stratified sandstone; Hammer for scale is 32 cm long (C) a transition from trough cross bedded upper shoreface to planar foreshore (Hammer is 32 cm long). Soft sedimentation structure in the trough indicates that sandstone was deposited rapidly; (D) Upper shoreface sandstone containing *Diplocraterion* and *Skolithos*; Hammer is 32 cm long.

(A)

(B)

(C)

(D)

Fig. 1.7: Outcrop photographs of conglomeratic sandstone and laterally accreted sandstone facies association (FA 4). (A) Chert and pebble sandstone at the base of channel system marking the erosional surface; total length of Jacob staff is 1.5 m with 5 cm interval. (B) Laterally accreted cross stratified sandstone; geologist for scale is 1.8 m tall. (C) Outcrop view of amalgamated meandering channel. (D) Outcrop view of meandering channel deposit showing lateral accretion.

(A)

(B)

(C)

Fig. 1.8: Photographs of tidal influenced sandstone facies association (FA 5). (A) Trough cross sandstone bed overlain by alternative fine and coarse grained sandstone; hammer head is 17 cm long. Lenses of fine grained sandstone and alternative fine and coarse grained sandstone indicates the rapid change in environment and suggests the tidal processes. (B) Spindle shaped crack (synaeresis crack?); pen for scale is 15 cm long. Synaeresis crack

represents the deposit in subaqueous environment (B) Ripple laminated green siltstone with mud drapes suggests tidally influenced environment.

A.

B.

Fig. 1.9: Photographs representing coastal plains facies association. (A) Intercalation of variegated mudstone and very fine grained sandstone; variegated color indicates changing condition of oxidation. (B) Calcareous nodules. Note irregular 'potato' shaped nodules; acid water bottle is 5 cm long.

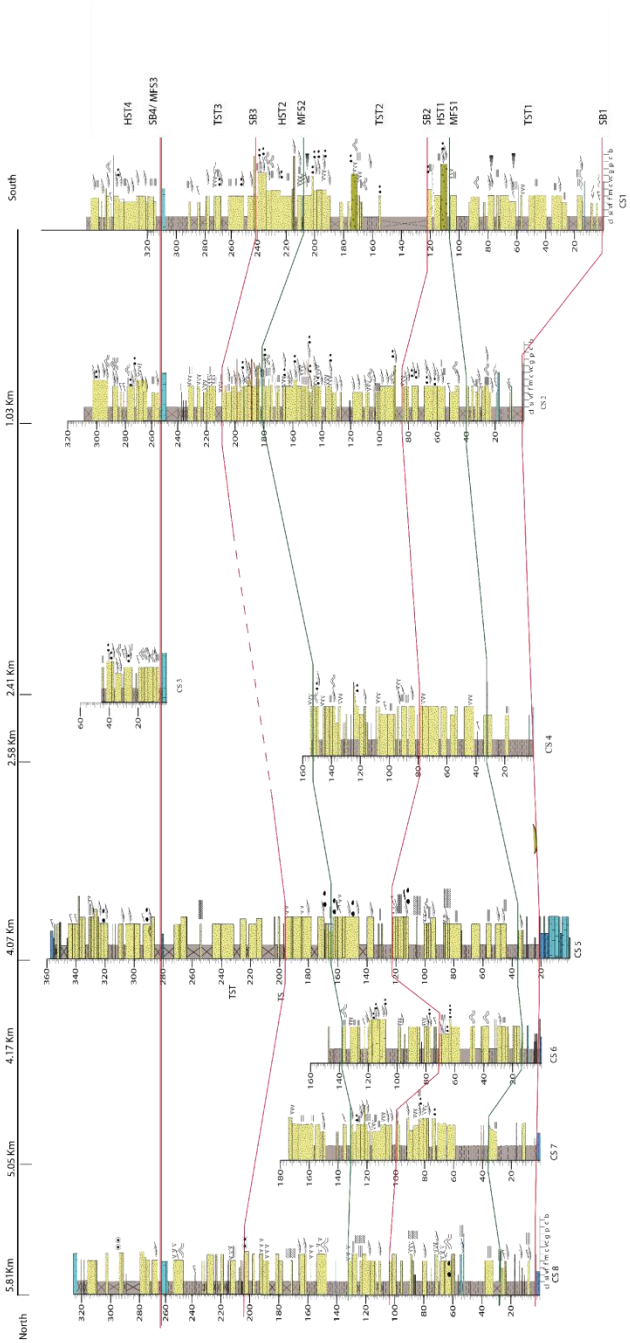

Fig. 1.10: Cross section showing Interpreted correlation of the Cox sandstone; please refer to Fig. 1.3 for section location and Fig. 1.11 for key to symbols used in this cross section. The Cox consists of four sequences.

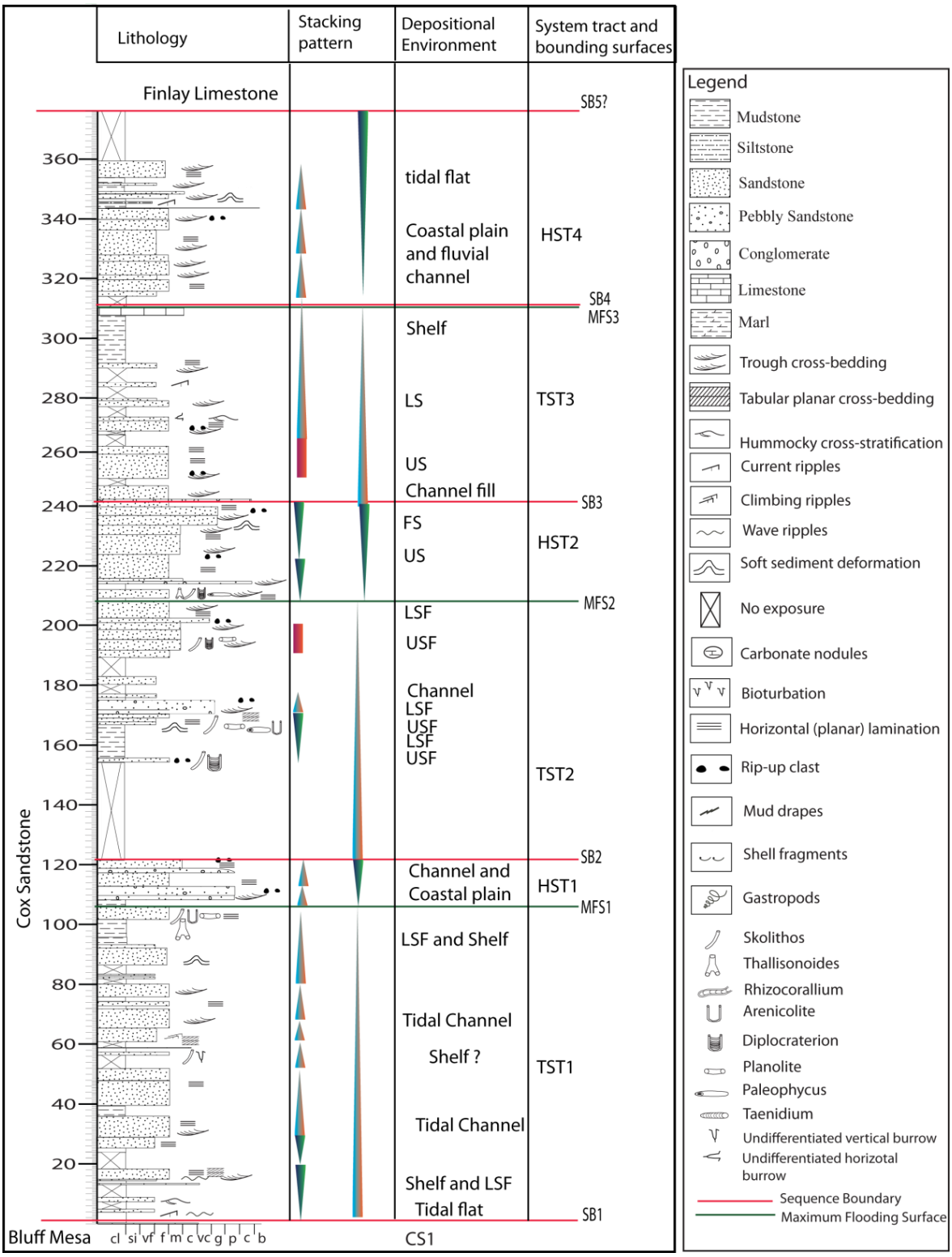

Fig. 1.11: Representative section of the Cox showing elements of sequence stratigraphic architecture. (Section CS1 in Fig. 1.3). Triangles show inferred transgressive and regressive trends.

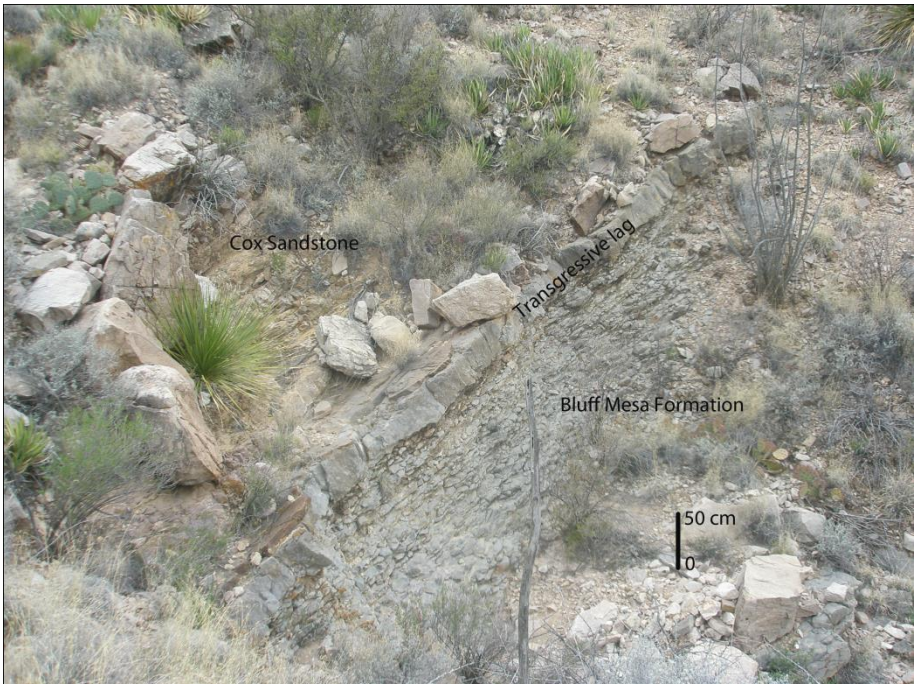
Cox Sandstone
Transgressive lag
Bluff Mesa Formation
50 cm
0

(A)

(B)

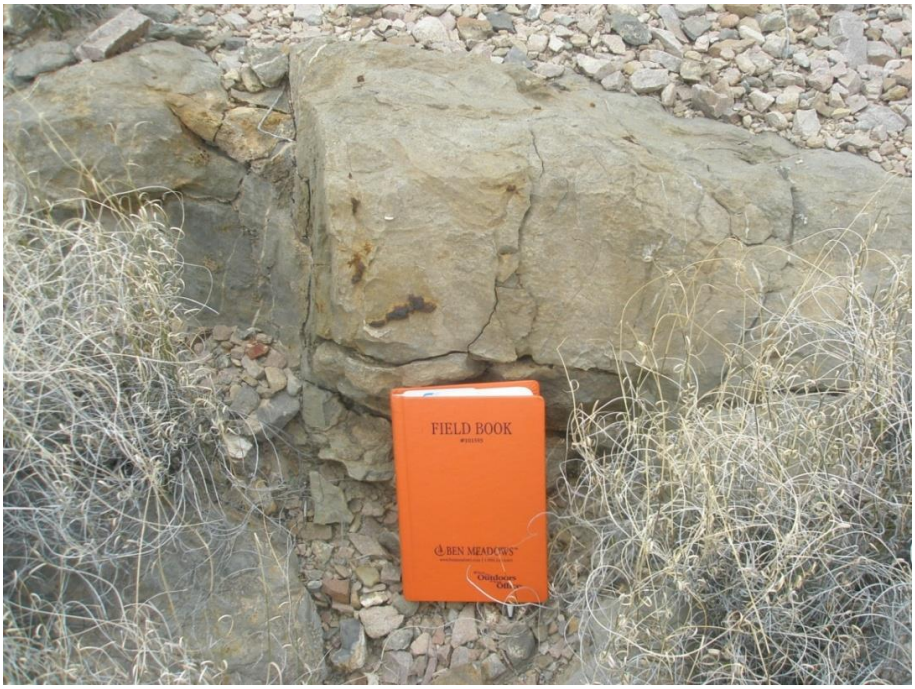

(C)

(D)

Fig. 1.12: Photographs illustrating key features of sequence 1. (A) Transgressive lag separating the upper Cox Sandstone and lower Bluff Mesa Formation. (B) Close up view of lag in the southern part. (C) Close up view of lag in the northern part. (D) Channel fill sandstone lying on the top of transgressive lag.

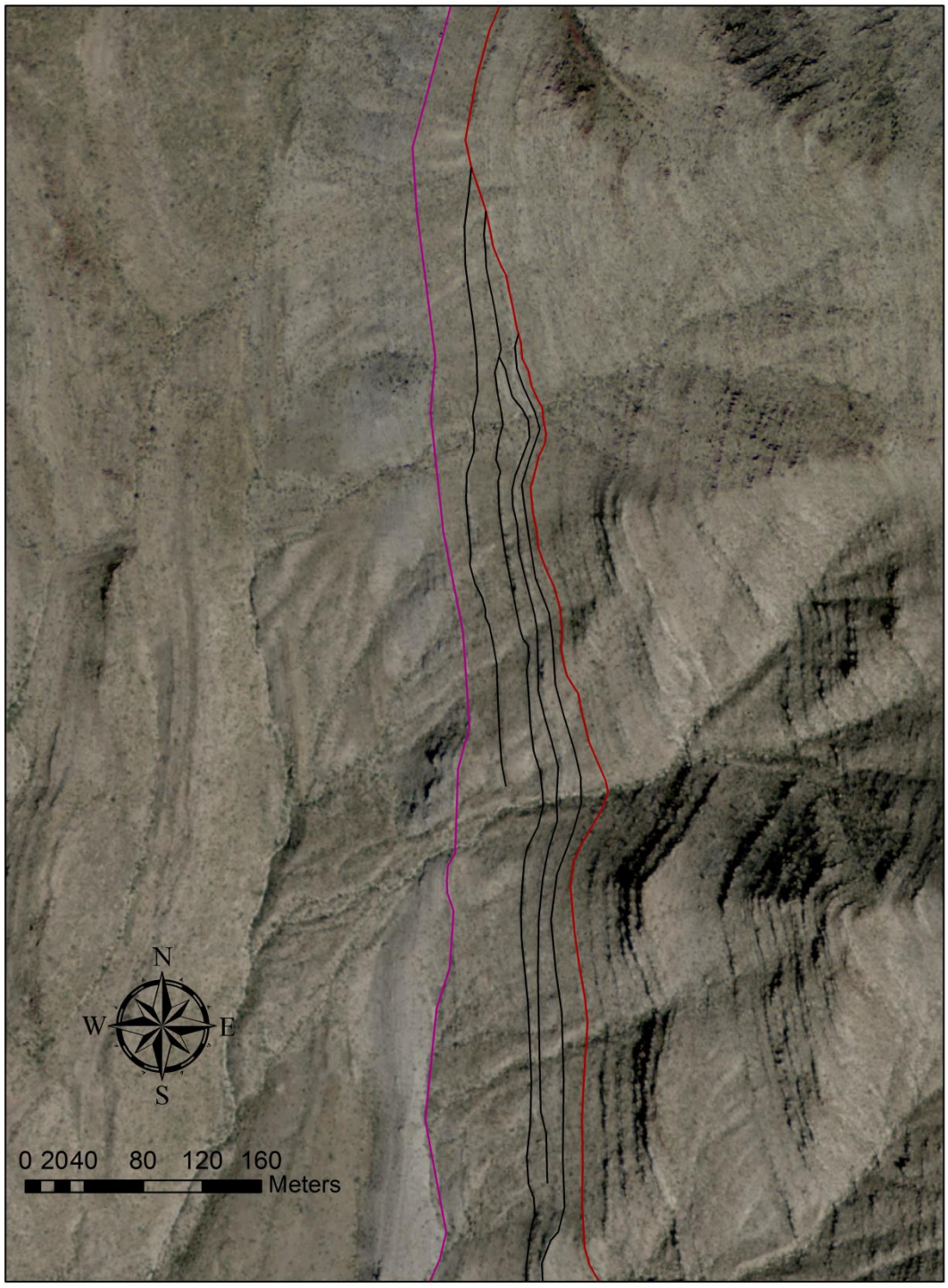

Fig. 1.13: High resolution satellite imagery showing erosional surface associated with truncation of strata. The black colour beds are onlapping the red coloured Sequence Boundary. Also shown is the Sequence Boundary at the base of the Cox Sandstone. Note thickening of beds to the south. Sequence is thickening to the south due to erosion and rotation of beds.

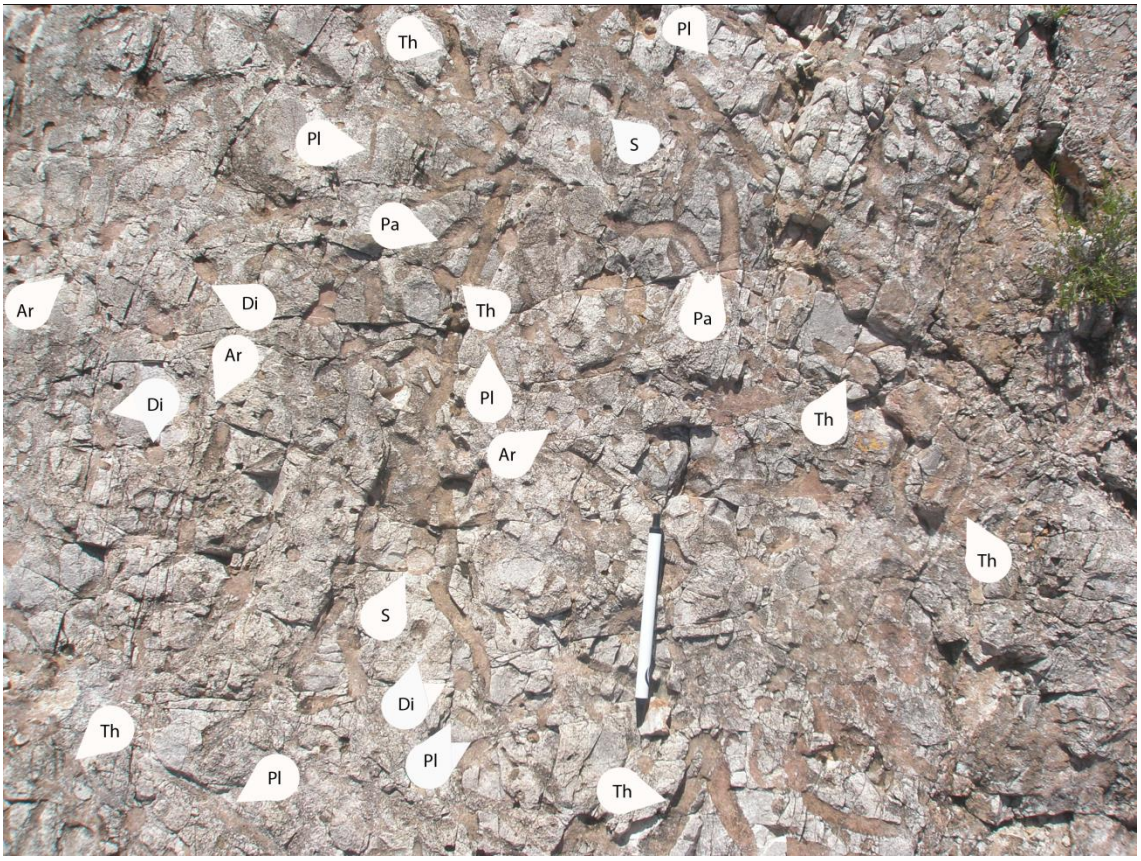

Fig. 1.14: Glossifungites ichnofacies containing *Thalassinoides* (Th), *planolite* (Pl), *Paleophycus* (Pa), *Diplocratarion* (Di), *Arenicolite* (Ar), and *Skolithos* (S) interpreted to be maximum flooding surface. Pen for scale is 12 cm long.

Fig. 1.15: Sequence boundary (SB4) separating marine limestone from non-marine coastal plain and fluvial deposits. Note the fluvial channel sandstone (FA 4) on the ridge crest.

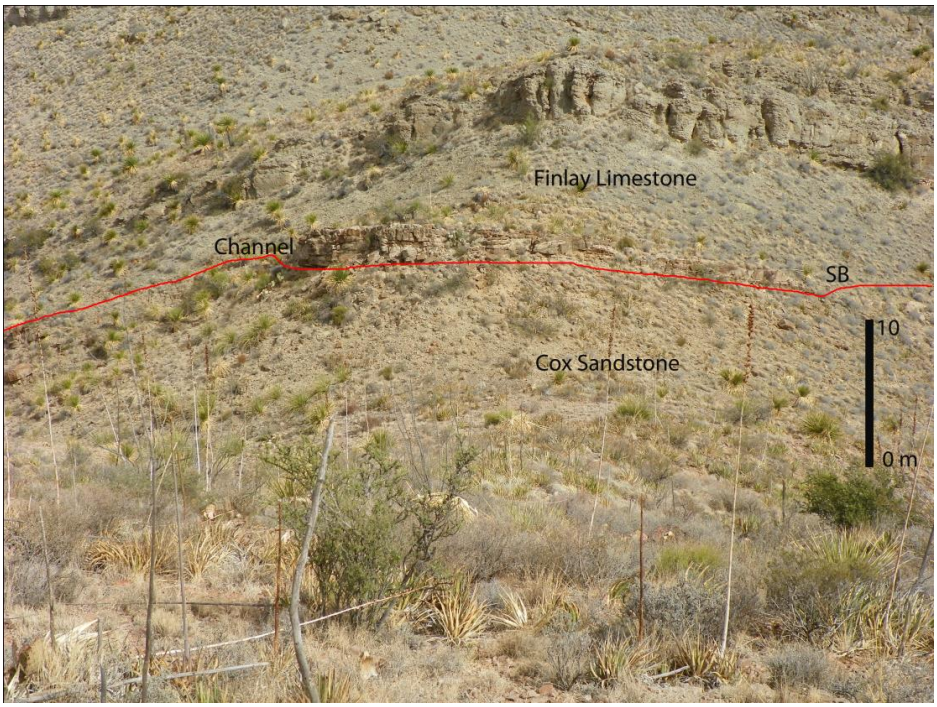

(A)

(B)

Fig. 1.16: (A) Photograph showing the contact between the Cox Sandstone and Finlay Limestone. Note channel deposit at the top of the Cox which consist of alternations of fossiliferous sandstone and limestone. (B) Enlarged view of channel deposit. Pen is 12 cm long.

SECTION 2

Geological and Geophysical Signatures for Delineating a Freshwater-Brackish Water Contact, an Example from the Hueco Bolson, El Paso, Texas

2.1 Abstract

El Pasoans depend on ground water for most of their drinking water supply. The Hueco Bolson Aquifer which is located between the Hueco Mountains in the west and the Franklin Mountains in the east contributes about 40% of the yearly drinking water supply to El Paso's community when sufficient water can be taken from the Rio Grande. The Hueco Bolson contains both fresh and brackish water. We used microgravity and well log data in a highly urbanized area to demarcate subsurface faults that appear to control the locations of fresh and brackish water in the Hueco Bolson. In this study 28 gravity anomalies were identified that correlate with previously mapped (Collins and Raney, 2000) and new faults and some of them can be extended further south to south east to join with previously mapped faults by Collins and Raney (2000) and Marrufo (2011). Interestingly, these faults are not offset more than 0.6 mGal. Because of large distance between individual wells, well logs correlations themselves do not resolve the existence of faults; however, structural cross sections suggest that at least some faults are present between them. The four depositional environments inferred from the gamma log responses and their stacking patterns are consistent with the previous interpretation of Doser and Langford (2006) and Marrufo (2011). The calculated salinity from the SP log generally matches with the measured salinity by El Paso Water Utilities.

2.2 Introduction

Since Texas and other States have experienced severe drought for the past few years, it is imperative to manage water wisely. People from the Borderland region (El Paso, USA-Ciudad Juarez, Mexico) depend on ground water for most of their drinking water supply. The Hueco Bolson Aquifer (HBA) contributes about 40% of the yearly drinking water supply to El Paso's

community when sufficient water can be taken from the Rio Grande. In drought years when river water is minimal, the HBA supplies an even greater percentage of the local water supply. According to Heywood and Yager (2003), the ground water level had declined by 60 meters in some areas under the Borderland region by 1996.

The Franklin Mountains and the Hueco Mountains define the eastern and western boundaries of the Hueco basin, which extends southward to the Sierra del Presidio in Mexico (Figure 2.1b). The northern boundary is a groundwater divide separating the Hueco basin from the Tularosa basin. However, our study is only limited to the El Paso region as outlined in Figure 2.1a.

The HBA contains both fresh and brackish water. El Paso has one of the largest desalination plants in the world and in order to efficiently process brackish water from HBA it is important to understand the location of the fresh-brackish water boundary and structural/stratigraphic controls on this boundary. Work by Marrufo (2011) suggests a fault serves as the barrier between fresh and saline in central northern bolson; however, we do not know where this contact extends within the northern part of the basin and if the fault remains the controlling mechanism for the freshwater-brackish water contact. By mapping the boundary between the freshwater and brackish water we will be better able to determine an estimate of the volume of freshwater for groundwater budget and sustainable resource management. This study also helps us to predict where we might be more likely to encounter fresh water in other basins that have not yet been explored in adjacent regions. In addition, it is important to locate the subsurface Quaternary faults as these represent possible earthquake sources and can be used in updated seismic hazards analysis of the region. The most recent felt earthquakes in El Paso (magnitude ~ 2.5, on March 6, 2012) is believed to have occurred along one of these concealed faults.

2.3 Geological Setting

The geological history of the El Paso region ranges from Precambrian to Cenozoic in age, and is shaped by complex geological processes. The details of these geological processes are beyond the scope of this paper. Interested readers are referred to Lovejoy (1975), LeMone (1983), Seager and Mack (1986), Baldridge (2004); McMillan et al. (2000). The Precambrian Castner Marble represents the oldest strata exposed in the El Paso region which were deposited along the shoreline as shallow marine limestone and later metamorphosed into marble (LeMone, 1983; Baldridge, 2004). This was followed by basalt volcanism and deposited a thin layer of Mundy Breccia. Lanoria Quarzite, shallow marine sand containing a sequence of metamorphosed quartz, sandstone, silt and shale overlies the Castner Marble and Mundy Breccia. The suggested depositional environments of these Precambrian rocks are within a shallow rift basin (Bickford et. al., 2000). About 1120-1080 Ma ago, the El Paso region experienced volcanic activity and was covered with ignimbrite and tuffceous rocks of the Thunderbird Group. During the same time, all these sequences were intruded by the Red Bluff Granite. These Proterozoic metasedimentary and igneous rocks crop out in the northern Franklin Mountains.

The Cambrian marine Bliss Sandstone nonconformably rests on Precambrian rocks following a gap in depositional history of about 550 Ma (LeMone, 1983). The mixed clastic-carbonate rocks of the Bliss Sandstone is overlain by thick sequences of carbonates deposited during the Ordovician (El Paso Group and Montoya Group), Silurian (Fusselman Dolomite), Devonian (Percha Shale and Canutillo Formation), Mississippian (Helms and Rancheria Formations), Pennsylvanian (Magdalena Group) and Permian (Hueco Group) (LeMone, 1983). The early Mesozoic was quiet period of time in the El Paso region where there was little or no tectonic activity. There was no deposition of Mesozoic rocks until the middle Cretaceous. Paleozoic and Cretaceous rocks are exposed in the Franklin Mountains, Hueco Mountains, Sierra de Juarez and other parts of El Paso (Figure 2.2).

Cenozoic tectonic events in El Paso and surrounding regions have had great influence on changing the landscape through widespread magamatic activity, crustal deformation and shortening, and rifting and extension. Throughout the latest Cretaceous to the middle Eocene subduction of the Farallon Plate beneath North American continental crust caused compressional deformation and shortening of this region (Seager and Mack, 1986; Baldridge, 2004; Seager 2004). As a result, mountains were uplifted in Colorado, New Mexico and Texas, including the Sierra de Juarez, Mexico (Chapin and Seager, 1975; Lovejoy, 1975; Baldridge, 2004). Magmatic activity during middle Eocene to Oligocene time resulted in intrusion of the Cerro de Cristo Rey, the Campus Andesite and other smaller intrusive bodies in the El Paso and Sierra de Juarez area (Hoffer, 1970; Lovejoy, 1975; Keller et al., 1990). The intrusion of these magmatic bodies, postdate the Laramide orogeny but predate Cenozoic extensional event (McMillan et al., 2000). Transition from compressional (Laramide orogeny) to extensional stress (Rio Grande Rift and Basin and Range) began around 36 Ma (McMillan et al., 2000) to 30 Ma (Henry and Price, 1985) and is recorded in volcanic rocks of El Paso and surrounding areas. The Rio Grande Rift began with the cessation of the Laramide orogeny and continues to today (Chapin, 1979).

The Rio Grande Rift extends from central Colorado to west Texas and northern Chihuahua, Mexico (Keller and Baldridge, 1999) and can be broadly divided into the northern Rio Grande Rift and the southern Rio Grande Rift. The Rio Grande Rift consists of series of north trending, interconnected asymmetrical grabens, including the Hueco bolson (Chapin, 1971; Seager et al., 1984; Collins and Raney, 1991; Keller and Baldridge, 1999). The northern part of a rift is the distinctive feature that separates the Great Plains to the east and the Colorado Plateau to the west; however, the boundary of the southern rift is the subject of controversy (Seager et al., 1984; Keller and Baldridge, 1999, McMillan et al., 2000). The Rio Grande rift has experienced two phases of extension producing two different styles of basins (Seager et al., 1984; Morgan and Golombek, 1984; Morgan el al., 1986). Early extension (mid-Oligocene to early Miocene) resulted in formation of broad and relatively shallow basins with low angle normal faults, while the late extension (mid-Miocene to Quaternary) produced high angle fault

bounded, relatively deep and narrow basins (Morgan and Golombek, 1984; Keller and Baldridge, 1999). The extension of the Rio Grande rift is still active today along Quaternary normal faults which can be mapped using geophysical and petrophysical techniques (Avilla, 2011; Maruffo, 2011).

2.3.1 HUECO BOLSON STRATIGRAPHY

Hueco basin stratigraphy (Figure 2.3) has been studied and described by several authors in the past (Albritton and Smith, 1965; Strain, 1966; Willingham, 1980; Riley, 1984; Stuart and Willingham, 1984; Vanderhill; 1986; Gustavson, 1990, 1991; Hawley and Kernodle, 2000; Hawley et al., 2002; Hawley and Kennedy, 2004). The basin fill is primarily composed of unconsolidated to poorly consolidated fluvial, lacustrine and aeolian sediments of Tertiary to Quaternary age (Hadi, 1991; Anderholm and Heywood, 2003; Heywood and Yager, 2003; Buck et al., 1998) but little is known about Tertiary sediments due to lack of outcrop and core data (Collins and Raney, 1991; Hawley et al., 2004). These basin fill sediments are commonly described as "alluvial" in the literature (Ashworth, 1990; Kernodle, 1992; Haywood and Yager, 2003) despite the variability of mixed depositional environments such as fluvial, lacustrine and aeolian (Gustavson, 1990; Hadi, 1991; Buck et al., 1998; Hawley et al., 2000; Hawley et al., 2009).

The basin fill deposits can be broadly divided into lower basin fill, upper basin fill and surficial deposits (Collins and Raney, 1991). The Pliocene- Pleistocene Fort Hancock and Camp Rice Formations (Strain, 1966) represent the upper part of the upper basin fill (Collins and Raney, 1991). The Fort Hancock Formation mostly consists of lacustrine and proximal to distal alluvial fan deposits (Hawley et al., 2002, Gustavson, 1990). Fluvial facies have also been reported in the Fort Hancock Formation (Willingham, 1980; Riley, 1984). According to Riley (1984), a meandering stream system was responsible for depositing the fluvial facies in the Fort Hancock Formation. A regional unconformity separates the overlying Camp Rice Formation from the underlying Fort Hancock Formation (Strain, 1966). The Camp Rice Formation mostly

consists of sand and gravel of braided stream system and alluvial fans. It also contains lacustrine and flood deposits in minor amounts (Collins and Raney, 1991). Albritton and Smith (1965) identified five Pleistocene gravel units, namely the Miser, Madden, Gills, Ramey and Balluco gravels, which were deposited on piedmont slopes and arroyo terrace environments. These units overlie the Fort Hancock and Camp Rice Formations and underlie the windblown, fluvial and alluvial deposits of the present Rio Grande (Albritton and Smith, 1965).

Haywood and Yager (2003) have divided the sediments of the Hueco basin into fluvial, alluvial-fan, lacustrine- playa and recent alluvial facies. Based on grain size analysis and well logs, Marrufo (2011) identified an additional playa margin facies in the HBA adjacent to this study area. The fluvial facies consists of relatively course grained sand and gravel interbedded with silt and clay. The predominant geologic formation of this facies is the Camp Rice Formation. The fluvial deposits of the HBA are mostly related to the ancient Rio Grande as described by many authors (Gustavson, 1990; Mack and Leeder, 1998; Haywood and Yager, 2003; Hutchison, 2006; Marrufo, 2011). Between 3.8 to 0.76 Ma, the Ancestral Rio Grande entered the Hueco Bolson through Fillmore Gap between the Organ and Franklin Mountains and discharged sediments into Lake Cabeza de Vaca (Strain, 1971; Gustavson, 1990; Mack and Leeder, 1998). By about 2.25 Ma, the upper and lower Rio Grande integrated replacing the existing Lake Cabeza de Vaca, and the ancestral Rio Grande flowed through the entire Hueco basin (Gustavson, 1990). According to Mack et al. (2006), the ancestral Rio Grande was a braided system, mostly depositing pebbly medium to coarse sand. The alluvial fan facies of the Camp Rice Formation consists of poorly sorted gravel and sand mainly derived from the present day Organ and Franklin Mountains. According to Gustavson (1991), lacustrine sediments represent the Fort Hancock Formation, most of which were carried to the basin by the northern ancestral Rio Grande. This facies predominantly occurs at the central, eastern and southeastern parts of the basin beneath the fluvial and alluvial-fan facies.

2.4 Methodology

In order to answer the research questions stated above, we used a geophysical and petrophysical approach as integration of these disciplines have been successfully applied to solve the similar problems (Marrufo, 2011). A previous study has shown the success of using a combination of water well logs, well cuttings and microgravity data to locate faults that appear to separate zones of fresh and saline water in the HBA within south-central El Paso (Marrufo, 2011). The logs and cuttings from this previous study also helped to define a sedimentological and stratigraphic framework that could be applied to other parts of the HBA. In our current study we have collected additional information from 9 water wells and microgravity data from the north-central and northwestern HBA (Figure 2.4) in an effort to trace the faults and stratigraphic facies across the basin.

2.5 Gravity Survey

This study is the extension of a previous study carried out in El Paso and surrounding areas. In this study we collected 502 gravity data points and combined them with existing gravity data available from the UTEP gravity data base. Because we did not have permission to collect data in the Fort Bliss Military area, our gravity points are sparse east of the rail road (Figure 2.4). The gravity survey was performed with 75 to 300 m spacing using a Lacoste and Romberg model G-1115 gravimeter and Topcon GB 1000 GPS with ground plane. This gravimeter has an accuracy of 0.01 mGal. The GPS base points were submitted in receiver independent exchange (RINEX) format to National Geodetic Survey (NGS) via the web based On-line Positioning User Service (OPUS) (http://www.ngs.noaa.gov/OPUS/). OPUS processes the GPS points with respect to three reference sites and the processed points are sent back to the user via email (Mader et al., 2003). We postprocessed our data using OPUS solutions which allowed us to achieve a high accuracy of elevation (<5 cm) and associated latitude and longitude.

A secondary base station (sub-base) was established near Painted Dunes Golf Course (hereafter called “golf base”), El Paso by tying with the absolute base station situated at the Kidd

Memorial Seismological Observatory on the UTEP campus (hereafter called "Kidd station"). The properties of these base stations are summarized in Table 2.1. Gravity points were collected in loop style and survey loops were closed on the golf base station on every 2-3 hours to reduce the effects of tides. Also, repeated gravity measurements at the base allow a drift correction to be made to the gravity reading at the other stations (Lowrie, 1997). The repeatability of the gravity value at base stations is approximately 0.01-0.04 mGal. The golf base station was tied at the beginning and end of each day to the absolute gravity station at UTEP.

Since the readings taken with the gravimeter are not in gravity units (milligals, mGal), a dial calibration factor provided for Lacoste and Romberg gravimeter model G-1115 was applied to each reading to convert them into mGals.

Gravity readings are affected by several variables including latitude, elevation, tides, density of materials, and topography. The following corrections were applied for the gravity reduction:

Free-air correction (C_F):

$C_F = 0.3086 * h$ mGal ---------- (eqn 1)

Where h is elevation in meters

Bouguer correction (C_B):

$C_B = 0.0419 * \rho * h$ mGal ---------- (eqn 2)

Where ρ is rock density in g/cm^3

Bouguer anomaly (ΔBA) = $g_{obs} - g_{theor} + C_F - C_B$ ---------- (eqn 3)

Where g_{obs} is the observed absolute gravity and g_{theor} is theoretical gravity

2.5.1 GRAVITY MAP

Geosoft's Oasis Montaj software with 200 m grid size and minimum curvature gridding technique was used to generate a Bouguer anomaly map with contour interval of 1 mGal as shown in Figure 2.5. An average crustal density of 2.67 gm/cm^3 was chosen for the Bouguer

correction to remove the gravity slab effect. A terrain correction was not applied to the gravity data since all gravity points collected in this study area are in a region of relatively flat topography.

The Bouguer anomaly map shown in Figure 2.5 represents the basic map for overall interpretations in this study. This map shows variation in anomaly value from -114.3 to -169.6 mGal. These anomalies show the strong correlation with the structural high and lows known from the previous study (Burrows, 1984; Hadi, 1991; Burgos, 1993). High gravity anomalies are related with the high density rocks of the Franklin Mountains and low anomalies are associated with low density basin fill deposits. Gravity values decrease from west to the east indicating more basin fill sediments to the east. The NE corner of the area shows the lowest gravity anomaly (>-168.2 mGal) representing the deepest part of the basin. The basin bounding fault situated near the east side of the Franklin Mountains and other smaller faults are reflected in the gravity anomaly map (Figure 2.5). The gravity signatures of these small scale structures are not necessarily identifiable in the Bouguer anomaly map alone.

To interpret these anomalies we created several simple profiles showing Bouguer values versus distance and topography in an Excel spreadsheet as shown in Figure 2.6. Profiles were created in such a way that all gravity values lie along the profile line as much as possible because any values offset from this line can give high or low values and results can be misinterpreted. Figure 2.6 is an example of a simple profile along McCombs Rd that shows the relationship between the Bouguer anomaly in mGal, and elevation and distance in meters between the first and last gravity stations of the loop. There is no correlation between topography and gravity between points T19 and T20, while point T21 coincides with a change in the topography. Anomaly at T21 has symmetric shape but the other two have asymmetric shapes. From left to right (North to South), the difference between consecutive stations for anomalies T21, T19 and T20 are 0.05, 0.2 and 0.09 mGal, respectively. We interpreted T21 as related topography, while the other two are related to fault anomalies. Gravity signatures in the hanging wall block of a normal fault show a decrease in gravity values as the equivalent section on the downthrown

block is lower in elevation (Burger, 1992). To satisfy these signatures, we need two faults so that T19 and T20 will be on the upthrown side of the fault block (Figure 2.6 and 2.8). Our all interpretation were based on the assumption that the upthrown block should show a higher gravity values than the downthrown block, although there might be another scenario where this general rule of thumb does not work for normal faults. Density contrasts in extensional basins are due to variations in densities in the accumulating basin fill. Depending on the depth of density contrasts the change in measured gravity at the surface may be broad, or shallower and more localized.

We selected three lines to model gravity profiles along that cut across major structures of the study area (Figure 2.5). Figure 2.7 show the three profiles modelled using Geosoft's GM-SYS software which is based on the forward modeling technique of Talwani et al. (1959), and Talwani and Heirtzler (1964). Regional geology, subsurface lithostratigraphy, density and thickness of formations are reasonably well understood from previous studies (Burrows, 1984; Collins and Raney, 1991; Hadi, 1991; Burgos, 1993; Hawley, 2000, 2004; Granillo, 2004; Avilla, 2011; Marrufo, 2011) Geologic maps and cross sections by Collins and Raney (2000), Hawley et al. (2009) and Marrufo (2011) were used for geologic contacts and fault constraints. Densities used in gravity modelling are shown in Table 2.2.

2.5.2 PROFILE AA'

The west-east extending profile AA' is located along the Texas-New Mexico state line, at the northern edge of the study area (Figure 2.5). The profile passes across several faults including, the East Boundary fault of the Franklin Mountains (Richardson, 1909, Lovejoy, 1975) (Figure 2.7a). The East Boundary fault is east dipping, high angle normal fault that bounds the western margin of the Hueco Bolson, and is marked by steep gravity gradient. Fault I, II and III are previously mapped faults (Collins and Raney, 2000). Anomalies labelledFault1 and Fault 2 coincide with the Fault I and Fault II (Figure 2.7a). Three anomalies appear to correspond to new faults (Fault 1, 2 and 3). These newly interpreted faults are NE dipping normal faults.

Interestingly, the anomalies associated with these faults are not more than 0.5 mGal. The high gravity anomaly on the west side of the profile is related to the denser rocks of the Franklin Mountains. A mafic intrusion with density of 3 gm/cm^3 was added beneath the Franklin Mountains to match the observed and calculated gravity anomaly (Figure 2.7a). This mafic body has been used in several previous gravity models (Hadi, 1984; Burgos, 1993; Avilla, 2011; Marrufo, 2011). The northeast part of the study area with the lowest gravity values represents the deepest part (4.1 Km) of the basin within the study area. This profile closely resembles a cross section shown by Hawley (2004) based on well log data and helps to constrain the geology and position of the faults.

2.5.3 PROFILE BB'

Profile BB' is also an west-east extending profile which runs from the foothills of the Franklin Mountains along Loma Real Avenue and crosses Dyer Street and Railroad Drive (Figure 2.5). This profile is similar to AA' except for the presence of more newly identified faults, which do not cut profile AA'. From west to east, we observed six anomalies and interpreted these as normal faults (Figure 2.7b). Faults XVI, VII and IV are previously mapped faults by Collins and Raney (2000), whereas Faults 15, 14, 9 and 8 are newly recognized buried faults. Fault 23 coincides with the previously mapped Fault XVI. Most of the faults are east to north-east dipping, except Fault 9, which is dipping south-west. This fault can be extended to the south-east to join the south-west dipping fault (Fault IX) of Collins and Raney (2000) (Figure 2.8). Similarly, Fault 12 can be joined with the fault (Fault A) identified by Marrufo (2011) (Figure 2.8). We do not know if Fault 10 extends further to the south-east due to the lack of available data in the Fort Bliss area (east of Railroad Drive). The block between Fault 8 and Fault 9 represents a horst bounded on both sides by normal faults, which is consistent with structures mapped by Collins and Raney (2000) to the east of study area (Figure 2.8).

2.5.3 PROFILE CC'

Profile CC' is a south-west to north-east extending profile which runs along Railroad Drive, and cross profiles AA' and BB' (Figure 2.5). It cuts across most of the NW-SE striking structures. We identified 11 anomalies along this section and interpreted them as related to normal faults (Figure 2.7c). Three faults (Fault 1, 2 and 7) interpreted in this section coincide with the previously mapped faults (Fault I, II and VII) (Collins and Raney, 2000) (Figure 2.7c). This section also cuts across Fault 8 and Fault 9 and the block between them represents a horst as in profile BB'. Fault 12 interpreted in this section can be joined with the fault (Fault A) identified by Marrufo (2011). We do not know if Fault 10 extends further to the south-east due to the lack of available data in the Fort Bliss area (east of Railroad Drive) (Figure 2.8).

2.6 Well Log Analysis

Well logs provide insight on the different properties of sediments, minerals and fluids of an aquifer. These can be used to estimate hydrogeological properties such as Shale volume (Vsh), water resistivity (Rw) and salinity, and to correlate these values with specific rock formations from well to well. Nine EPWU water well logs were used in this study (Figure 2.4). Gamma ray, resistivity and spontaneous potential logs are commonly run in EPWU wells to estimate hydrogeologic properties. Also, the well log header for some wells includes borehole diameter, drilling fluid and mud properties, and temperature, which are very useful in correcting resistivity logs. Unfortunately, wells 29B, MNST03, MNST 05 and MNST 06 do not have information about drilling mud resistivity (Rm) and mud filtrate resistivity (Rmf). Thus we could not use these wells for water resistivity and salinity calculations, although we used these wells for correlation purposes.

The gamma ray log responds to natural radioactivity of minerals that are emitted from the decay of Uranium, Thorium and Potassium atoms. The gamma ray log is primarily used to differentiate coarse grained sandstone from shale, as quartz is often the principal component of sandstone and has little radioactivity. But care must be taken when other minerals, for example

feldspars, mica and heavy minerals, are present in the coarse grained sediments. These minerals contain radioactive elements and can lead to erroneous interpretations of fine grained sediments, which often have higher amounts of Uranium. Similarly, carbonates containing organic matter and evaporites with potassium content also show radioactivity, whereas pure carbonates and evaporites do not show strong gamma ray signatures. Patterns in the gamma logs are used to infer depositional environments, and correlate formations from well to well.

Resistivity, the inverse reciprocal of conductivity, is the ability of fluid and sediments to impede electrical current and has units of ohm-m. Resistivity depends on rock composition, formation fluid types, pore geometry, grain size and temperature. Some rocks, such as tight sandstone and limestone, salt, anhydrite, coal and gypsum, show high resistivity. When salt comes in contact with water, its resistivity greatly reduces. The saltier water has lower resistivity than the fresh water. The greater the salt concentration in the water, the greater the conductivity and lower the resistivity. A decrease in the sediment grain size also results in lower resistivity as the relationship between resistivity and grain size depends on irreducible water content in a mineral (Rider, 2002). Finer grain sediments have a larger surface areas and higher irreducible water compared to coarser grain sediments (Rider, 2002).

Most of the EPWU water well logs come with two resistivity curves- 16" (shallow) and 64" (deep) normal resistivity logs. Since resistivity is affected by borehole diameter, invasion and bed thickness, it is necessary to apply resistivity corrections so that the vertical resolution of beds and boundaries look similar to the gamma ray log (Serra, 1984; Doser and Langford, 2006). We applied resistivity corrections (bed thickness and bed boundary asymmetry) using excel spreadsheets outlined by Doser and Langford (2006). This correction is based on log spacing, borehole diameter, and the ratio of measured resistivity to drilling-fluid resistivity and based on the work of Serra (1984).

The spontaneous potential (SP) log measures the natural potential difference in millivolts (mV) between the well and the surface, and is commonly used to detect permeable beds, determine water resistivity (R_w), and evaluate salinity of formation water. Any deflection of the

SP log from the shale baseline indicates a contrast in salinity between the drilling fluids and formation water. The higher the deflection, the greater is the contrast. Deflection of the SP log to the left and right from a shale baseline indicates that the salinity of formation water is greater or less than that of the drilling fluid.

The empirical relationships used to derive water resistivity and water salinity from the SP log, drilling fluid resistivity and temperature logs are shown in equations 4, 5 and 6 which follow the procedures outlined in charts SP-1 and SP-2 in the Schlumberger Log Interpretation Chart (Schlumberger, 1991).

$$SSP = -K_c \mathrm{Log}(R_{mfeq}/R_{weq}) \text{----------} \quad \text{(eqn 4)}$$

$$K_c = (60 + 0.133T_f) \text{----------} \quad \text{(eqn 5)}$$

$$R_{mfe} = R_{mf}[(T_{mf} + 6.77)/(T_f + 6.77)] \text{----------} \quad \text{(eqn 6)}$$

Where,

SSP= Static SP (mV) [SP deflection opposite from the shale baseline]

R_{mfe}= Equivalent mud filtrate resistivity at formation temp (ohm-m)

R_{weq}= Equivalent formation water resistivity (ohm-m)

T_{mf}= Mud filtrate temperature (^{0}F)

T_f= Formation temperature (^{0}F)

After calculating water resistivity using the above equations, we determined the water salinity using the resistivity to salinity conversion formula (eqn 7) given by Asquith and Gibson (1982). Figure 2.9 shows the salinities calculated from the method described above. Comparison between the calculated salinity from the SP log and the salinity calculated from water sampling by EPWU is shown in Table 2.3. The salinity derived from the SP log approximately matches with the actual measurement determined from chemical analysis by EPWU except in well FBT 04. Water analysis of well FBT 04 indicates a brackish water quality. Because of lack of limited well log data and well log header information, our interpretations are limited. Still, it seems that a conversion from the SP derived water resistivity to salinity works well for fresh water wells.

Salinity=0.001/{exp[1.06355In(Rw(T-3.047)/129.953)-7.52144]-1.9*10^-6}---------- (eqn 7)

Alternatively, we can also determine R_w from the resistivity method and convert it into salinity using eqn 7. Calculating salinity from resistivity is useful in case of bad SP curve.

The relationship between water saturation (Sw), water resistivity (Rw), formation resistivity (Rt) and porosity (Φ) is given by Archie's equation (Archie, 1942) (eqn 8).

$S_w^n = aR_w / \Phi^m R_t$ ----------(eqn 8)

The cementation factor (m) depends on sediment type and shape, pore system, shaliness, specific surface area and degree of compaction (Salem, 2001). Common value of m for consolidated sandstone is between 1.8 and 2, and for unconsolidated sands is 1.3, respectively. The tortuosity factor (a) depends on compaction and consolidation of sediments, pore structure and grain size. The common value of a is considered to be 1. There are several published literatures available, which provide the valuable information about these Archie's parameters. It is important to note that Archie's equation break downs in the presence of fresh water and clay as this equation was derived for clean sand and saline water. Unfortunately, Archie's equation with traditional a and m value does not work in our study area as it contains both fresh water and shaly sand. The salinity converted from the resistivity log derived water resistivity is shown in Table 2.3, which gives higher salinity value.

2.7 Depositional Environments

Previous authors have analyzed grain size variation from cuttings in wells 601, 605, 610, 615 and 509A, and interpreted depositional environments based on grain size distribution and log responses (Doser and Langford, 2006; Marrufo, 2011). Most of the logs are provided with simple cutting descriptions by the EPWU based on the unified soil classification system which does not help much in inferring depositional environments. Due to the proximity of study area to the study area of Marrufo (2011), we used cuttings of well 601 as a reference and compared these to our log responses and the unified soil classification based lithology (Figure 2.10). We also used the

'electroseqence analysis' (Rider, 2002) or 'sequential analysis' (Rider, 1986) concept to decipher geological information from geophysical logs. This concept is based on identification of electrofacies (baselines, trends, shapes, abrupt breaks and anomalies) (Rider, 2002). We used gamma logs to identify these features, although multiple logs are desirable for this technique. Electrofacies is defined as *"a suite of wireline log responses and characteristics sufficiently distinctive to be able to be separated from other electrofaceis"*, which might be different from the 'facies' used in geological sense (Rider, 2002, p. 232). The depositional facies identified through log responses and their stacking patterns were stacked vertically and grouped together to form facies associations. One facies association can have single or multiple facies. After establishing characteristics facies, surfaces such as flooding surfaces, erosional surfaces, or unconformities were identified. We found this method very suitable for well log correlation. For example, a sandstone resting on the top of a shale and a shale sitting on the top of a sandstone were identified and interpreted as an erosional surface and flooding surface, respectively (Figure 2.10). Figure 2.10 also shows abrupt breaks in a log which indicates changes in lithology or a structural break (unconformity, fault etc).

Five facies inferred from logs of the Hueco bolson were grouped into four facies associations and their corresponding depositional environments (Table 2.4). Log characteristics, stacking patterns, and surfaces used to characterize depositional facies are presented in Figure 2.10. The facies associations are used as a guide to correlate wells. Bell, funnel, serrated and blocky shapes represent fining up, coarsening up, alternative fine and coarse grained, and no or little change in lithology, respectively.

2.7.1 CHANNEL FILL DEPOSIT FACIES

This facies shows variation in log response, thickness, and stacking pattern and varies from well to well. A sharp base with bell shaped to slightly cylindrical gamma log signature indicating channel fill deposits, is a very characteristic features of this facies. Rounded to well-rounded gravels and coarse sands of mixed lithology have been reported from cuttings that come

from this facies where clean gravels bearing units become sandier upward showing a typical bell pattern with a sharp base in the gamma ray log (Marrufo, 2011). In logs gravels are recognized as having low to moderate gamma readings and high resistivity. The high gamma with high resistivity signatures of conglomerates can be distinguished from high gamma with low resistivity of shales. The channel fill deposit correlates with the EPWU lithology descriptions of SW (well graded sands) and GP (poorly graded gravels).

Single to multi-storey channels superimposed on each other can clearly be observed in well logs. Based on the gamma response, the position of channel in the sedimentary sequences and grain size distribution, they can be further subdivided into two different distinct sub-facies. The first type of channel facies consists of thick, multi-storey, fining up channel deposits in which individual channels are separated by a sharp gamma peak. This facies can be interpreted to have been deposited in a braided channel system with episodes of flooding. The braided channel facies ranges from 20 to 60 ft in thickness. The second type of facies is single, isolated channels encased in shale or in finer sediments. Some logs show a conglomerate signature in this facies, but they are not common. They also vary in thickness from 10 to 30 ft. This facies is interpreted as channel fills intebedded with the alluvial plain deposits.

2.7.2 PROXIMAL ALLUVIAL FAN FACIES

The proximal alluvial facies is common at the foothills of the Franklin Mountains and can be best observed in well THNH1. Mostly this facies consists of poorly graded gravels (GW), silty gravels (GM), and clayey gravels (GP) and sometimes interbedded with shale. These are mostly thick, amalgamated, multi-storey conglomerate bodies that show serrated to slightly coarsening up shaped gamma log signatures. The serrated shape might be due to poor internal stratification or the lack of bed development, as in debris flow deposits. This coarsening up conglomerate dominant facies is interpreted to be a prograding proximal alluvial fan deposit.

2.7.3 DISTAL ALLUVIAL FAN FACIES

The distal alluvial fan facies consists of well graded gravel (GW), clayey gravel (GC), clayey sands (SC) and clay (CL). Typical log responses in this facies are serrated, bell, funnel and dumb-bell patterns and can be further divided into three sub-facies. The dumb-bell shape facies consists of alternating upward fining and coarsening upward, 15 to 35 ft thick facies suggesting abrupt changes in grain size. Another distinctive facies is the funnel shaped coarsening upward facies. These facies are 10-25 ft thick. Sequences that become coarser upward are interpreted as prograding alluvial fan deposits, while abrupt changes in grain size from lower coarser to upper finer grains are interpreted as due to flashy discharge with discrete flood events. The blocky facies are 20-30 ft thick; however, they are internally serrated and comprised of interbedded medium to fine grained sandstone and siltstone or shale. The serrated facies signifies sandy sheet-flood events and are interpreted as distal alluvial fan deposits. The serrated signatures are less developed in this facies than in the flood plain and deltaic facies and sandy-silty facies.

2.7.4 FLOOD PLAIN AND DELTAIC FACIES

Continuous, very thick, multi funnel shape facies stacked on top of each other and separated by high gamma peak makes this facies unique amongst others. Also, this facies consists of alternating fine and coarse grained sediments depicting a serrated pattern in the gamma log. In well logs, a funnel shaped gamma log response corresponds with increasing grain size from clay, silt to sand. Gravels are often identified in this facies. Flood plain deposits are characterized by alternating fine and coarse grained sediments making serrated shapes. A coarsening up facies with shale on the top represents prograding delta deposits with episodes of flooding.

2.7.5 Sandy-silty facies

There are two types of characteristic log responses in the sandy-silty facies. The most common one is a serrated pattern. Another pattern is blocky with internally serrated structure.

The blocky pattern suggests very little or no change in lithology, while the serrated pattern is evidence of alternating silty/sandy and clayey deposits. This facies can be found in several environments.

2.7.6 FACIES ASSOCIATIONS

Due to the limitation of available logs, distance between wells and complexity of the area, it is not easy to correlate all facies. The facies and the depositional environments can change vertically and laterally within a short distance. In order to overcome this problem, we grouped five facies and associated sub-facies described above into four facies associations according to environments of deposition. Figure 2.11 is a schematic representation of the depositional environments of the study area.

2.7.6.1 Facies Association 1

Facies association 1 is interpreted to have been deposited in the fluvial environment. The channel fill deposit facies is the dominant facies of this association. It consists of thin to thick bedded, single to multi-storey or isolated channel fill deposits with episodes of flooding. Due to the proximity of the Franklin Mountains, larger grain size, stacking patterns and the lack of observed point bar deposits, the channels are interpreted to be associated with braided systems; however, a meandering stream channels could be possible as there are numbers of finer grained, isolated channels with fining up sequences.

2.7.6.2 Facies Association 2

Facies association 2 is mainly dominated by gravel deposits in the proximal part and gravels to coarse grained sand deposits in the distal part of alluvial fan. The gravels in the distal alluvial fan are variably rounded with limestone and granite matrix and finer grained sands than fluvial deposits (Doser and Langford, 2006). Doser and Langford (2006) also observed coarse grained sands with sparse gravel clasts and compared this facies with the exhumed intervals of the Santa Fe group in the Hueco and Mesilla bolson.

2.7.6.3 Facies Association 3

Flood plain and deltaic facies and sandy-silty facies are grouped together in this association and interpreted to represent playa margin and deltaic deposits. This sequence is mainly composed of clays silts and silty clay with sands and gravels. ML (inorganic silts and very fine sands), CL (clays), SC (clayey sands), and GC (clayey gravels) are the major lithologies described in the EPWU based lithology which match the description provided by Doser and Langford (2006), and Marrufo (2011). These authors have also reported carbonate nodules and white silty sands and sandy silts in this unit.

2.7.6.4 Facies Association 4

This association contains sandy-silty facies. Just based on the unified soil classified system, this unit is difficult to separate from playa margin deposits, as it contains the same lithology. However, it has distinct log signatures compared to the playa margin. This unit shows repeated coarsening up cycles in the gamma log response. From the cuttings analysis, 10-100 ft thick, variegated silty clays and clayey silt have been reported. When the sediment load enters into the water body, the suspensed load settles out, leading to accumulation of fine grained sediments. The thick shale indicates a stable period of time, whereas alternating sands and clays or silty-clayey successions are the result of multiple sheet flooding or repetitive stream invasion (Mader, 1985).

2.8 Discussion

Figures 2.13 through 2.16 depict four structural cross sections with their tops at ground elevation. Well logs were correlated using Schlumberger's Petrel software. The locations of the sections, previously mapped faults by Collins and Raney (2000) and Marrufo (2011), and newly identified faults in this study are shown in Figure 2.12. Faults numbered with Roman numeral have the surface expressions that were mapped by Collins and Raney (2000). Faults labeled with alphabets are the faults mapped by Marrufo (2011) and the faults marked with numbers are the interpreted faults in this study. Seven key erosional surfaces (ES1-7) were identified based on

gamma and resistivity signatures that can be correlated between wells. In well logs, low gamma and high resistivity resting on the top of high gamma and low resistivity are the key features to identify these erosional surfaces.

Section p1p2 extending from the foothills of the Franklin Mountains to the east of Railroad Drive incorporates wells THNH1, TH43A, 29B, 40A, and FBT 04 (Figure 2.13). There are offsets between key surfaces in each well indicating faults in the location of which are in agreement with the interpretation made by the gravity study. Faults 14 and 15 were identified between wells THNH1 and TH43A, and both faults are east dipping. There is also an offset in underlying strata between wells TH 43A and 29B. Because of very limited gravity data between these wells, we were unable to locate faults based on gravity data between these two wells. Since these wells are located about 2.86 Km apart and covered by a highly urbanized area, it is difficult to pinpoint the exact location of the faults between wells TH 43A and 29B. Also, between wells 29B and 40 A, fault 12 was identified using gravity data. Interestingly, most of the erosional surfaces in well 29 B have dropped down to the east in well 40A except erosional surface ES 6. This implies that there might be two faults between these wells: east dipping fault 12 and another small subsurface fault that dips to the west. Faults 9, 10 and 11 were interpreted between wells 40A and FBT04. Faults 9 and 10 can be extended further southeast and joined with the Faults IX and X mapped by Collins and Raney (2000).

Section q1q2 extends from north to south and passes through wells E-3A, THNH2 and TH 43A (Figure 2.14). Faults 16, 17 and 18 were identified and located between wells E-3A and THNH2; however, we do not know the direction in which the faults strike (Figures 2.5 and 2.8). Additional gravity survey between McCombs Road and Martin Luther King Jr Boulevard would need to be conducted to identify the extension of these faults. But well log data suggests that at least one south to southwest dipping normal fault passes between these wells.

Section r1r2 is a northwest-southeast extending section which encompasses wells E-3A, MNST3, MNST2, MNST5 and FBT 04 (Figure 2.15). Here wells E-3A, MNST3 and MNST2 show stepwise normal faults. Interpreted faults (Fault 19 and 20), plus one additional previously

identified west dipping fault (Fault XV) are located between these wells. Unfortunately, the gravity data did not resolve this west dipping fault. Additional microgravity survey within this area will be helpful in locating position of these faults. Due to lack to microgravity data between Fault 10 and 25, we are unable to determine whether Fault 10 extends further north and merges with Fault 25 or if these are two separate faults. From the well log data, it is clear that the key surfaces of well MNST5 have dropped down with respect to well FBT04, which implies the existence of a down to the west fault (Fault 9) (Figures 2.8 and 2.15).

s1s2 is another north-south trending profile which extending from well MNST6 encompassing well MNST3 and 40A and ending with well 601 in the south (Figure 2.16). Fault 7 is previously identified by Collins and Raney (2000) and is apparent in this study as well (Figure 2.12). Section s1s2 cuts across this fault between wells MNST6 and MNST3. We identified faults three faults (Fault 12, 24 and 27) between well MNST3 and 601. The offset in strata between wells 40A and 601 represents Fault 12. A small fault dipping southwest near well 40A probably represents the fault between wells MNST3 and 40A; however, additional data are desirable to prove this.

Four stratigraphic sections were created along the same structural profile to determine change in geometry and thickness of the sediments (Figures 2.17-2.20). Stratigraphic sections were created by hanging all logs along the first erosional surface ES1 (Figures 2.17-2.20). Compare to east west sections, the north-south stratigraphic sections (q1q2 and s1s2) show very little change in thickness (Figures 2.17 and 2.18). The p1p2 section shows dramatic change in sediment thickness between erosional surfaces from east to west (Figure 2.17). Wells THNH1 and TH43A show thick sedimentary units that gradually thin towards east. In all sections, the downthrown side of the faulted block is thicker than the upthrown side, which suggests continuous deposition of the sediments in the hanging wall during faulting.

The salinity of the Hueco Bolson varies from well to well and the groundwater quality degrades with the depth and to the north, east and south (Figure 2.21). Compared to the southern Hueco bolson, there are few wells in the northern region and they are located far apart. This

makes it difficult to judge the true distribution of the Total Dissolved Solid (TDS) anomaly across the study area. Concentration of TDS is used to characterize the water quality and chloride is one of the components of the TDS. The potable limit of TDS and chloride concentration in Texas is 1000 mg/L and 250 ppm, respectively. Paine and Collins (2002) have mentioned two schemes of salinity classification based on TDS concentration in their report, which is shown in Table 2.5. In our study we have used the salinity classification scheme of Freeze and Cherry (1979) in which water with salinity greater than 1000 mg/L is considered as brackish water.

It has been observed that the Chloride limit often exceeds drinking water standard before TDS in some of the wells in Hueco bolson (Bredehoeft, et al., 2004). For this reason, Chloride concentration data can be used alternatively to map the distributions in salinity (Bredehoeft, et al., 2004). Chloride concentration between 250-500 mg/l is considered as transitional between fresh and brackish water. Several possible causes such as sewage outfalls, irrigation activities, and river/aquifer hydrodynamics have been suggested as the possible sources of salinity in the Hueco Bolson (Hibbs and Darling, 2005; Hibbs and Merino, 2006). Based on study of Cl/Br ratios at San Elizario Island near Fabens, Hibbs and Merino (2006) suggested upwelling of saline water from deeper sources as a primary factor in salinization.

Because of sparsely distributed wells and the poor quality of well logs in the northern Hueco bolson, well log data are not sufficient to depict salinity distributions over study area (Figure 2.23). We used Chloride concentration maps prepared by Bredehoeft et al. (2004) to aid in our interpretations (Figure 2.22 through 2.25). Figures 2.22, 2.23, 2.24 and 2.25 show interpreted faults and Chloride concentration maps at elevation 1048.48, 1024.43, 904.34 and 731.52 m respectively. It can be clearly observed that the Chloride concentration is increasing with decreasing elevations or increasing depth. Assuming a 1219.20 m (4000 ft) average elevation in the study area, Chloride concentration maps at elevation 1048.48, 1024.43, 904.34 and 731.52 m correspond to 134.72, 194.77, 314.86 and 487.68 m depth, respectively.

At a depth of 134.72 m fresh to transitional water dominates the study area except in the eastern part where Chloride concentration is very high and represents a brackish water zone.

Well THNH1 is located in this area (Figure 2.22). At this depth there are also some other pockets of brackish water zone. Interestingly, they are separated from fresh or transitional water zones by faults as shown in Figure 2.12. From 134.72 to 194.77 m depth, water quality changes from the fresh to transitional salinities, as indicated by blue to turquoise blue color (Figure 2.23). Similarly, Chloride concentration in the pockets of brackish water zone increases at this depth. Water quality at depths 314.86 and 487.68 m is brackish except in the area depicted by blue to turquoise blue color (Figures 2.24 and 2.25). Note that on the east side of Martin Luther King Boulevard the salinity is extremely high (with greater than 1000 mg/l chloride concentration) it and remains constant at all depths (Figures 2.22-2.25). This area lies in the vicinity of the East Franklin Boundary Fault Zone. Also, numbers of other smaller new faults have identified within this area (Figures 2.12 and 2.22).

The dual behavior of a fault has been reported by several authors (Rawling et al., 2001; Bense et al., 2003; Bense and Person, 2006). Faults can act as a barrier to lateral groundwater flow and thus prevents invasion of brackish water into fresh water. They can also provide migration pathway along the fault plane for deep aquifer water to enter into shallow groundwater aquifers as in South Louisiana (Stoessel and Prochaska, 2005) and thus cause mixing of deep brine water with shallow groundwater. Cataclasis, particulate flow, clay smearing and diagenesis are major deformation processes that reduce the effect of hydraulic conductivity in the fault zone (Bense et al., 2003). Clay is considered as a primary factor for controlling lateral movement of fluids in the faulted segments (Bense and Person, 2006). Marrufo (2011) noticed that clay volume in the Hueco basin increases towards the east from well 601 to 610, creating hydraulic anisotropy and impeding the flow of brackish water into the freshwater zone. We also observed the similar trend between wells MNST5 and FBT04 and between MNST3 and MNST2 where volume of clay increases gradually to the east. The distribution of Chloride concentration, presence of Quaternary faults, and increase in clay volume indicate the controlling role of faults in the fresh-brackish water contact. We made a slightly unusual observation in well NHH1 where water is brackish at shallow depth. Because this well is located just near the deep East Franklin

Boundary fault there might be a possibility that the shallow aquifer is somehow connected to deep saline aquifer and fault served as a conduit for fluids mixing freshwater with brackish water, as in South Louisiana where contamination of freshwater with brackish water is mainly due to halite dissolution (Stoessel and Prochaska, 2005). However, our speculation remains open until further research is carried out.

2.9 Conclusions

The microgravity survey was effective method in identifying small displacement faults in a highly urbanized environment. We noted 28 gravity anomalies that correlate with previously mapped and new faults. The East Franklin Boundary fault was recognized by a sharp change in gravity gradient; however, other smaller faults do not show an obvious change in gravity values, as they exhibit of less than 0.6 mGal. By careful comparison of Bouguer gravity to change in elevation and distance between gravity stations seems to be an effective method to recognize such small anomalies. This interpretation technique can be misleading when combined with previously collected gravity data if the gravity stations are too apart or the associated data errors are large. The interpreted faults appear to coincide with the freshwater brackish water boundary determined from limited water well information.

The gamma log responses and their stacking patterns were used to infer depositional environments. Based on electrofacies (baselines, trends, shapes, abrupt breaks and anomalies), five facies, namely channel fill deposit, proximal alluvial fan, distal alluvial fan, flood plain and deltaic, and sandy silty facies, were grouped into four facies associations corresponding to fluvial, alluvial, playa margin and playa lake environments. Identification of these depositional environments is consistent with the previous interpretation of Doser and Langford (2006) and Marrufo (2011).

Seven erosional surfaces identified in gamma and resistivity logs were used for well log correlation. Structural cross sections were created from ground elevation level, whereas first erosional surface (ES1) were used to create stratigraphic cross sections. The structural cross

sections support the interpretation of faults made from the microgravity survey. The stratigraphic correlation suggests less change in thickness of sediments in a north-south direction, while we observe abrupt changes in thickness from west to east.

The salinity calculated from the SP log generally resembles the true water salinity determined from the water salinity by EPWU. It can serve as a 'quick look' method to calculate salinity. Due to limited available logs and lack of log header information, determining Rw from resistivity is challenging. Salinity calculation using traditional values of Archie's parameters (a and m) gives higher salinity values. It is recommended to use Poupon-Leveaux (Indonesian) or Waxman-Smits-Thomas and dual-water equations for shaly sand aquifers, which is an area of future research.

2.10 Acknowledgments

This research was partly supported by the West Texas Geological Society (WTGS). Pawan Budhathoki was a recipient of the 2013 WTGS Terra Nova Scholarship. The authors are very grateful to Alfredo Ruiz of El Paso Water Utilities for providing the well logs. The authors thank Galen Kaip, Niti Mankhemthong, Felix Ziwu, Victor Avilla, Martin Sandoval, Mark Lucero, and Alay Gebregiorgis for assisting in the fieldwork. The authors thank Sandy Marrufo for providing the gravity data used in this study. We would also like to thank Dr. Mark Baker for discussions related to well log analysis and Carlos Montana for handling computer problems.

References

Albritton, C.C., Jr., Smith, J.F. Jr., 1965, *Geology of the Sierra Blanca area, Hudspeth County, Texas*: U.S. Geological Survey Professional Paper 479, 131 p.

Anderholm, S.K., and Heywood, C.E., 2003, *Chemistry and age of ground water in the southwestern Hueco Bolson, New Mexico and Texas:* U.S. Geological Survey Water-Resources Investigations Report 02-4237, 16 p.

Ashworth, J.B., 1990, Evaluation of groundwater resources of the El Paso Valley, Texas, Texas Water Development Board, open-file report.

Asquith, G., and Gibson, C., 1982, *Basic well log analysis for geologists*: AAPG Methods in Exploration Series, 216 p.

Avilla, V.M., 2011, *An investigation of the seismic hazards of the el paso-juarez region: The nature and extent of the southern east franklin mountains fault zone*: Unpublished M.S. Thesis, Univ. of Texas at El Paso, El Paso, TX, 51 p.

Baldridge, W.S., Olsen, K.H., and Callender, J.F., 1984, Rio Grande rift: problems and perspectives: *New Mexico Geological Society Guidebook Rio Grande Rift*, No. 35, pp. 1-12.

Baldridge, W.S., 2004, *Geology of the American Southwest A Journey through Two Billion Years of Plat-Tectonic History*: Cambridge University Press, 280 p.

Bense, V. F., Van den Berg, E. H., and Van Balen, R. T., 2003, Deformation mechanisms and hydraulic properties of fault zones in unconsolidated sediments; the Roer Valley Rift System, the Netherlands: *Hydrogeology*, Vol. 11, pp. 319-332.

Bense, V.F., and Person, M.A., 2006, Faults as conduit-barriers to fluid flow in siliclastic Sedimentary aquifers: *Water Resources Research*, Vol. 42, W05421, pp. 1-18.

Bickford, M.E., Soegaard, K., Nielsen, K.C., and McLelland, J.M., 2000, Geology and geochronology of Grenville-age rocks in the Van Horn and Franklin Mountains area, west Texas: Implications for the tectonic evolution of Laurentia during the Grenville: *Geological Society of America Bulletin*, Vol. 112, pp. 1134-1148.

Bredehoeft, J., Ford, J., Harden, B., Mace, R., Rumbaugh, J., III., 2004, *Review and interpretation of the Hueco Bolson groundwater model: Prepared for El Paso Water Utilities* Report 39: Electronic document, available at www.epwu.org/water/hueco_bolson.html

Buck, B.J., Kipp, J.M., Jr., and Monger, H.C., 1998, Eolian stratigraphy of intrabasinal fault depressions inthe northern Hueco and southern Tularosa Basins: Evidence for neotectonic activity: *New Mexico Geological Society*, 49th Field Conference, pp. 79-86.

Burger, Robert H., 1992, *Exploration geophysics of the shallow subsurface*: Prentice Hall, New Jersey, 489 p.

Burgos, A., 1993, *A gravimetric study of the thickness of the unconsolidated materials in the Hueco Bolson aquifer, Juarez area, Chihuahua Mexico*: Unpublished M.S. Thesis, Univ. of Texas at El Paso, El Paso, TX, 259 p.

Burrows, L., 1984, *A gravity and magnetic survey in the Hueco Mountains, Western Diablo Pleteau, Texas*: Unpublished M.S. Thesis, Univ. of Texas at El Paso, El Paso, TX, 54 p.

Bjorlykke, K., 1989, *Sedimentology and Petroleum Geology*: Springer-Verlag, Berlin, 363p.

Chapin, C. E., 1971, The Rio Grande rift part 1: modifications and additions: *New Mexico Geological society*, Annual Field Conference Guidebook, No.22, pp.191-201.

Chapin, C.E., and Seager, W.R., 1975, Evolution of the Rio Grande rift in the Socorro and Las Cruces areas: *New Mexico Geological Society Guidebook*, 26th Field Conference., pp. 297-322.

Collins, E. W., and Raney, J. A., 1991, Tertiary and Quaternary Structure and Paleotectonics of the Hueco Basin, Trans-Pecos Texas and Chihuahua, Mexico: The University of Texas at Austin, Bureau of Economic Geology, Geological Circular 91-2, 44p.

Collins, E. W., and Raney, J. A., 2000, Geologic map of West Hueco Bolson, El Paso Region, Texas: The University of Texas at Austin, Bureau of Economic Geology, Miscellaneous Map No. 40, scale 1:100,000, 24 p.

Doser, D.I., and Langford, R.P., 2006, *Characterization of Aquifer Extent and Quality for Desalination and Brine Disposal Projects*: Report W-06-04.

Freeze, R. A., and Cherry, J. A., 1979, *Groundwater*: Prentice-Hall, Englewood Cliffs, New Jersey, 604 p.

Granillo, J.A., 2004, *A gravimetric study of the structure of the northeast portion of the Hueco Bolson, Texas employing GIS technology*: Unpublished M.S. Thesis, Univ. of Texas at El Paso, El Paso, TX, 127 p.

Gustavson 1990, Timing and effects of integration of the northern and southern segments of the ancestral Rio Grande, Hueco Bolson, West Texas: *Geological Society of America Abstracts with Programs*, Vol. 22, p. 22.

Gustavson, T. C., 1991, Arid basin depositional systems and paleosols: Fort Hancock and Camp Rice Formations (Pliocene-Pleistocene) Hueco Bolson, West Texas and adjacent Mexico: The University of Texas at Austin, Bureau of Economic Geology, Report of Investigations 198, 49 p.

Hadi, J., 1991, *A Study of the structure and subsurface geometry of the Hueco Bolson*: Unpublished M.S. Thesis, Univ. of Texas at El Paso, El Paso, TX, 88 p.

Hawley, J. W., and Kennedy J.F., 2004, Creation of a Digital Hydrogeological Framework Model of the Mesilla Basin and Southern Jornada del Muerto Basin: *WRRI Technical Completion Report*, 332, 105 p.

Hawley, J.W., and Kernodle, J.M., 2000, Overview of the hydrogeology and geohydrology of the northern Rio Grande basin—Colorado, New Mexico, and Texas. In Ortega-Klett, C.T. (Editor), *Proceedings of the 44th Annual New Mexico Water Conference*, New Mexico Water Resources Research Institute Report 312, pp. 79-102. Available at http://wrri.nmsu.edu/publish/watcon/proc/proc44/contents.html

Hawley, J.W., Kennedy, J.F., Hibbs, B.J. and Cleary, M., 2002, Basin-fill aquifers of the southern New Mexico border region, USA and Mexico: Their hydrogeologic framework, and related aspects of groundwater flow and chemistry. In Integrated Trans-boundary Water Management: *Proceedings of a special joint conference of Universities Council on Water Resources (UCOWR), Environmental & Water Resources Institute of ASCE (EWRI), U.S. Army Corps of EngineersInstitute for Water Resources (CEIWR), and National Ground Water Association (NGWA)*, pp.164-172.

Hawley, J.W., Kennedy, J.F., Grandos-Olivas, A., and Ortiz, M.A., 2009, Hydrogeologic Framework of the Binational Western Hueco Bolson-Paso del Norte Area, Texas, New Mexico, and Chihuahua: Overview and Progress Report on Digital-Model Development: *New Mexico Water Resources Research Institute*, Technical Completion Report 349, 45 p.

Henry, C.D., and Price, J.G., 1985, Summary of the tectonic development of Trans-Pecos Texas: The University of Texas at Austin, Bureau of Economic Geology, Miscellaneous Map No. 36, 8 p.

Heywood, C.E., and Yager, R.M., 2003, *Simulated ground-water flow in the Hueco Bolson, an Alluvial-basin aquifer system near El Paso, Texas*: U.S. Geological Survey Water-Resources Investigations Report 02-4108, 55 p.

Hibbs, B. J., and Merino, M., 2006, A geologic source of salinity in the Rio Grande aquifer near El Paso, Texas: *New Mexico Journal of Science*, Vol. 46, pp. 165-181.

Hoffer, J.M., 1970, Petrology and mineralogy of the Campus andesite pluton, El Paso, Texas: *Geological Society of America Bulletin*, Vol. 81, pp. 2129–2136.

Hutchison, W.R., 2006, *Groundwater Management in El Paso, Texas*: Unpublished Ph.D. Dissertation, Univ. of Texas at El Paso, TX, El Paso, 329 p.

Keller, G.R., Morgan, P. and Seager, W.R., 1990, Crustal structure, gravity anomalies and heat flow in the southern Rio Grande rift and their relationship to extensional tectonics: *Tectonophysics*, Vol. 174, pp. 21-37.

Keller, G.R., and Baldridge, W.S., 1999, The Rio Grande Rift: A Geological and Geophysical Overview: *Rocky Mountain Geology*, Vol.34, pp. 121-130.

Kernodle, J.M., 1992, *Summary of U.S. Geological Survey ground-water-flow models of basin-fill aquifers in the southwestern alluvial basins region, Colorado, New Mexico, and Texas*: U.S. Geological Survey, Open-file Report 90-361, 81 p.

LeMone, 1983, Stratigraphy of the Franklin Mountains, EI Paso County, Texas, and Dona Ana County, New Mexico. In Allen, R. (Editor), *Delaware Basin*: West Texas Geological Society Publication, 82–76, pp. 85–87.

Lovejoy, E.M., 1975, An Interpretation of the Structural Geology of the Franklin Mountains, Texas: *New Mexico Geological Society Guidebook*, 26th Field Conference, Las Cruces, pp. 261-268.

Lowrie, W., 1997, *Fundamentals of Geophysics*: Cambridge University Press, 354 p.

Mack, G.H., and Leeder, M.R., 1998, Channel shifting of the Rio Grande, southern Rio Grande rift: implications for alluvial stratigraphic models: *Sedimentary Geology*, Vol.117, pp. 207-219.

Mack, G.H., Seager, W.R., Leeder, M.R., Perea-Arlucea, M., and Salyards, S.L., 2006, Pliocene and Quaternary history of the Rio Grande, the axial river of the southern Rio Grande rift, New Mexico, USA: *Earth-Science Reviews*, Vol. 77, pp. 141-162.

Mader, D., 1985, Braidplain, floodplain and playa lake, alluvial-fan, aeolian and palaeosol facies composing a diversified lithogenetical sequence in the Permian and Triassic of South Devon (England). In Mader D. (Editor), *Aspects of Fluvial Sedimentation in the Lower Triassic Buntsandstein of Europe.* Lecture Notes in Earth Sciences, Berlin, Vol. 4, pp. 15-64.

Mader, G. L., Weston, N. D., Morrison M. L., and Milbert, D. G., 2003, The On-line Positioning User Service (OPUS), *Professional Survey Magazine*, May 2003: Electronic document, available at www.profsurv.com

Marrufo, S.S., 2011, *An integrated geological and geophysical study of the fresh and brackish water boundary in the Hueco bolson, West Texas*: Unpublished M.S. Thesis, Univ. of Texas at El Paso, El Paso, TX, 108 p.

McMillan, N. J., Dickin, A. P., and Haag, D. 2000, Evolution of magma source regions in the Rio Grande Rift, southern New Mexico: *Geological Society of America Bulletin*, Vol. 112, pp. 1582–1593.

Morgan, P. and Golombek, M. P., 1984, Factors controlling the phases and styles of extension in the northern Rio Grande rift, *New Mexico Geoogical Society Guidebook., 35th Field Conf.*, 13–19.

Morgan, P., Seager, W. R., Golombeck, M. P., 1986, Cenozoic thermal, mechanical and tectonic evolution of the Rio Grande rift: *Journal of Geophysical Research*, Vol. 91, pp. 6263-6276.

Paine, J. G., and Collins, E. W., 2002, *Evaluating potential groundwater resources on State Lands in El Paso County, Texas using airborne geophysics*: report prepared for the General Land Office under contract no. 02-306R, 87 p.

Rawling, G.C., Goodwin, L.B., and Wilson, J.L., 2001, Internal architecture, permeability structure, and hydrologic significance of contrasting fault zone types: *Geology*, Vol. 27, pp. 43–46.

Richardson, G.B., 1909, *Description of the El Paso quadrangle, Texas*: U.S. Geological Survey Folio Series 166, 11 p.

Rider, M.H., 1986, *The geological interpretation of well logs*, John Wiley & Sons, New York, Whittles Publishing, 175 p.

Rider, M. H., 2002, *The geological interpretation of well logs*, 2nd edition: Rider-French Consulting Ltd, 280 p.

Riley, R. 1984, *Stratigraphic Facies Analysis of the upper Santa Fe Group, Fort Hancock and Camp Rice Fromations, Far West Texas and South-Central New Mexico*: unbuplished M.S. Thesis, Univ. of Texas at El Paso, El Paso, TX, 109 p.

Robinove, C. J., Langford, R. H., and Brookhart, J. W.,1958, *Saline-water resources of North Dakota*: U.S. Geological Survey, Water-Supply Paper 1428, 72 p.

Schlumberger, 1991, *Log Interpretation Charts*, Houston, Schlumberger, 172 p.

Seager, W.R., 2004, Laramide (late Cretaceous to Eocene) tectonics of southwestern New Mexico; in Mack, G.H., and Giles, K.J., eds., The Geology of New Mexico: A geologic history: *New Mexico Geological Society*, Special Publication 11, pp. 183-202.

Seager, W.R., and Mack, G.H., 1986, Laramide paleotectonics of southern New Mexico: *American Association of Petroleum Geologists Memoir*, Vol. 41, pp. 669-685.

Seager, W.R., Shafiqullah, M., Hawley, J.W., and Marvin, R.F., 1984, New K-Ar dates from basalts and the evolution of the southern Rio Grande: *Geological Society of America Bulletin*, Vol. 95, No.1, pp. 87-99.

Serra, O. 1984, *Fundamentals of Log Interpretation*, Vol. 1, Elsevier Press.

Stoessel, R. K., and Prochaska, L., 2005, Chemical evidence for migration of deep formation fluids into shallow aquifers in South Louisiana, Trans: *Gulf Coast Assoc. Geol. Soc*., Vol.55, pp. 794-808.

Strain, W. S., 1966, Blancan mammalian fauna and Pleistocene formations, Hudspeth County, Texas: *Texas Memorial Museum Bulletin,* No. 10, 55 p.

Strain, W. S., 1971, Late Cenozoic bolson integration in the Chihuahua tectonic belt. In Hoffer, J.M. (Editor), *Geologic framework of the Chihuahua tectonic belt*: West Texas Geological Society 71-59, pp. 167–173.

Stuart, C.J., and Willingham, D.L., 1984, Late Tertiary and Quaternary fluvial deposits in the Mesilla and Hueco bolsons, El Paso area, Texas: *Sedimentary Geology,* Vol. 38, pp. 1-20.

Talwani, M., Heirtzler, J.R., 1964, Computation of magnetic anomalies caused by two-dimensional structures of arbitrary shape, computers in the mineral industries: *School of Earth Sciences*, Stanford University (Publication), pp. 464-480.

Talwani, M.,Worzel, J.L., Landisman, M., 1959, Rapid gravity computations for two dimensional bodies with applications to the Mendocino Submarine Fracture Zone: *Journal of Geophysics,* Vol. 64, pp. 49-59.

Vanderhill, J.B., 1986, *Lithostratigraphy, vertebrate paleontology, and magnetostratigraphy of Plio-Pleistocene sediments in the Mesilla Basin, New Mexico*: Unpublished Ph.D. dissertation, The University of Texas, Austin, TX, 311p.

Willingham, D.L., 1980, *Stratigraphy and sedimentology of the upper Santa Fe Group in the El Paso regions, West Texas and South central New Mexico*: Unpublished M.S. Thesis, Univ. of Texas at El Paso, El Paso, TX, 93 p.

Table 2.1: Summarizing properties of Golf base station and UTEP KIDD station

	Golf Base Station	UTEP KIDD Station
Latitude	31.95671484	31.78936111
Longitude	-106.4062014	-106.5064167
Elevation (m)	1217.769	1186.5
Absolute Gravity (mGal)	979085.48	979107.52

Table 2.2: Density values used in gravity modelling based on Hadi (1991)

Age/ Formations	Lithology	Density(gm/cm^3)
Quaternary	Shale, sandstone	2.2
Tertiary	Shale, Sandstone	2.4
Paleozoic	Shale, Sandstone, Limestone, Dolomite	2.5
Precambrian	Granite	2.7
?	Mafic Intrusion	3

Table 2.3: Comparison of water salinity determined from water analysis by EPWU and salinity derived from the SP and resistivity logs

Well	Depth (ft)	Measured water salinity by EPWU (mg/L)	Water resistivity (Rw) determined from the SP log	Calculated salinity from the SP log using eqn 7	Calculated salinity from the resistivity log
40A	750	340	9.62	311	1390.05
TH 43A	560	766	3.58	892.64	3860.92
	680	1168	2.36	1393.21	1735.75
	720	1166	2.36	1393.21	3158.42
	820	1459	2.36	1393.21	6005.07
	953	973	3.12	1033.87	4351.98
FBT 04	990	3954	1.92	1735.02 **	7512
601	400	unknown (*)	5.22	597.49	2893.46
	500	unknown (*)	6.37	483.08	1809.11
	600	unknown (*)	6.37	483.08	6101.89
	750	unknown (*)	6.71	457.34	3749.32

*The water quality of well 601 is considered as fresh water.
** The quality of water in well FBT 04 is brackish.

Table 2.4: Facies, geophysical log characteristics and interpreted depositional environment

Facies	Geophysical log characteristics	Description	EPWU Description	Depositional Environment
Channel fill deposit facies	Sharp base with bell shaped to slightly cylindrical gamma signatures, gravels are recognized as low to moderate gamma reading and high resistivity	Rounded to well-rounded gravels and coarse sands of mixed lithology; thick, multi-storey, fining up channel deposits; isolated channel encased in shale	SW, GP, CL	Braided channel, alluvial plain
Proximal alluvial fan facies	Serrated to slightly coarsening up (funnel)	Thick, amalgamated, multi-storey conglomerate bodies	GW, GM, GP, CL	Proximal alluvial fan
Distal alluvial fan facies	Serrated, bell, funnel and dumb-bell patterns	Variable rounded with limestone and granite matrix and more fine grained sands than fluvial deposits	GW, SC, CL	Distal alluvial fan
Flood plain and deltaic facies	Several funnel shape facies stacked with each other and separated by high gamma peaks	Increasing grain size from clay, silt to sand, alternating fine and coarse grained sediments; gravel present sometimes	ML, CL, SC, GC	Play margin, Deltaic, Flood plain
Sandy silty facies	Serrated; blocky with internally serrated structure	Alternating silty/sandy and clayey deposit; variegated silty clays and clayey silts	ML, CL, SC, GC	Playa margin, Deltaic, Playa lake

Table 2.5: Salinity classification scheme based on TDS concentration

Classification (Robinove et al., 1958)	TDS range (mg/L)	Classification (Freeze and Cherry, 1979)
Fresh	0-1000	Fresh
Slightly saline	1000-3000	
Moderately saline	3000-10000	
Very saline	10000-35000	
Briny	35000	
	1000-10000	Brackish
	10000-100000	Saline
	100000	Brine

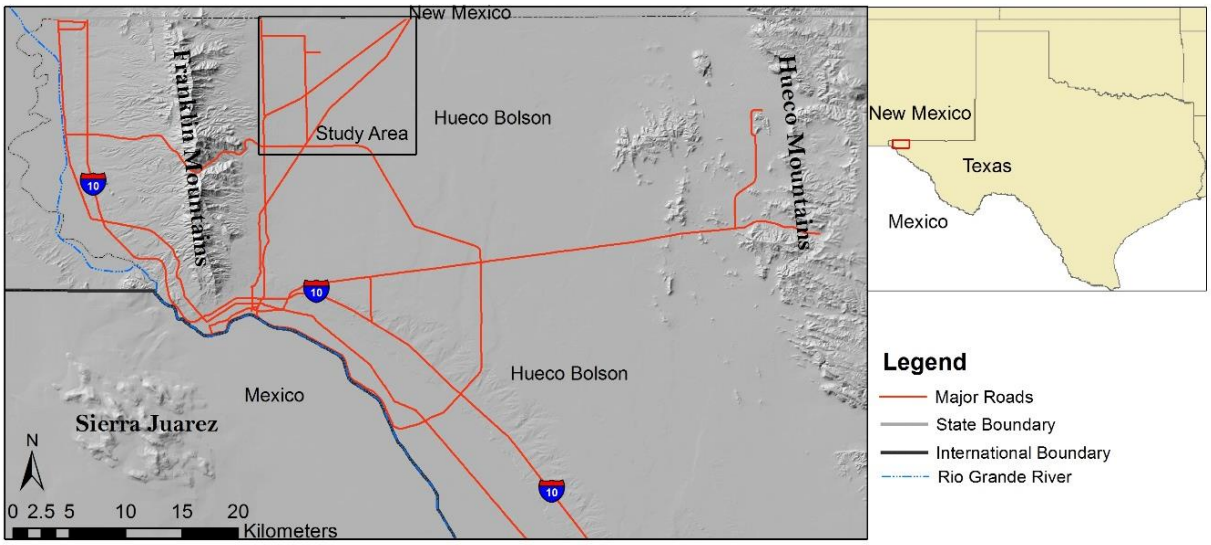

a)

b)

Figure 2.1: a) Location map of the study area. b) Outline of the Hueco basin which is bounded by Tularosa basin in the north and Mesilla basin in the west. Our study area lies in the northern part of the Hueco basin. (See Figure 2.1a)

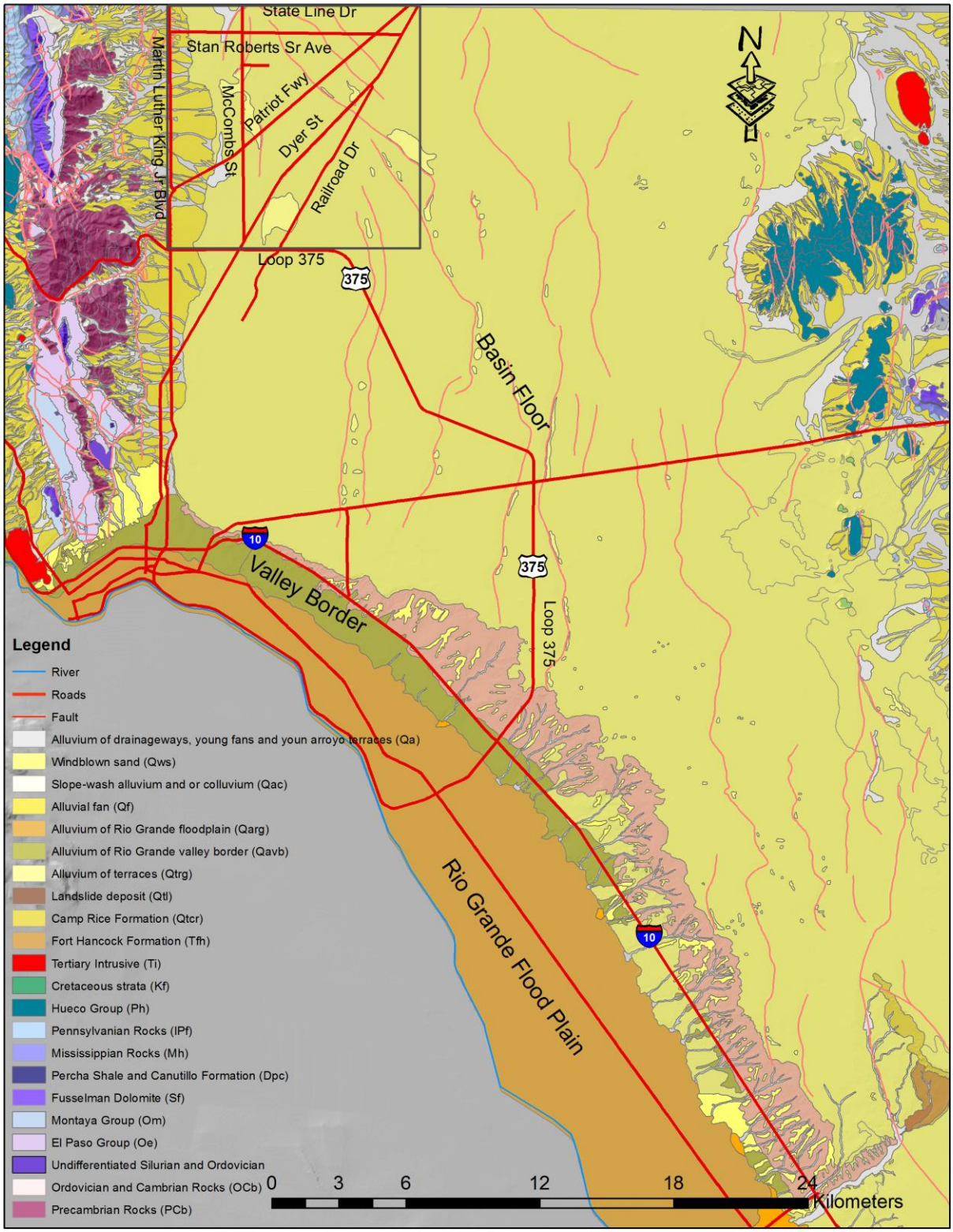

Figure 2.2: Geological map of the northern Hueco basin (Modified after Collins and Raney, 2000)

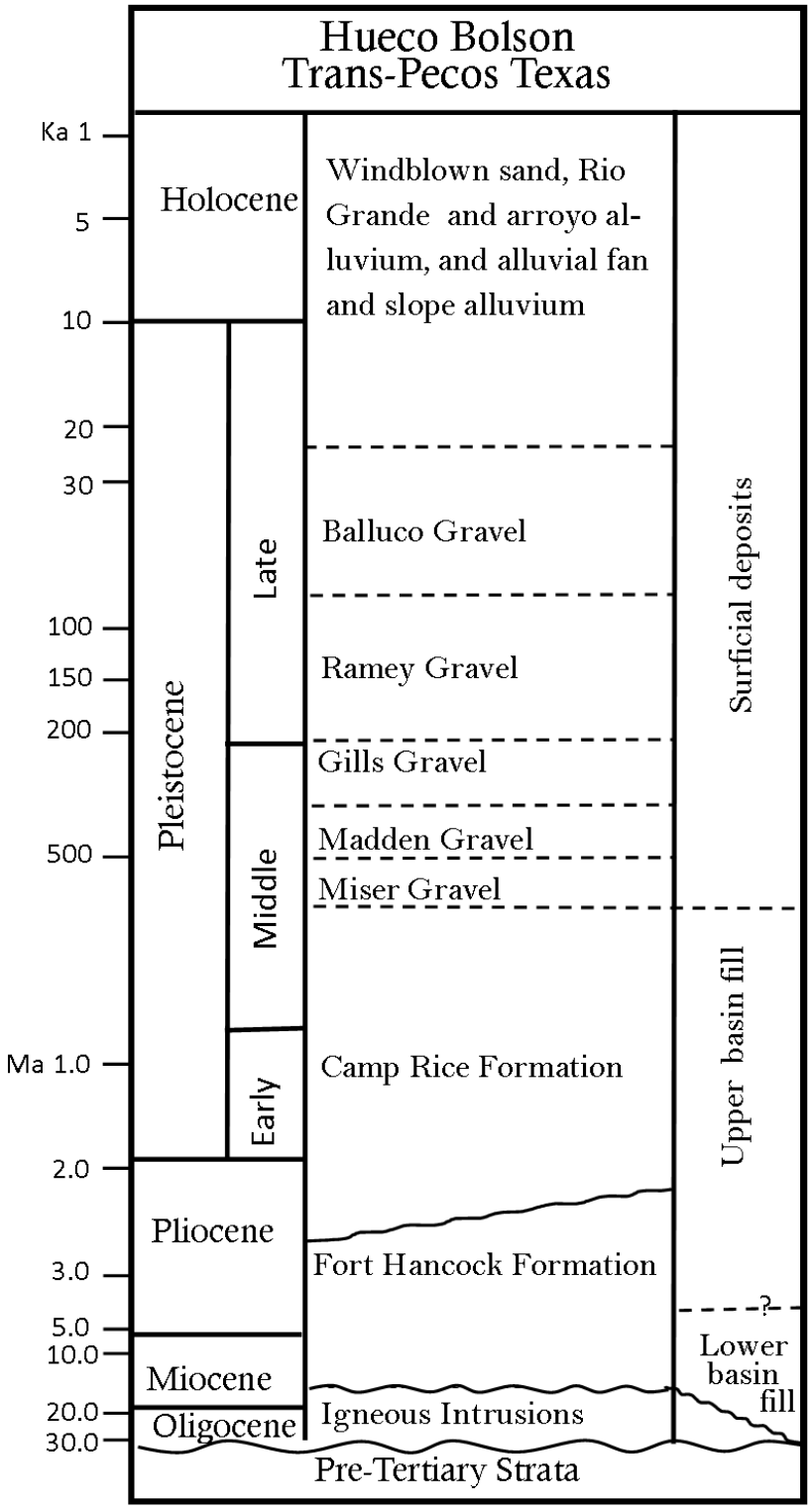

Figure 2.3: Hueco bolson stratigraphy (Modified after Collins and Raney, 2000)

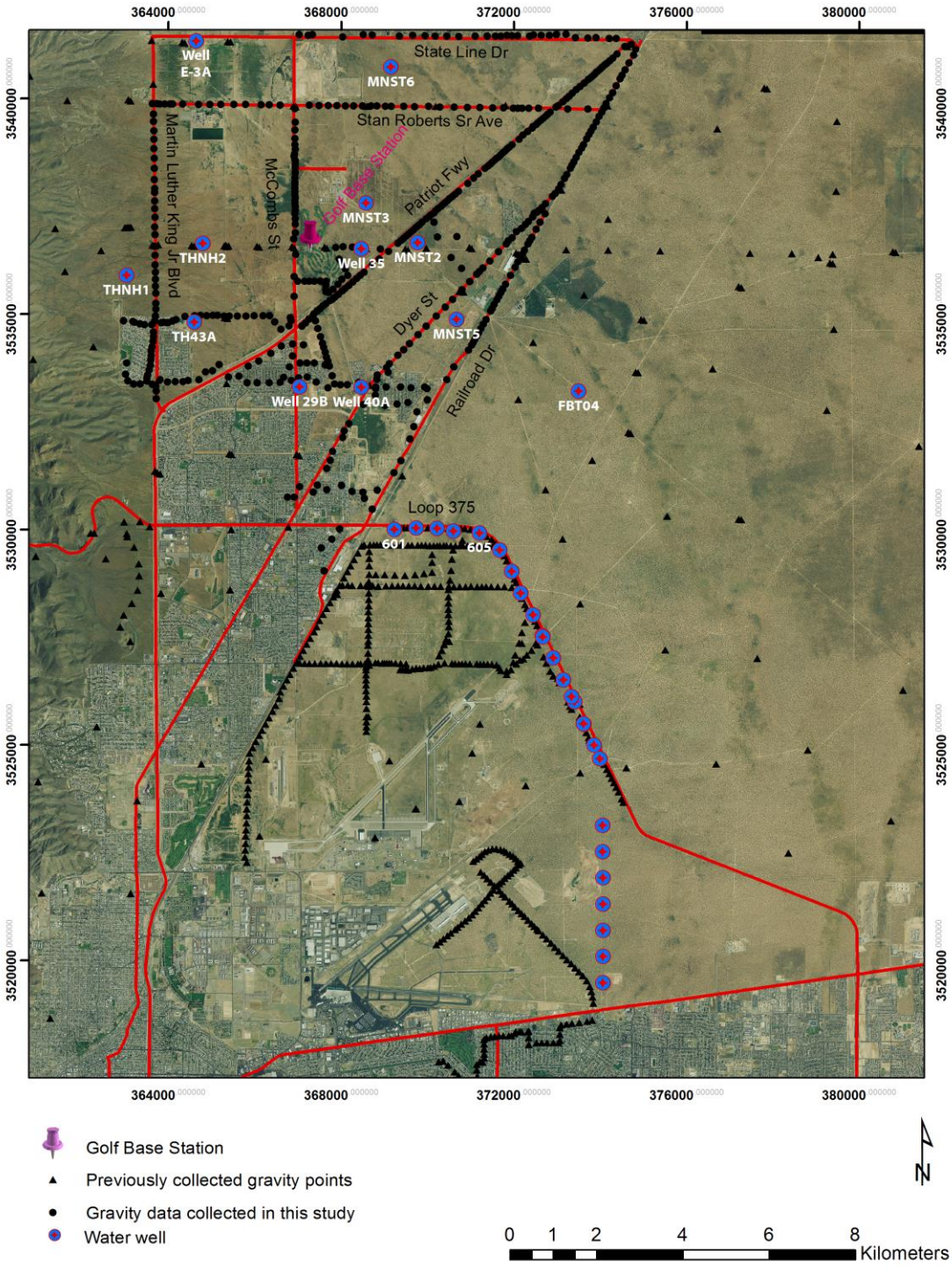

Figure 2.4: Map showing location of gravity stations and wells. Black dots represent the gravity data collected during this study. The gravity survey was performed with 75 to 300 m spacing using a Lacoste and Romberg model G-1115 gravity meter. Triangle signs are gravity stations previously collected by Marrufo (2011) and others. These data are available at the UTEP-PACES website. Water wells are indicated by star inside the circle signs.

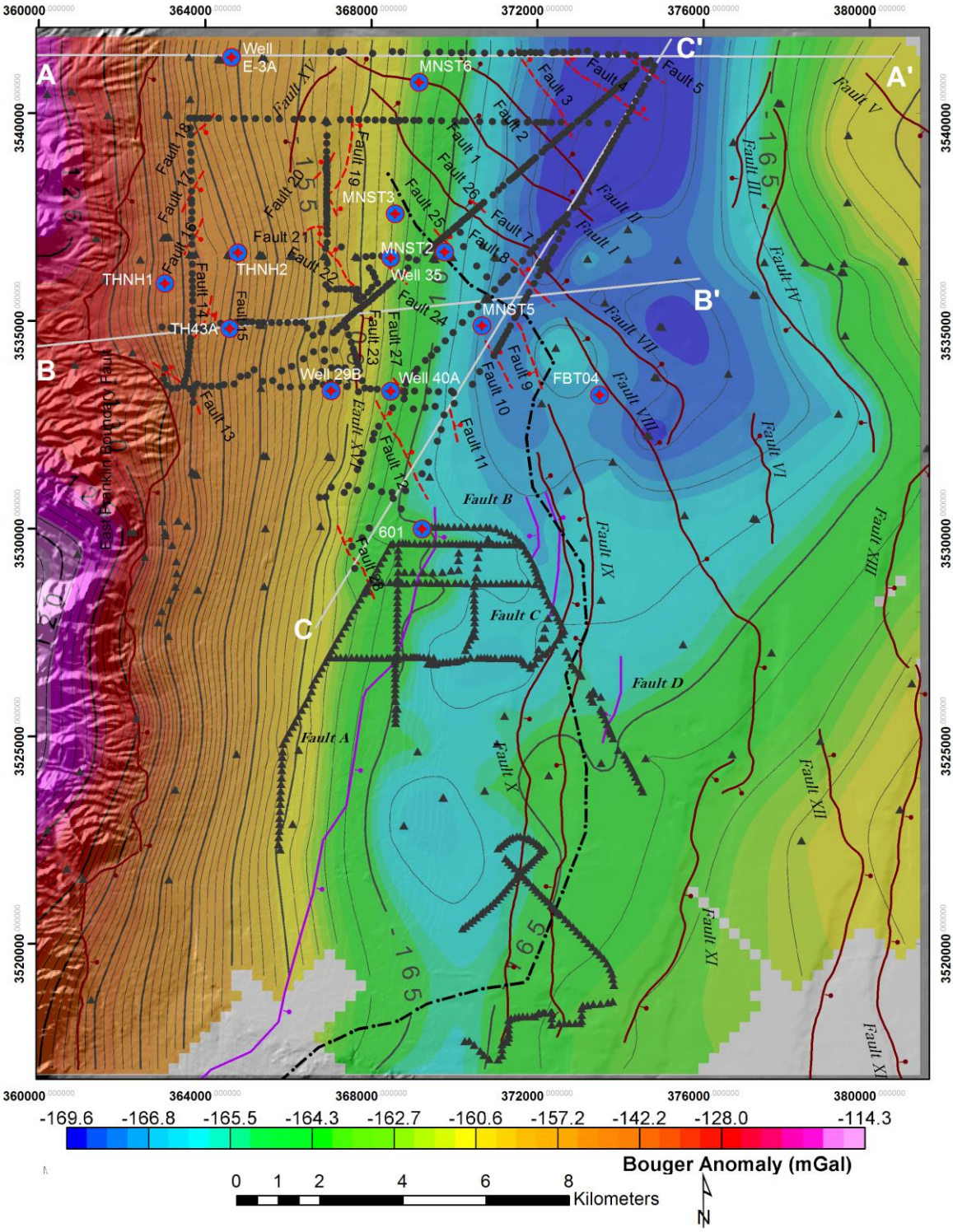

Figure 2.5: Bouguer gravity anomaly map contoured at a 1mGal interval. Hot and cool colors represent high and low gravity values, respectively. The mid northern part of area with low gravity values represents the deepest part of the basin. Previously identified faults are shown with solid lines and newly identified faults with dotted lines. AA', BB' and CC' are the location of profiles.

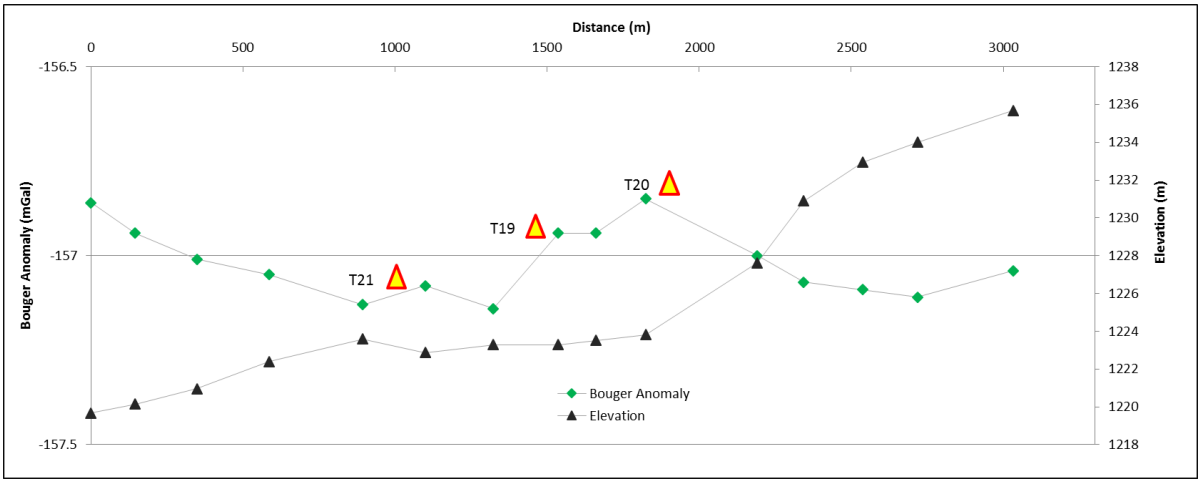

Figure 2.6: Figure showing the relationship between Bouger anomaly, elevation and distance between gravity stations. Anomalies T19 and T20 are fault related whereas anomaly T21 is elevation related (see text for details).

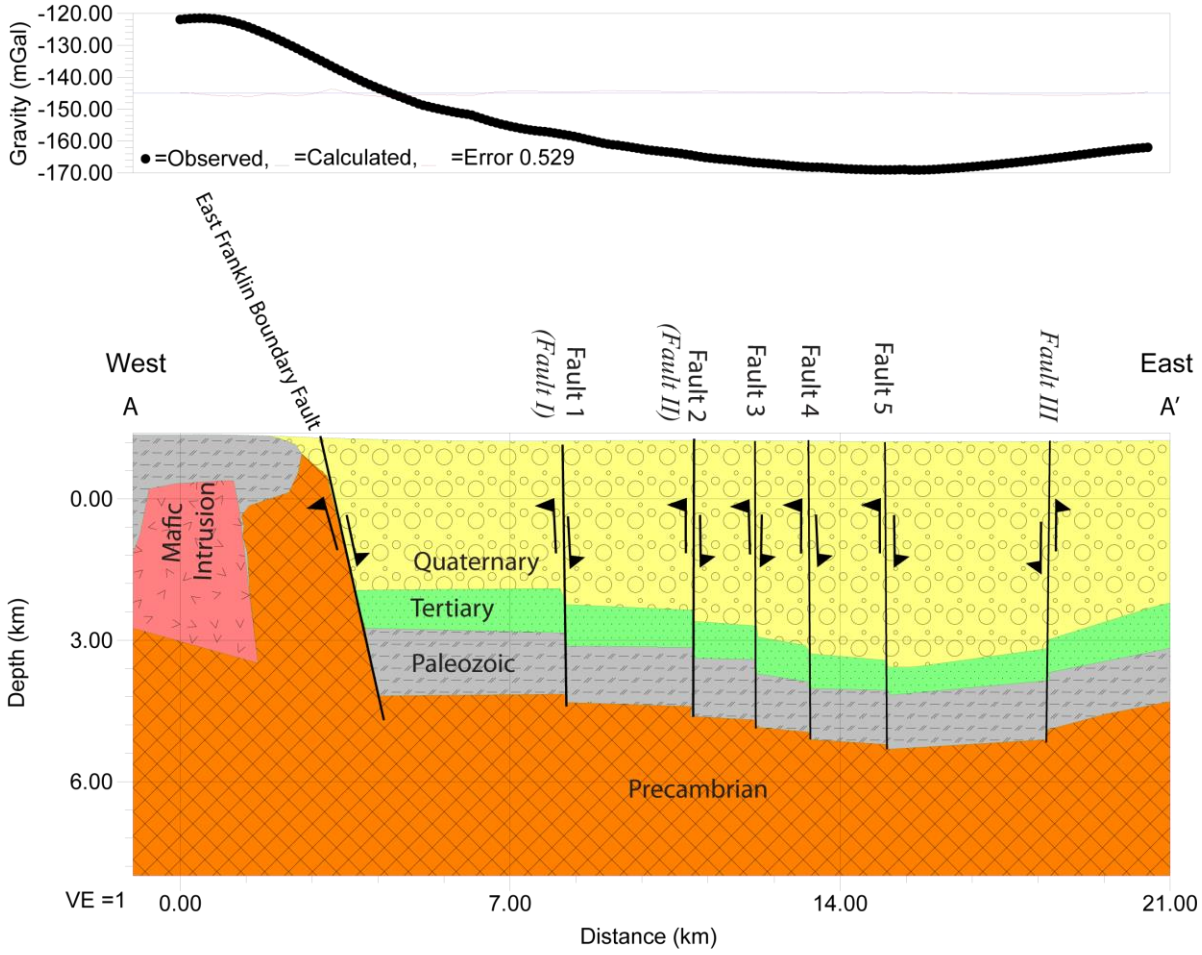
Gravity (mGal)
-120.00
-130.00
-140.00
-150.00
-160.00
-170.00
●=Observed, =Calculated, =Error 0.529
East Franklin Boundary Fault
West
A
Fault 1
(Fault I)
Fault 2
(Fault II)
Fault 3
Fault 4
Fault 5
Fault III
East
A′
Mafic Intrusion
Quaternary
Tertiary
Paleozoic
Precambrian
Depth (km)
0.00
3.00
6.00
VE =1
0.00
7.00
14.00
21.00
Distance (km)

a)

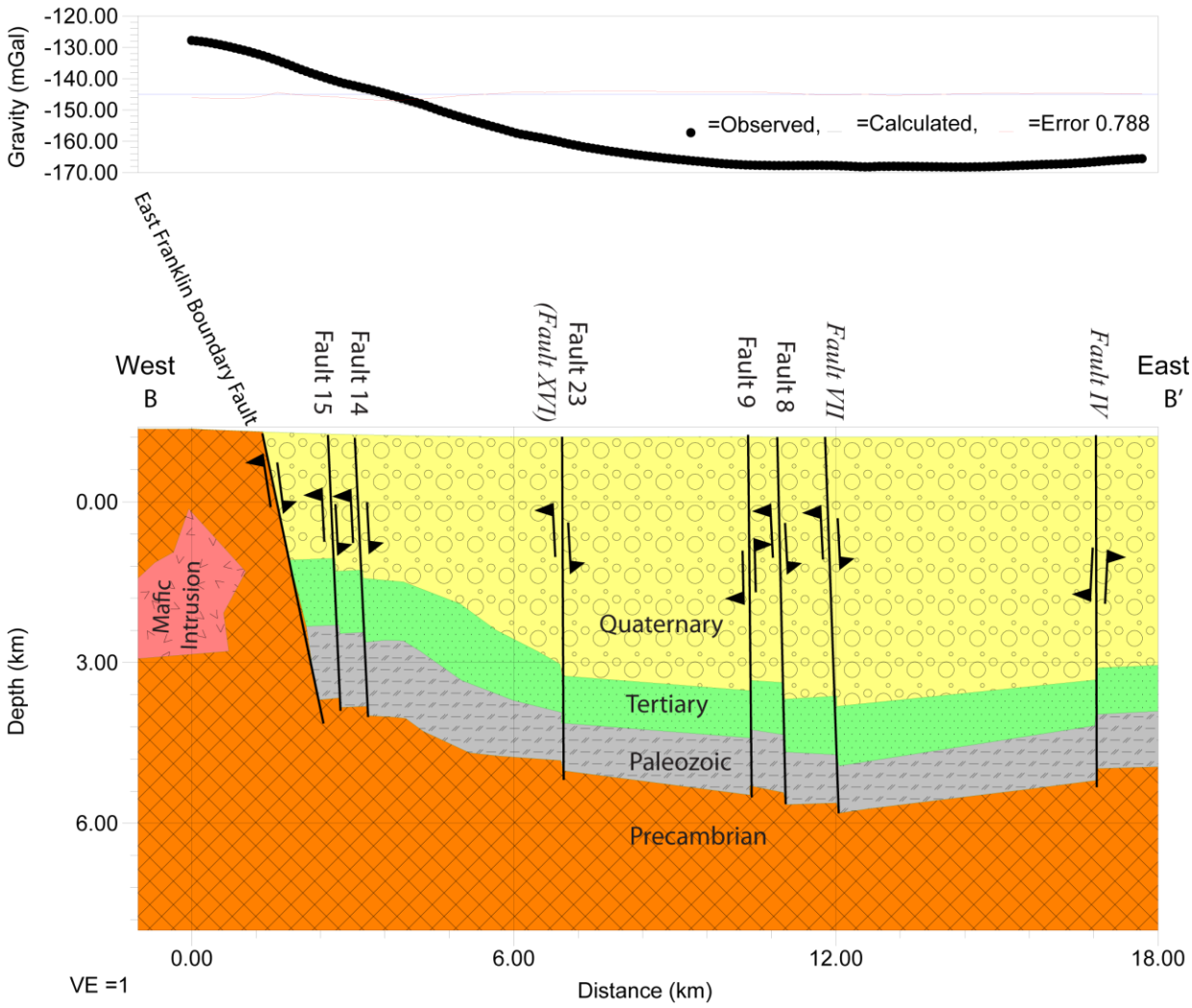
Gravity (mGal)
-120.00
-130.00
-140.00
-150.00
-160.00
-170.00
=Observed,
=Calculated,
=Error 0.788
East Franklin Boundary Fault
Fault 15
Fault 14
Fault 23
(Fault XVI)
Fault 9
Fault 8
Fault VII
Fault IV
West
B
East
B′
Mafic
Intrusion
Quaternary
Tertiary
Paleozoic
Precambrian
Depth (km)
0.00
3.00
6.00
0.00
6.00
12.00
18.00
VE =1
Distance (km)

b)

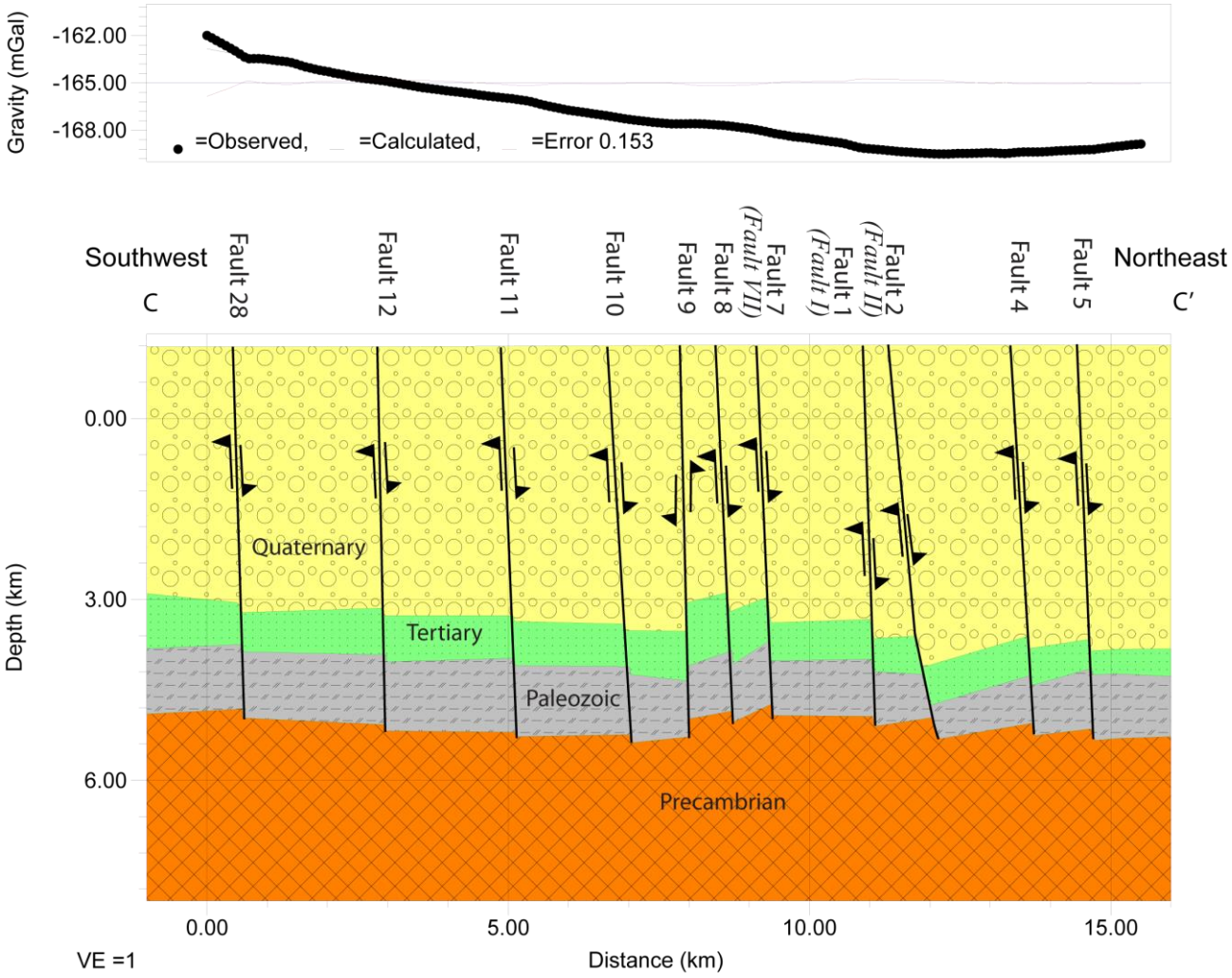

c)

Figure 2.7: Interpreted gravity profile along AA' (a), BB' (b) and CC' (c). The profile locations are shown in Figure 2.5. Faults labelled with Roman numerals are the faults mapped by Collins and Raney (2000).

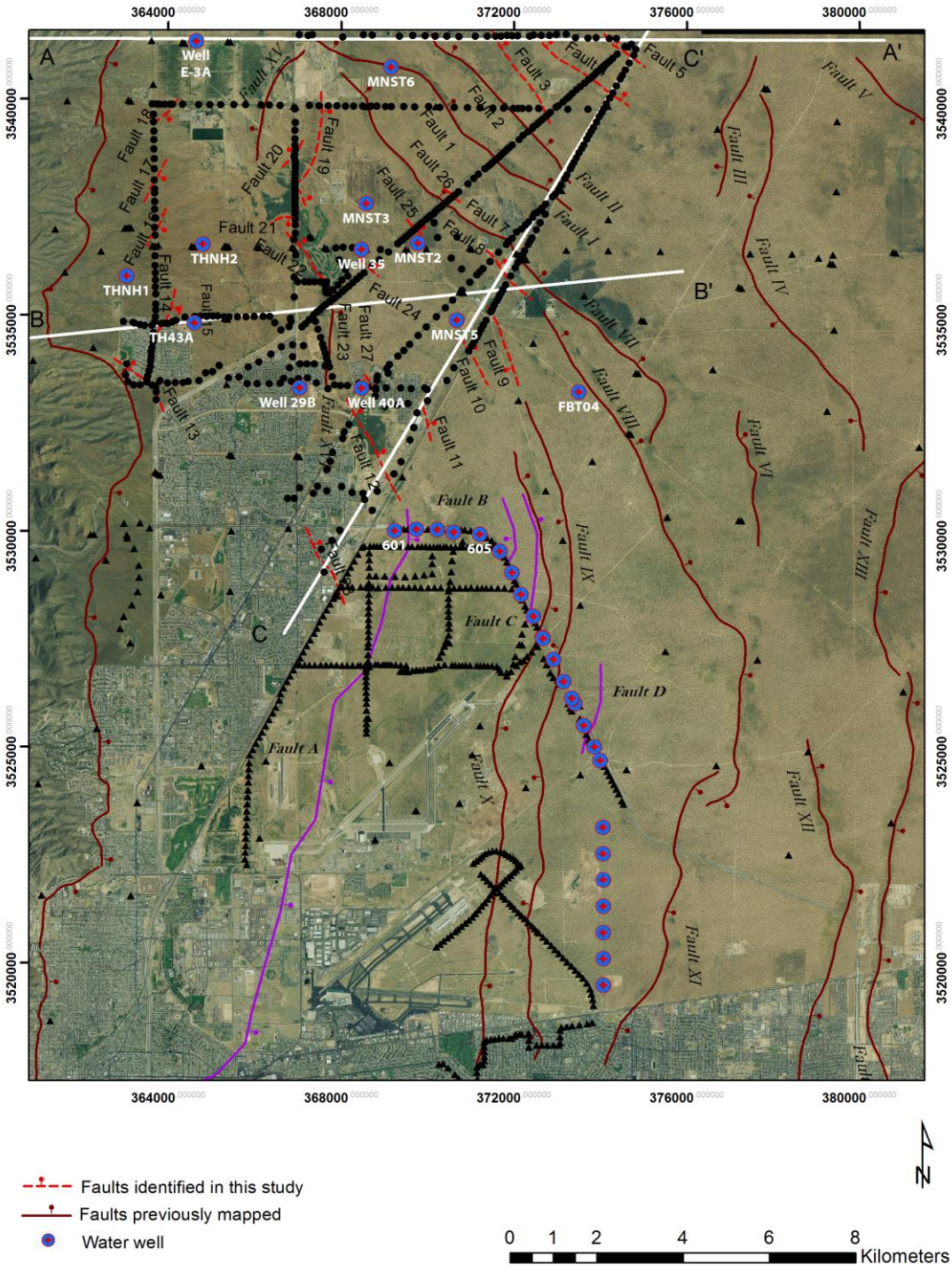

Figure 2.8: Map showing newly interpreted faults with relationship to fresh-brackish water boundary. Faults labeled with general numbers are newly interpreted faults in this study. Faults labeled with Roman numerals and with alphabets are previously mapped faults by Collins and Raney (2000) and Marrufo (2011), respectively. Brackish water is located to the east of the boundary. AA', BB' and CC' are the location of profiles.

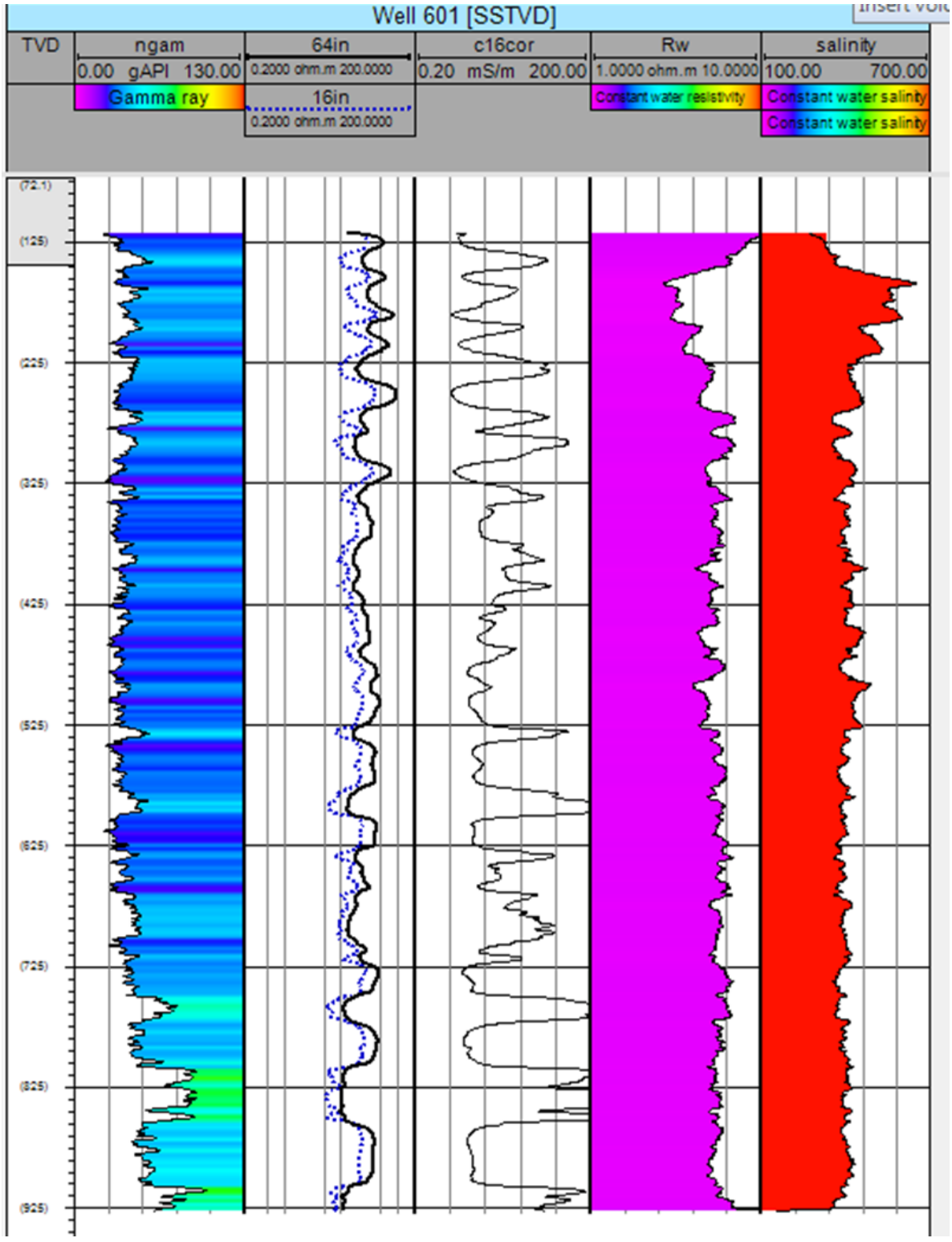

Figure 2.9: Figure showing water resistivity (Rw) calculated from SP method and converted it into salinity using eqn 7.

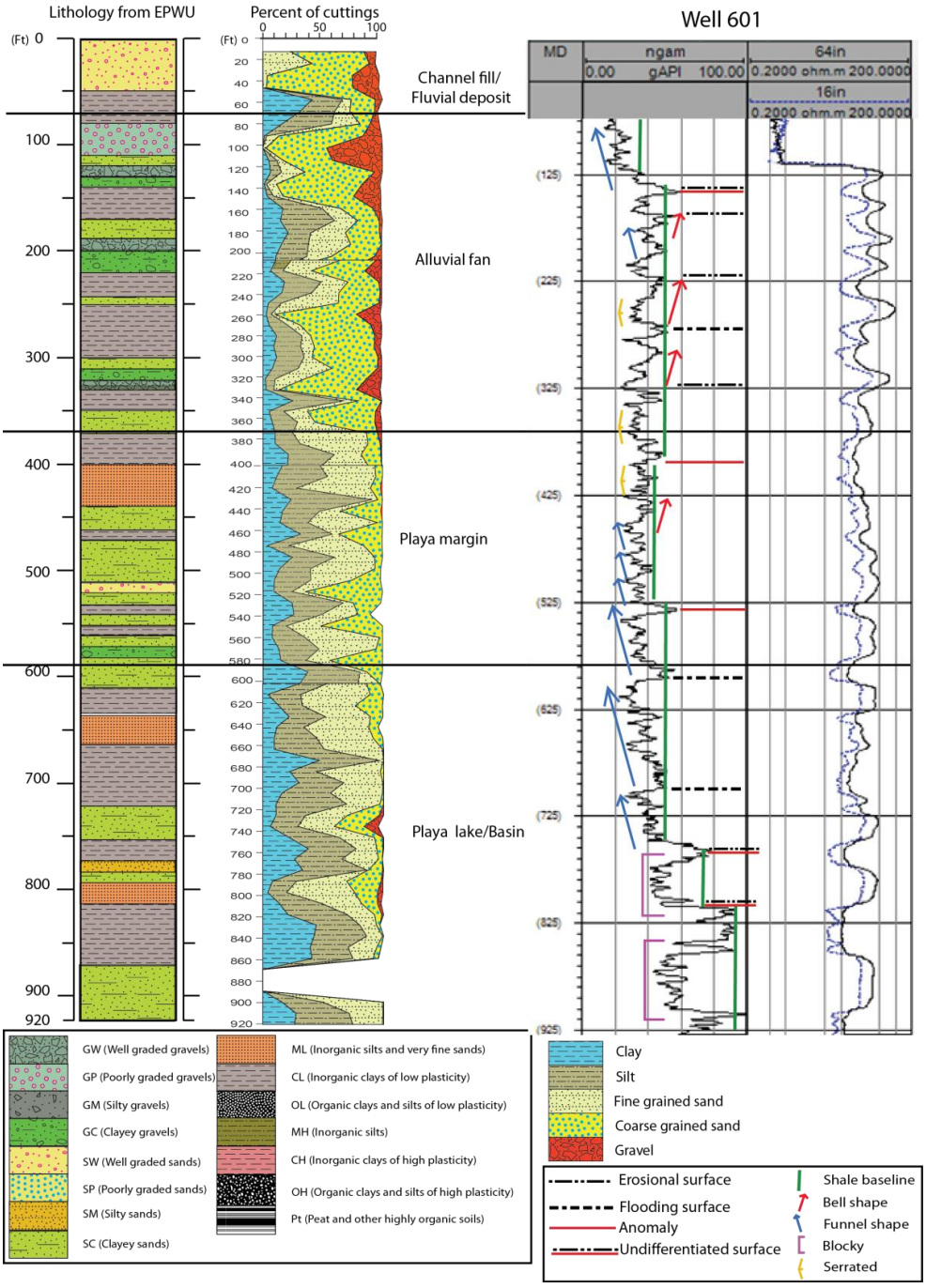

Figure 2.10: Comparison between grain size distribution, geophysical logs and lithology based on unified soil classification system from well 601.Figure for percent of cuttings is modified from Doser and Langford (2006). Sandstone (conglomerate) resting on top of shale is demarcated as an erosional surface; shale on the top of sandstone as a flooding surface and abrupt changes in shale baseline as an anomaly which can be either an unconformity or fault. Bell, funnel, serrated and blocky shapes represent fining up, coarsening up, alternative fine and coarse grained, and no or little change in lithology, respectively.

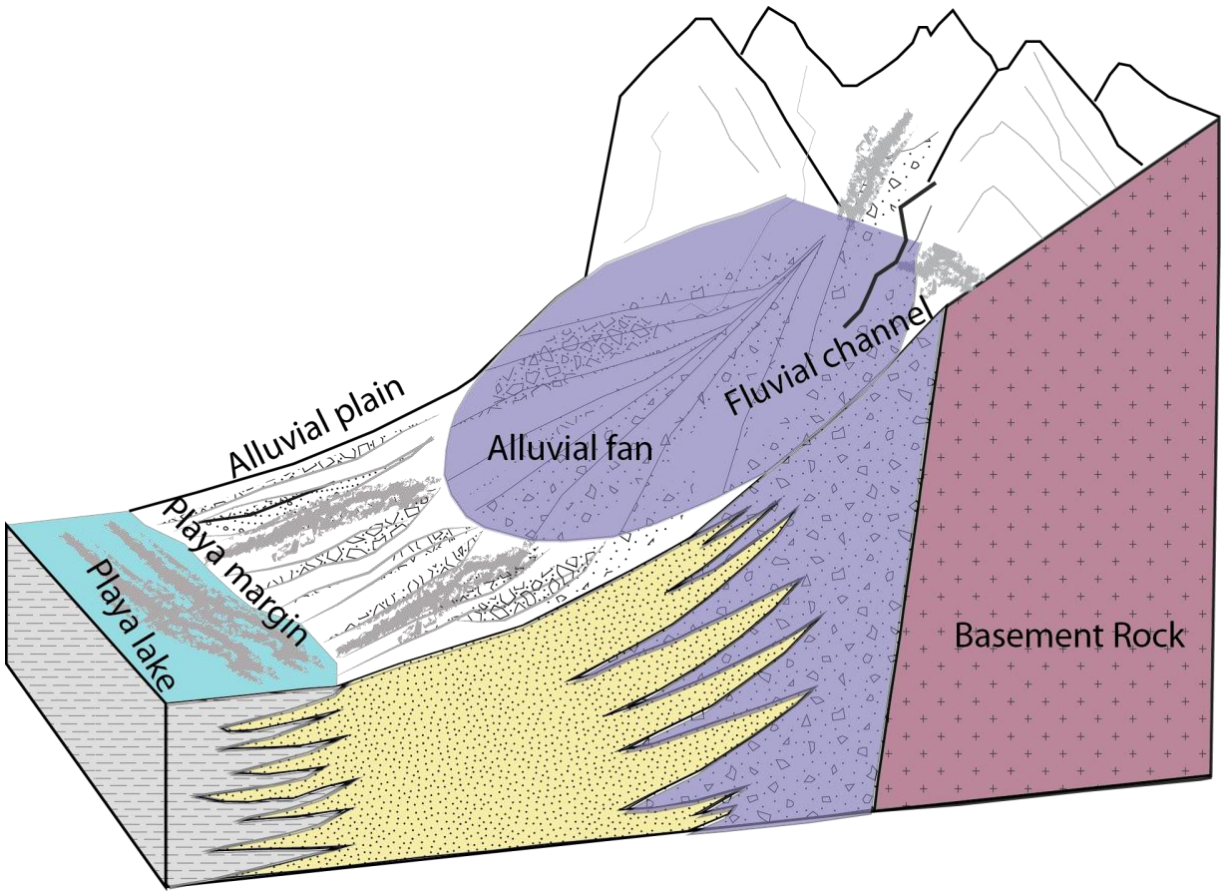

Figure 2.11: Schematic representation of alluvial fan system meeting playa lake (Modified after Bjorlykke, 1989).

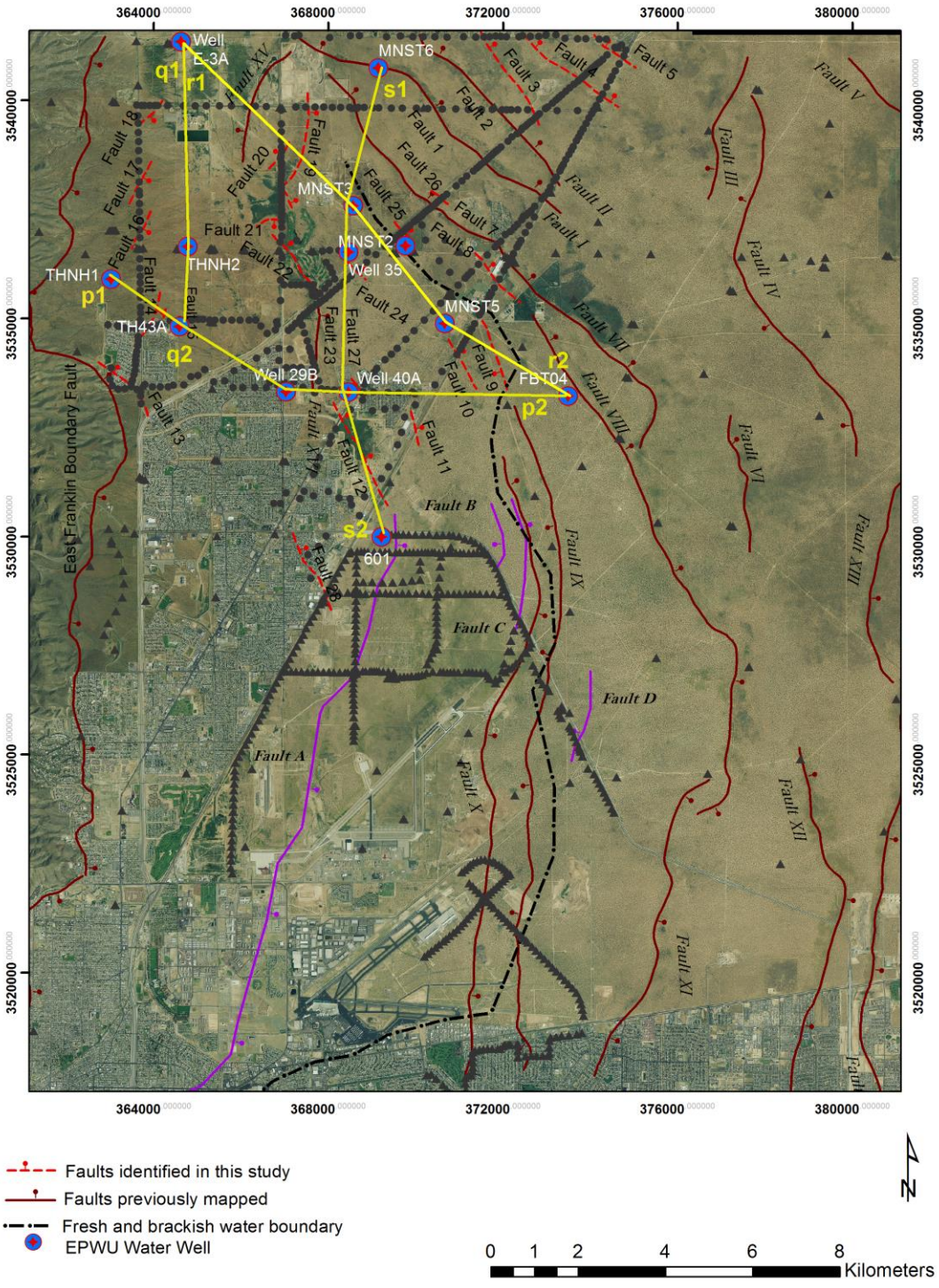

Figure 2.12: Map showing the location of well log sections, faults, and the fresh-brackish water boundary. p1p2, q1q2, r1r2 and s1s2 are the location of structural and stratigraphic cross sections.

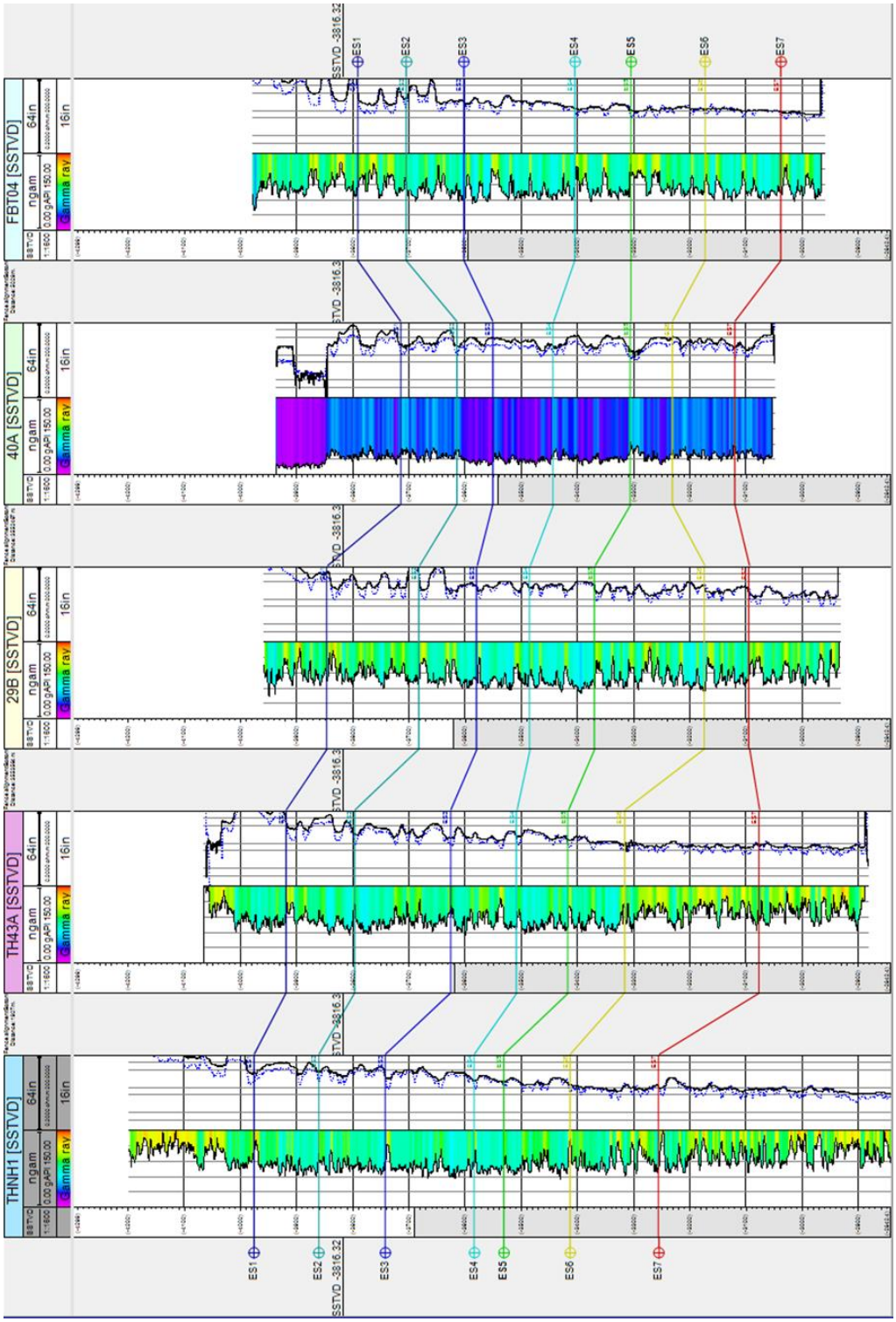

Figure 2.13: West-east extending structural section (p1p2) (Location is shown in Figure 2.12).

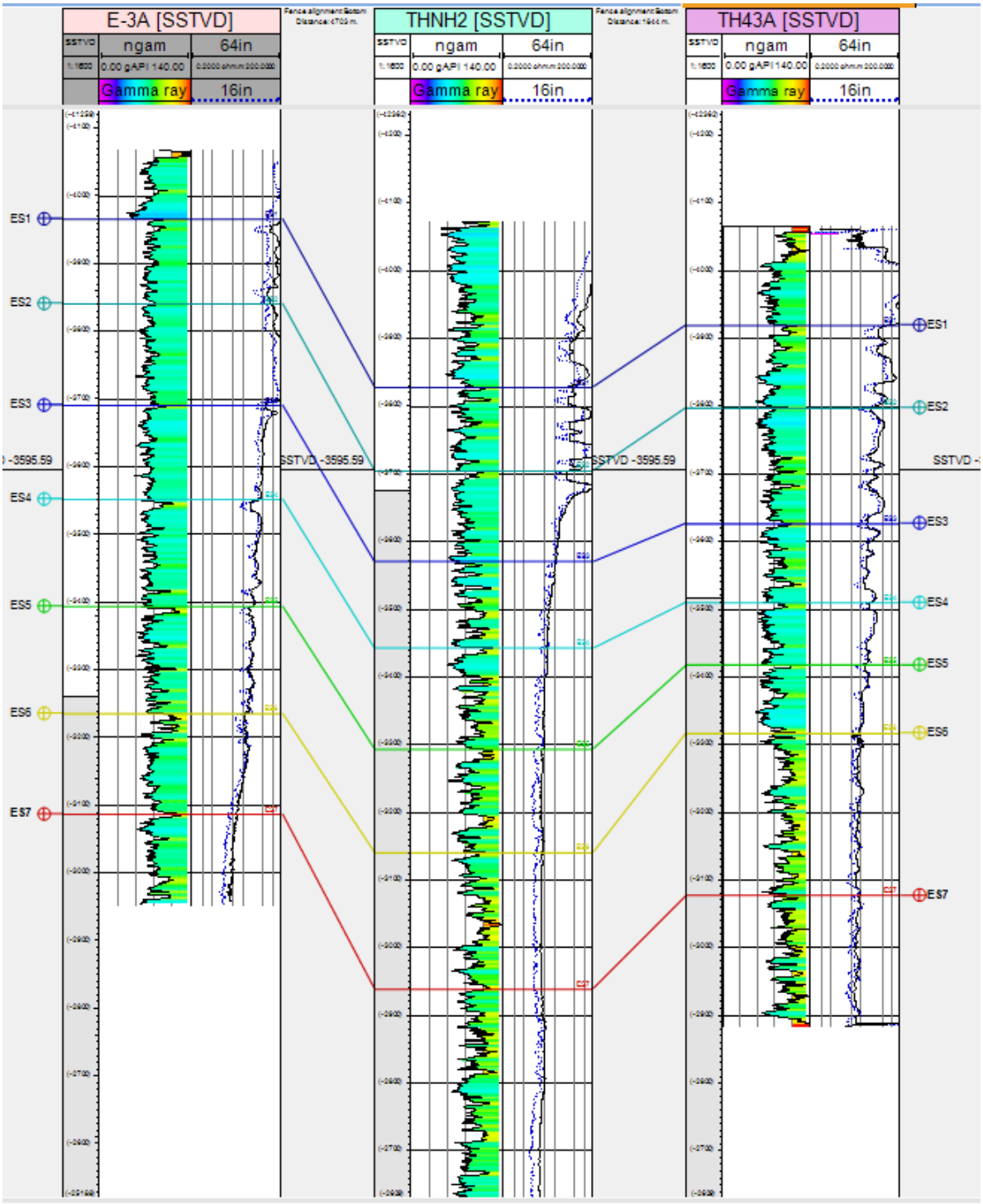

Figure 2.14: Structural cross section along q1q2 (Location of line is shown in Figure 2.12).

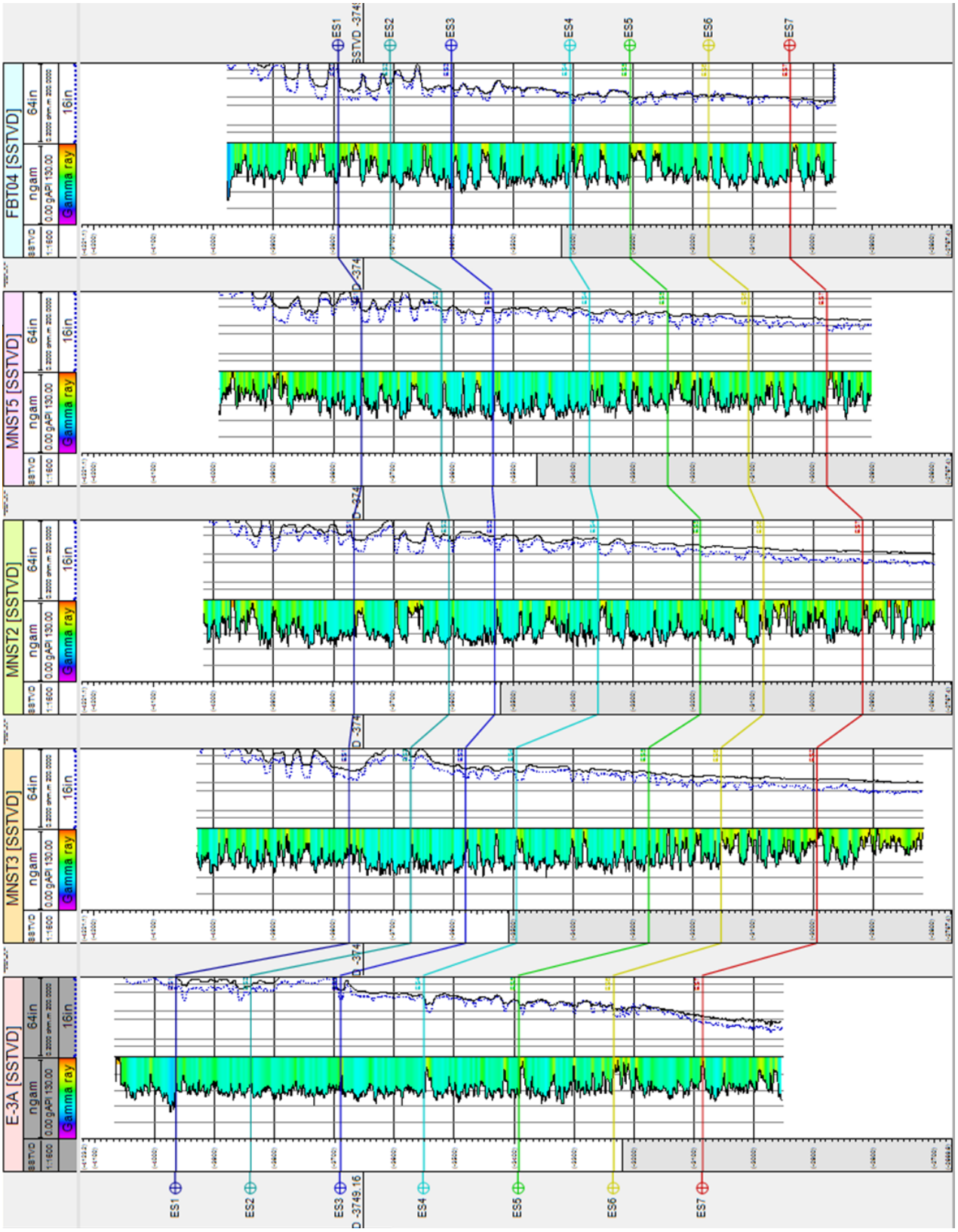

Figure 2.15: Structural cross section along r1r2 (Location of line is shown in Figure 2.12).

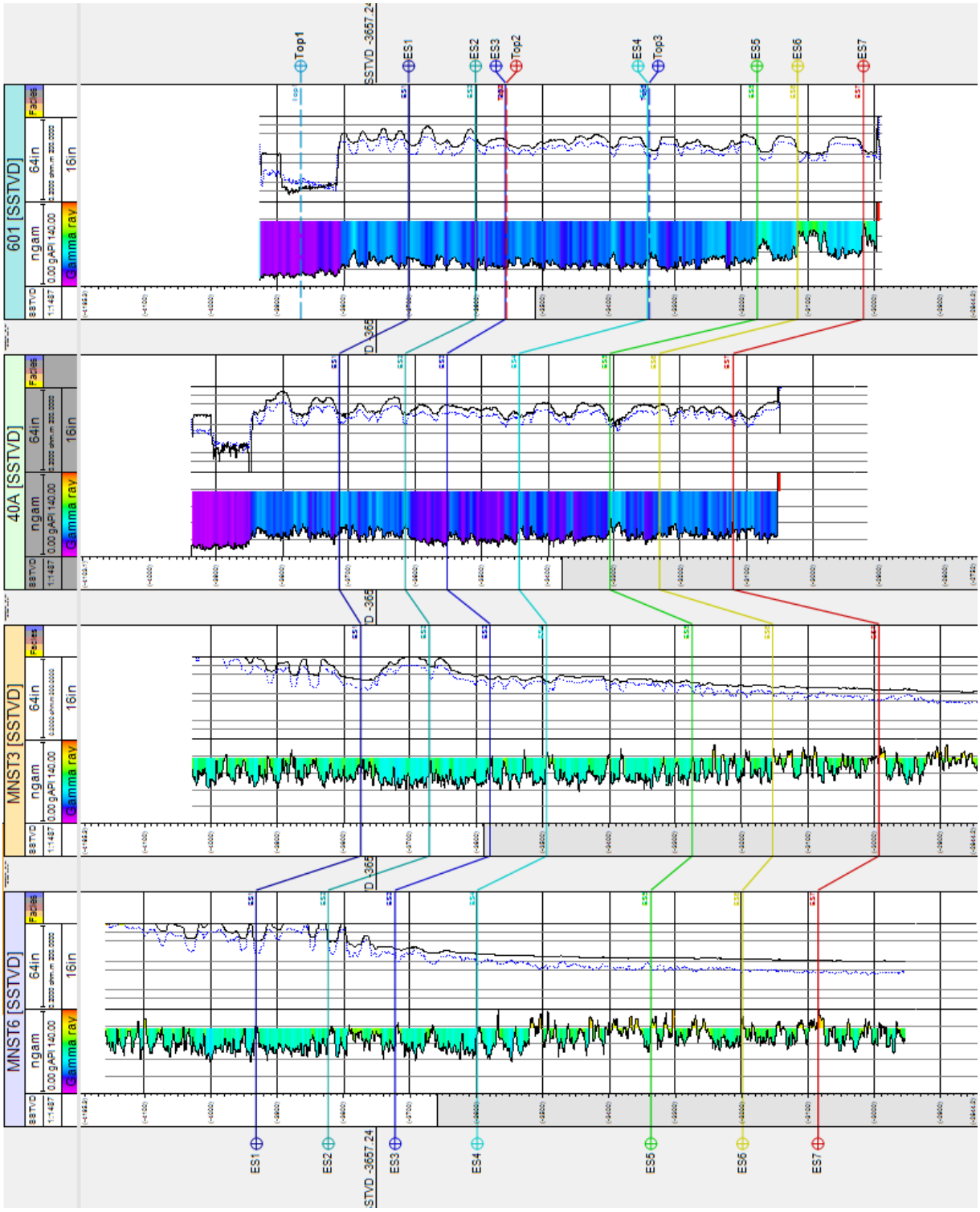

Figure 2.16: Structural cross section along s1s2 (Location of line is shown in Figure 2.12).

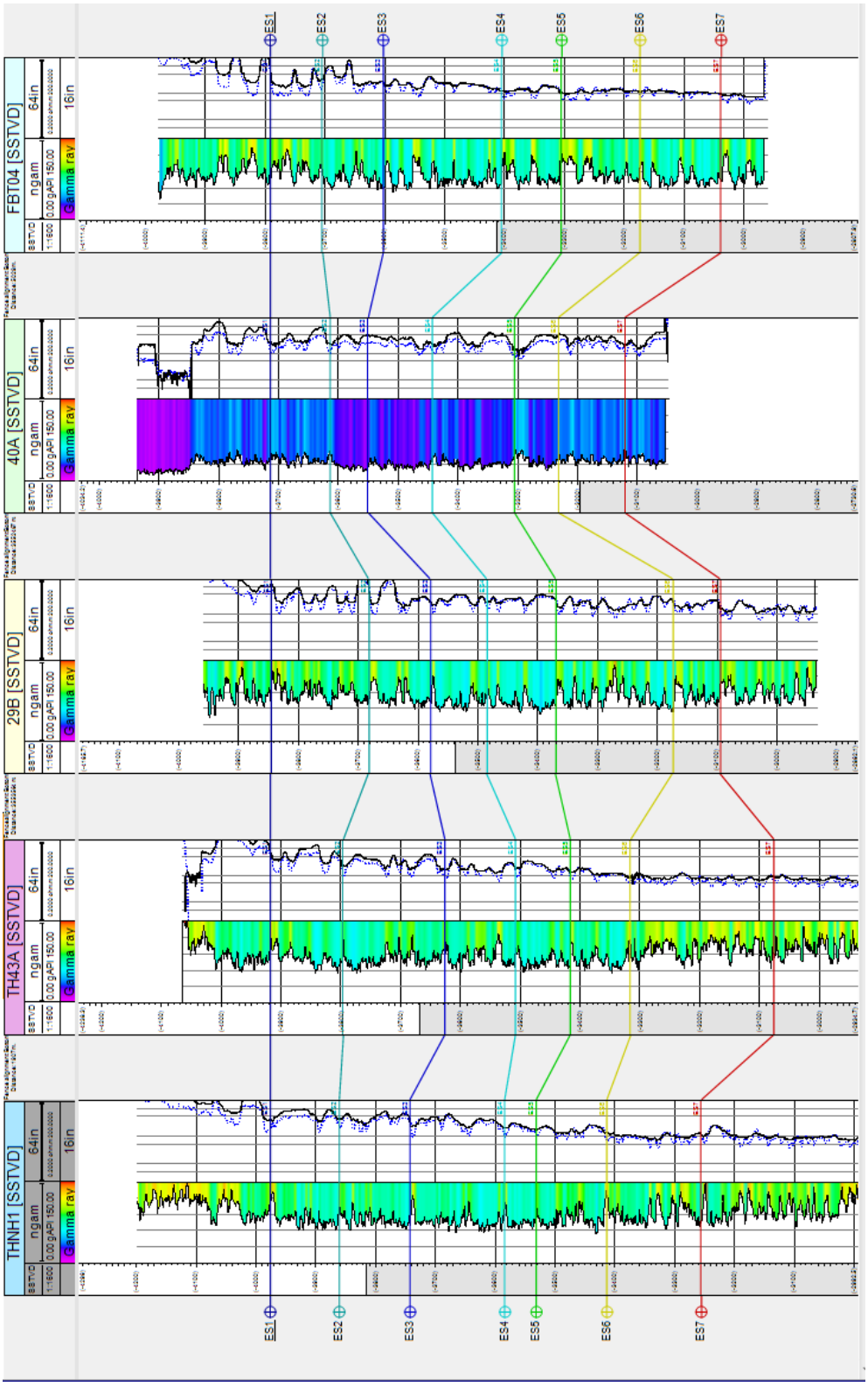

Figure 2.17: Stratigraphic cross section along p1p2.

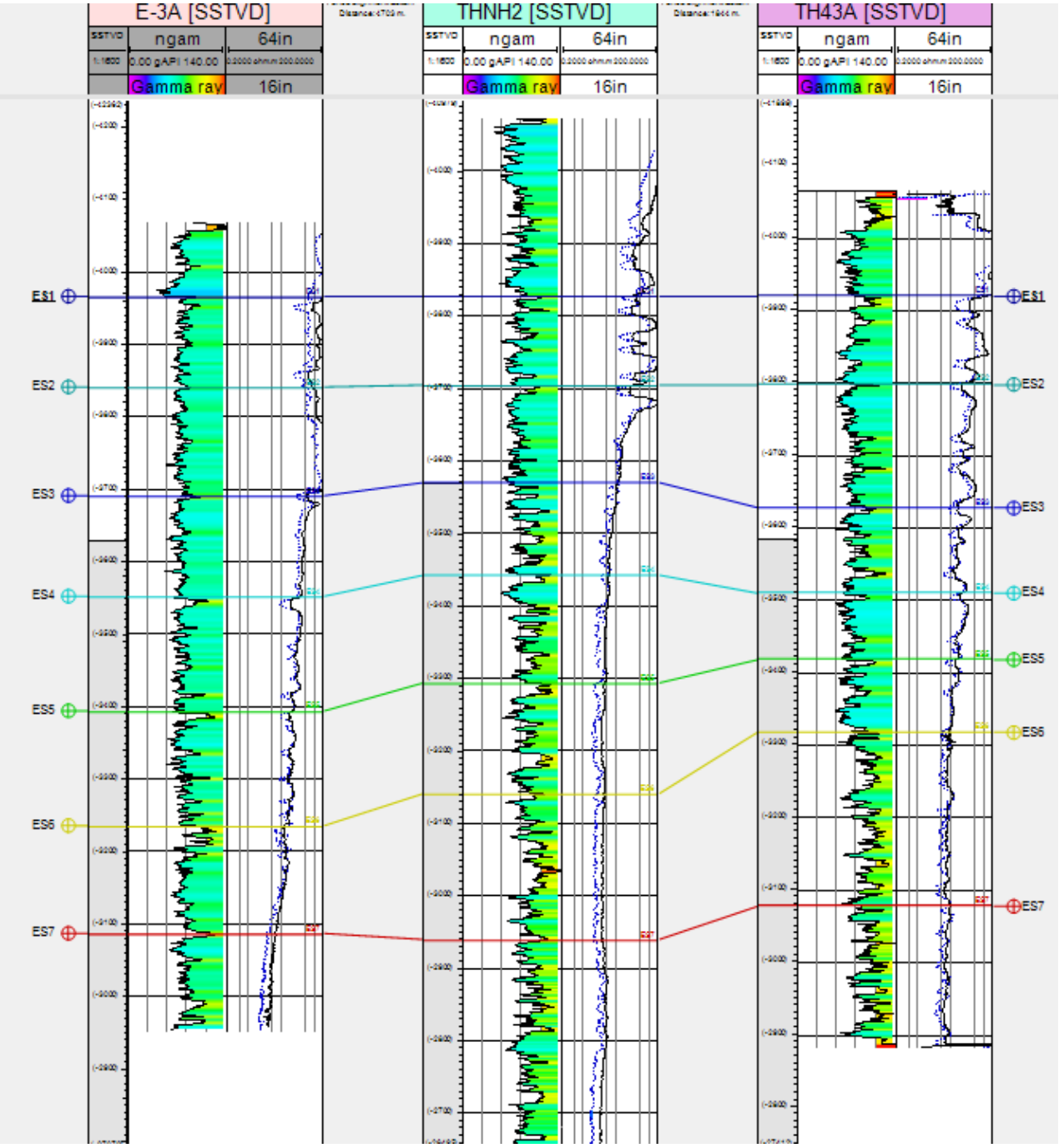

Figure 2.18: Stratigraphic cross section along q1q2.

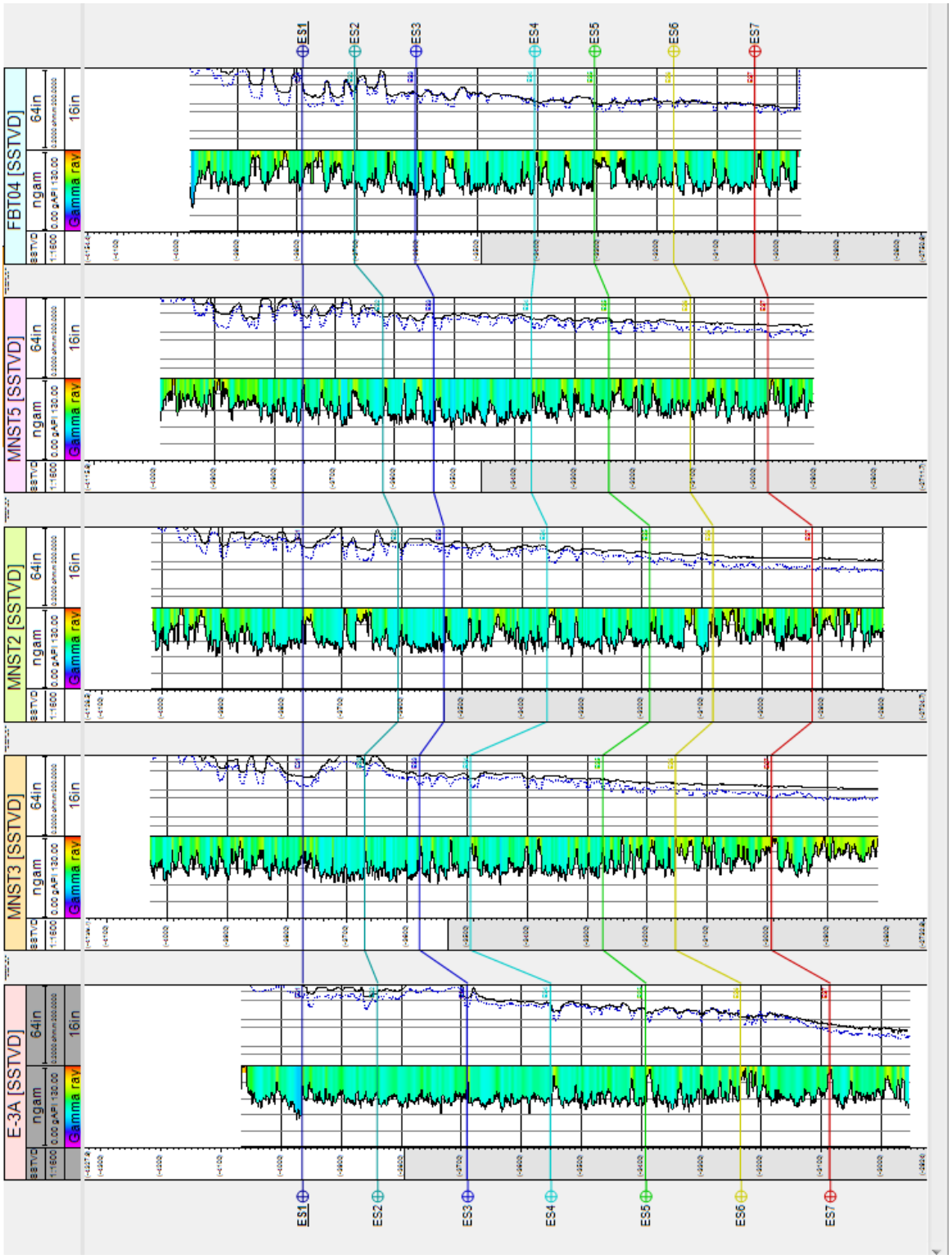

Figure 2.19: Stratigraphic cross section along r1r2.

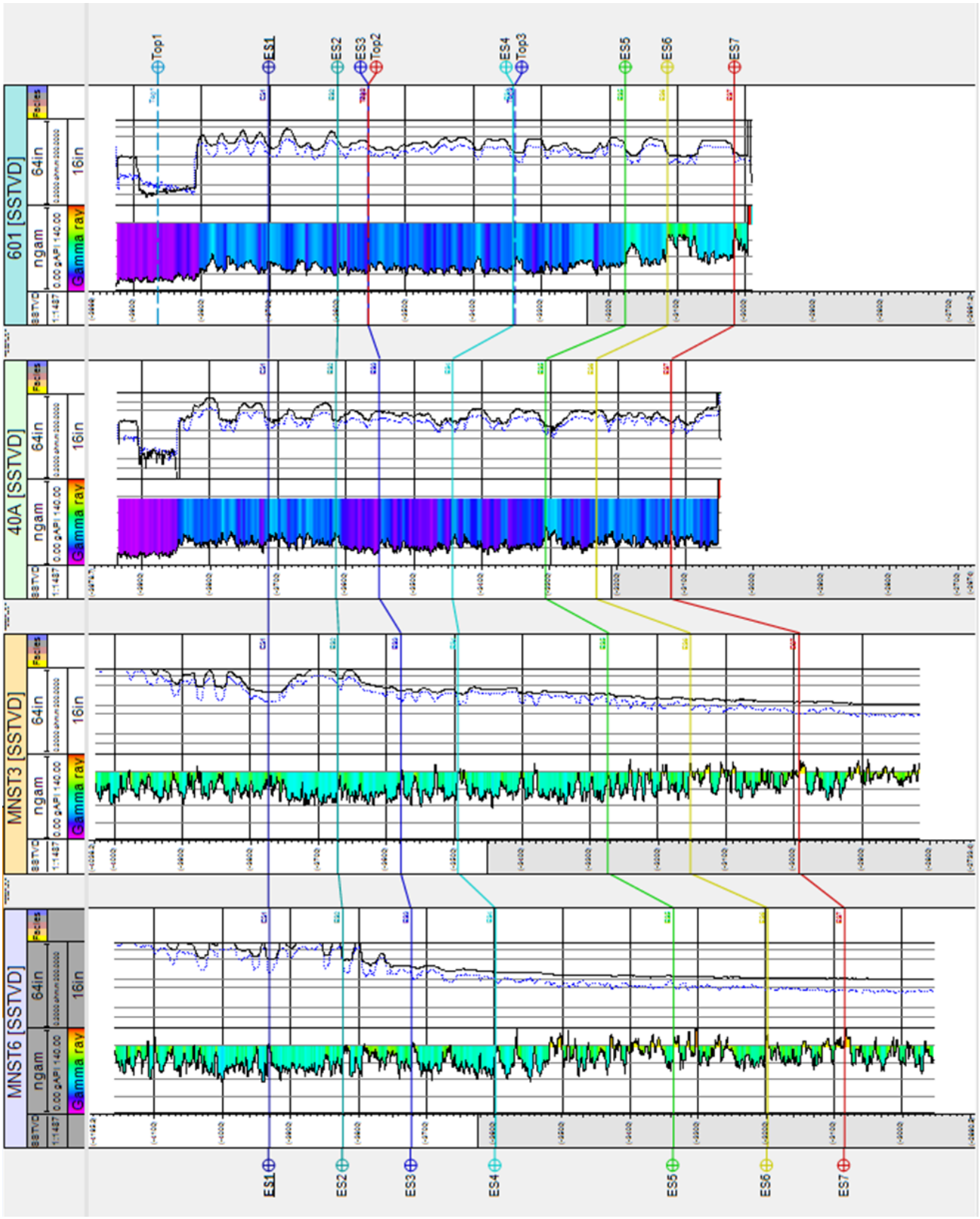

Figure 2.20: Stratigraphic cross section along s1s2.

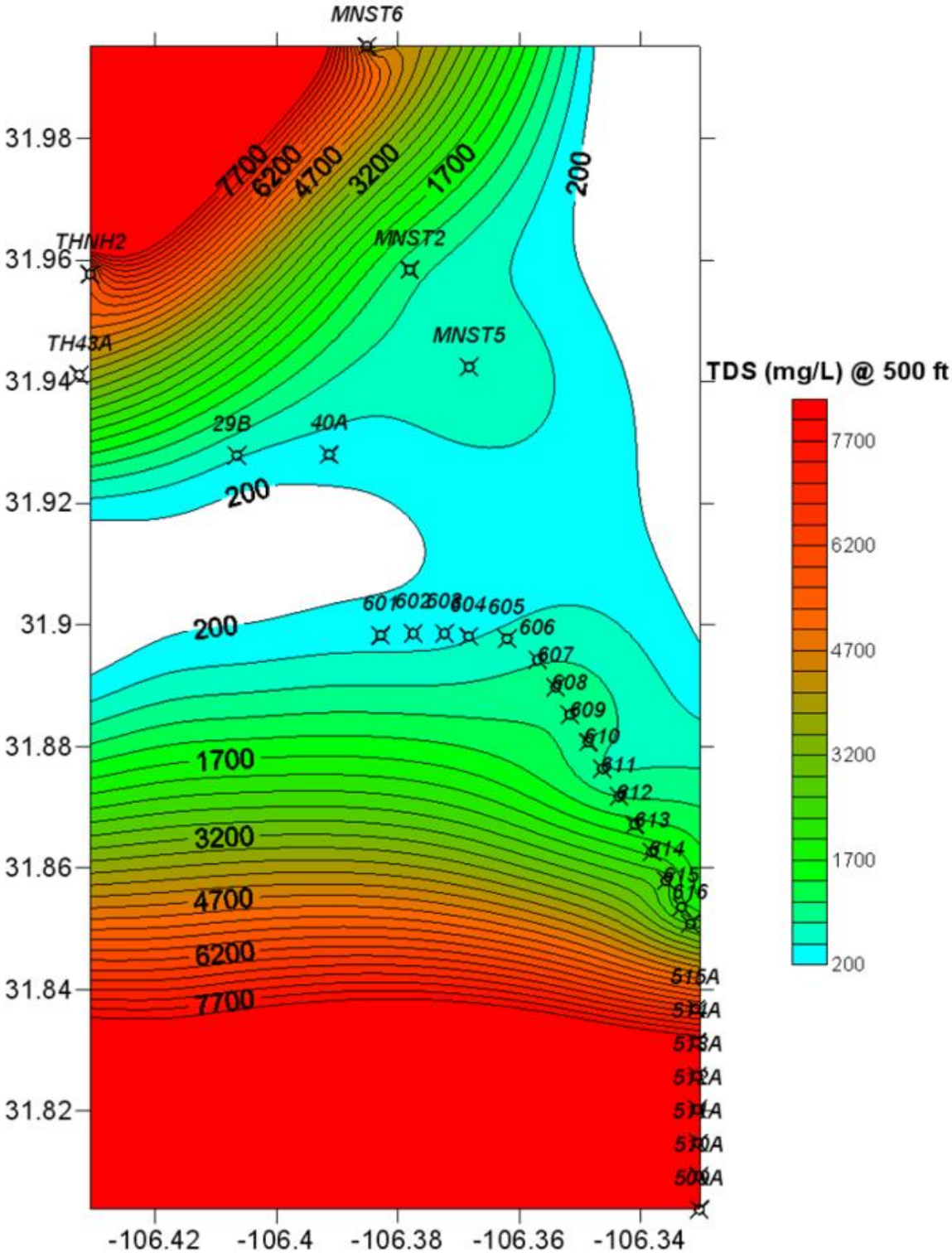

Figure 2.21: Map showing well locations and TDS. TDS values were obtained from EPWU, which ranges from 320 to 7410 mg/L (ppm) around 500 ft depth.

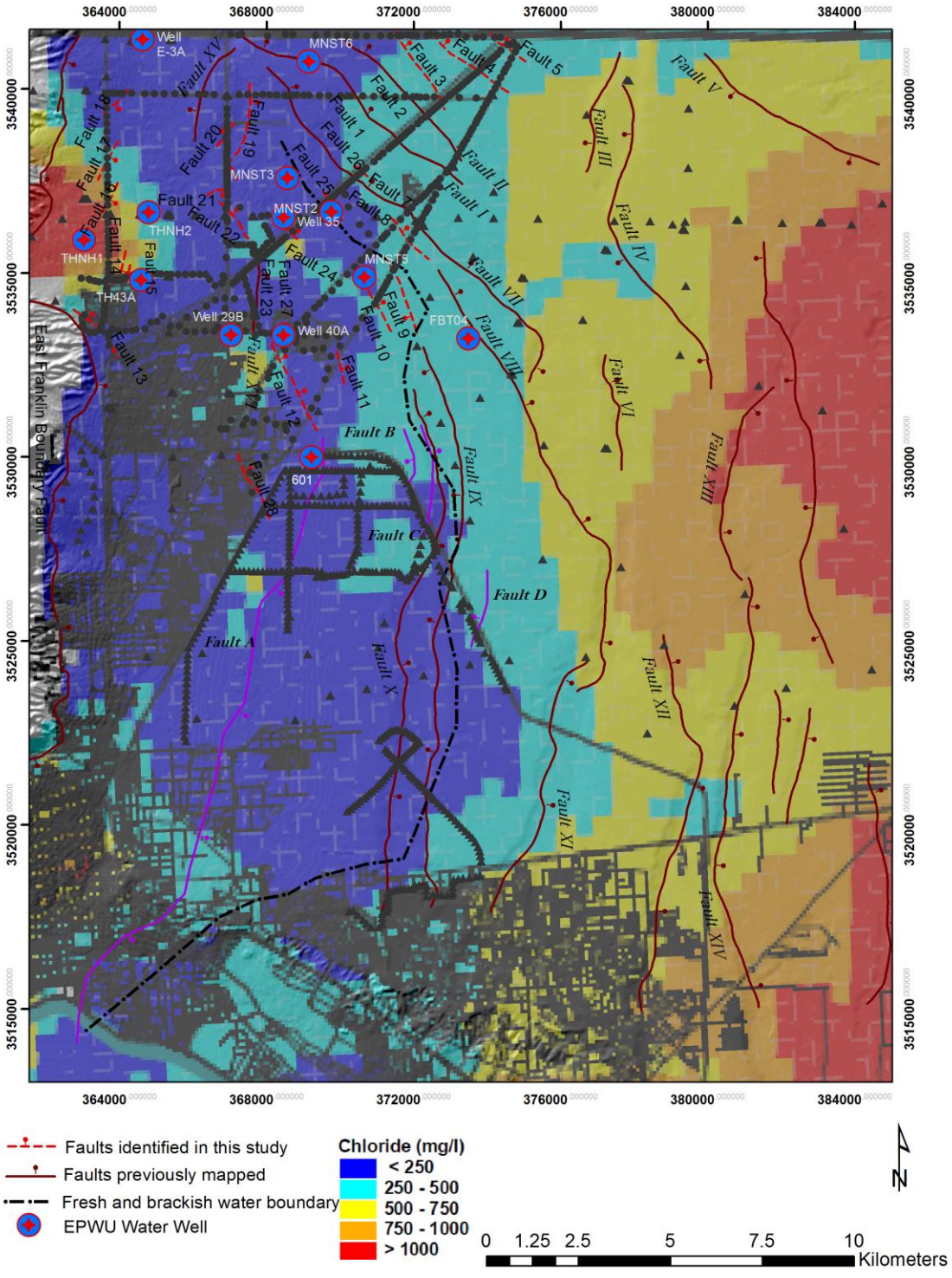

Figure 2.22: Choloride concentration map around 1084 m elevation. Chloride concentration map is from Bredehoeft et al. (2004).

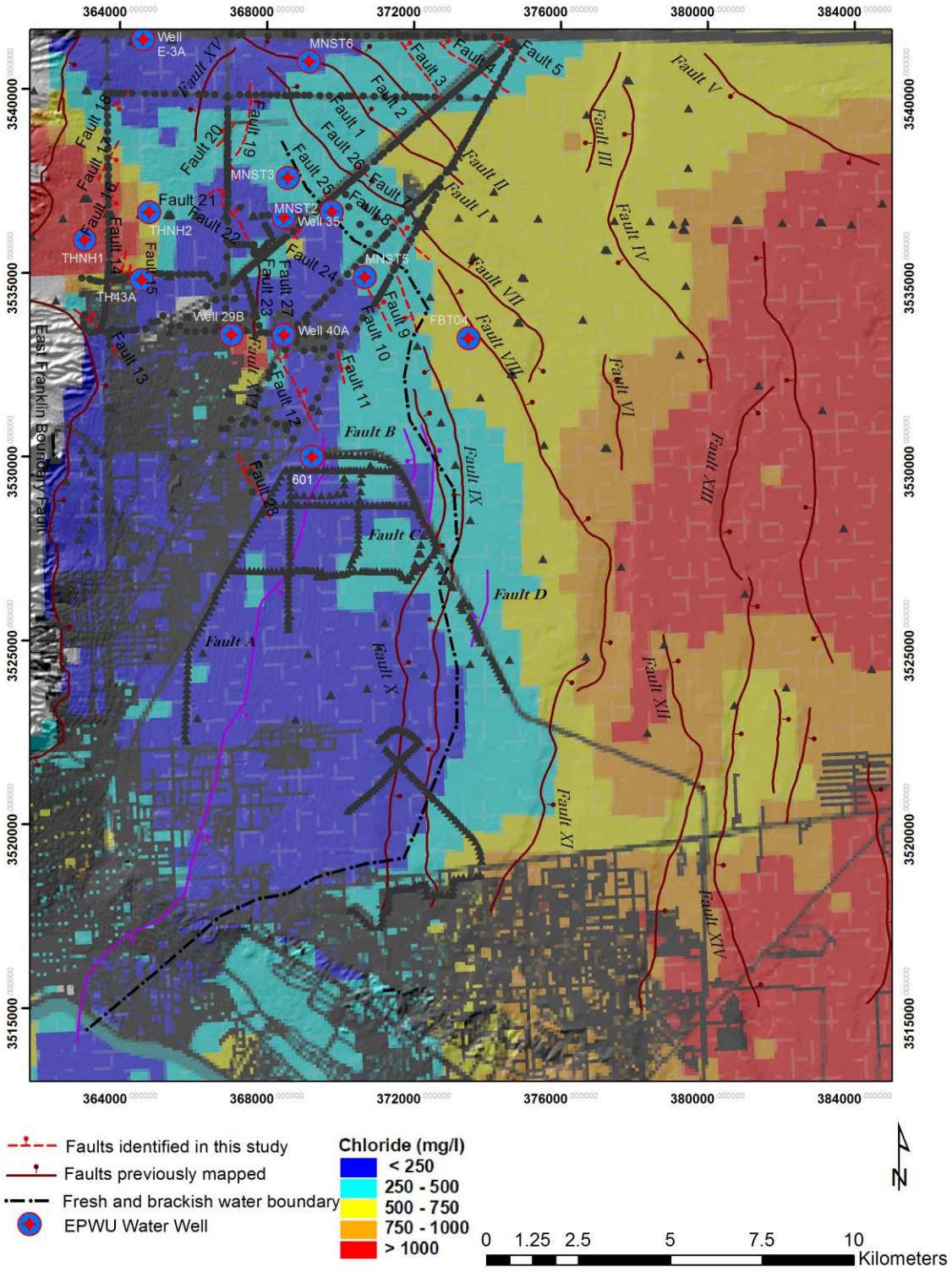

Figure 2.23: Choloride concentration map around 1024 m elevation. Chloride concentration map is from Bredehoeft et al. (2004).

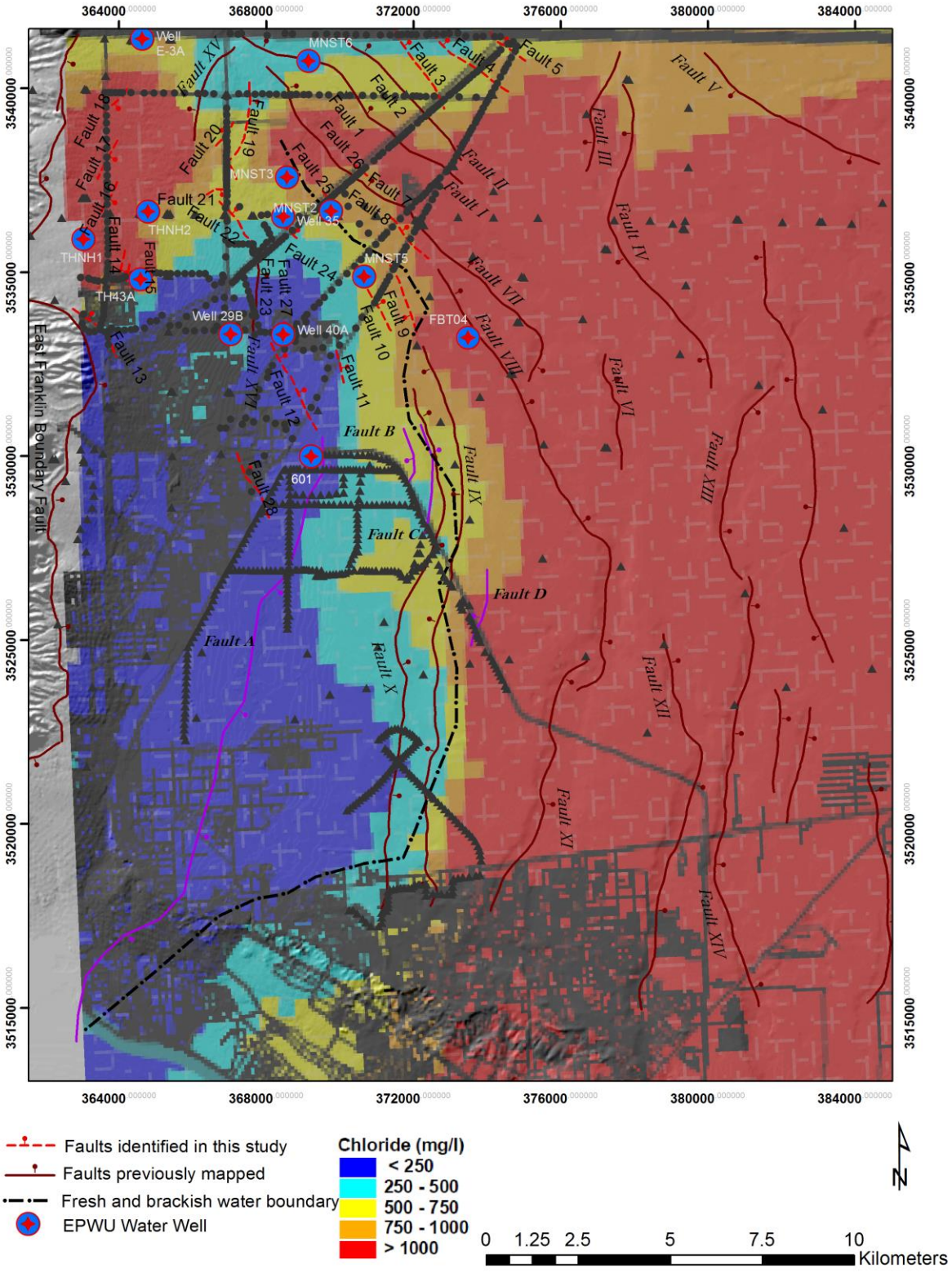

Figure 2.24: Choloride concentration map around 904 m elevation. Chloride concentration map is from Bredehoeft et al. (2004).

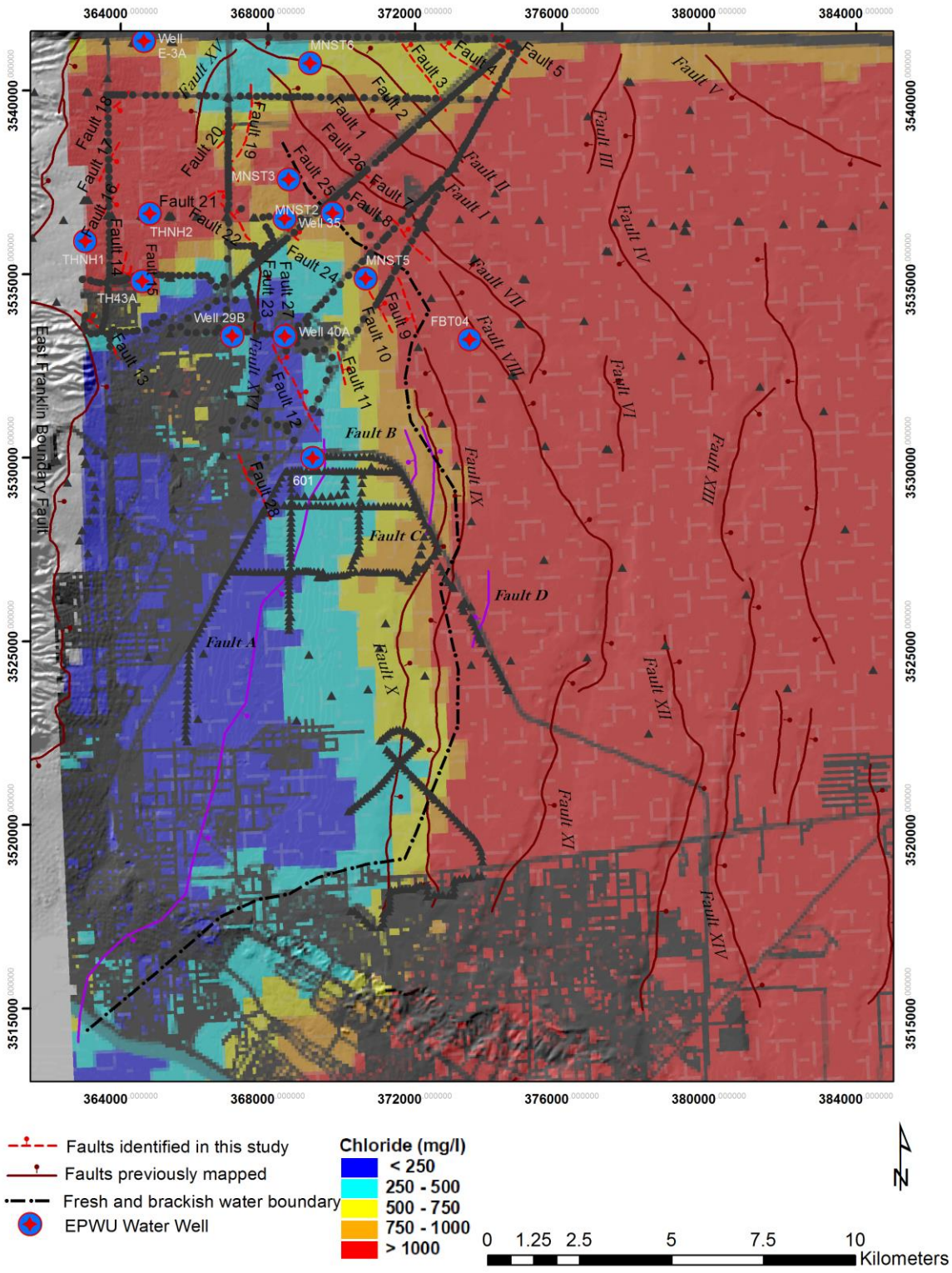

Figure 2.25: Choloride concentration map around 731 m elevation. Chloride concentration map is from Bredehoeft et al. (2004).

Vita

Pawan Budhathoki earned his Bachelor of Science degree in Geology in 2001, and Master of Science degree in Geology in 2006 from Tribhuvan University, Nepal. In 2008 he joined the doctoral program in Geology at The University of Texas at El Paso (UTEP).

He has presented his research in several national and international meetings. He has been the recipient of numerous awards including a Vernon and Joy Hunt Scholarship, a Frank B. Cotton Memorial Scholarship, an American Association of Petroleum Geologists (AAPG) Southwest Section Scholarship, and a West Texas Geological Society (WTGS) Terra Nova Scholarship. Moreover, he was the recipient of an AAPG SEAPEX Named Grant and various other grants from the Geological Society of America (GSA) and the American Association of Petroleum Geologists/Society of Exploration Geophysicists (AAPG/SEG). He was also awarded a Bruce Davidson Memorial Student Award for his outstanding contribution to the Department of Geological Sciences.

While pursuing his degree, he worked as an assistant instructor for the Department of Geological Sciences. He has interned with Texas Rare Earth Resources Corp (TRER) and with Baker Hughes. After graduation, he will begin work as a geoscientist with Baker Hughes.

He participated in several extracurricular activities. He served as president of the UTEP chapter of the Society of Exploration Geophysicists, and as Chair of the 26th Annual Geological Sciences Colloquium. In recognition of his service, he was awarded an SEG/Chevron Student Leadership Symposium Travel Grant.

His dissertation, *Integrated Geological and Geophysical Studies of the Indio Mountains and Hueco Bolson, West Texas*, was supervised by Dr. Richard Langford and Dr. Diane Doser.

Permanent address: Khanar-5
Sunsari, Nepal

This dissertation was typed by Pawan Budhathoki.